

AD-757 162

CALCULATION OF THE THREE DIMENSIONAL
PARTICLE TRAJECTORIES IN A ONE AND ONE-
HALF STAGE OF A COMPRESSOR

M. Fathy Hussein, et al

Cincinnati University

Prepared for:

Army Research Office-Durham

February 1973

DISTRIBUTED BY:

NTIS

National Technical Information Service
U. S. DEPARTMENT OF COMMERCE
5285 Port Royal Road, Springfield Va. 22151

DOCUMENT CONTROL DATA - R & D

(Security classification of title, body of abstract and indexing annotation must be entered when the overall report is classified)

1. ORIGINATING ACTIVITY (Corporate author)		2a. REPORT SECURITY CLASSIFICATION	
University of Cincinnati		Unclassified	
		2b. GROUP	
		NA	
3. REPORT TITLE			
Calculation of the Three Dimensional Particle Trajectories in a One and One-Half Stage of a Compressor			
4. DESCRIPTIVE NOTES (Type of report and inclusive dates)			
Technical Report			
5. AUTHOR(S) (First name, middle initial, last name)			
M. Fathy Hussein and W. Tabakoff			
6. REPORT DATE		7a. TOTAL NO. OF PAGES	7b. NO. OF REFS
February 1973		81	6
8a. CONTRACT OR GRANT NO.		9a. ORIGINATOR'S REPORT NUMBER(S)	
DAHC04-69-C-0016		Project Themis Report No. 73-34	
b. PROJECT NO.			
c.		9b. OTHER REPORT NO(S) (Any other numbers that may be assigned this report)	
d.			
10. DISTRIBUTION STATEMENT			
Distribution of this report is unlimited			
11. SUPPLEMENTARY NOTES		12. SPONSORING MILITARY ACTIVITY	
None		U.S. Army Research Office - Durham Box CM, Duke Station Durham, North Carolina 27706	
13. ABSTRACT			
<p>The equations of motion, in three dimensions, for solid particles moving in a compressible gas flow in a rotating cascade are solved for the case of the particles moving through a compressor guide vane followed by a compressor stage. The solution considers the particle impact and rebound with both the blade walls and the compressor casing. The three dimensional absolute paths of the particles, their trajectories relative to the compressor rotor, their velocity histories, and the combined particle velocity diagrams in the compressor cascades are given. The effects of flow parameters on the dynamic behavior of the solid particles throughout the compressor one and one-half stage are investigated. Parameters considered included particle mean diameter and material density, initial particle and gas velocities at the guide vane inlet, and compressor rotor rotational speed. Observations concerning the erosion damage to the blades of the compressor cascades are also discussed.</p>			
Key Words:			
Compressor Two-Phase Flow Trajectories			

DD FORM 1473
1 NOV 65FORM 1473 USE PREVIOUS EDITIONS 1 JAN 64, WHICH IS
OF GLENN T.O. 1-A MAY 64.

Unclassified

Security Classification

I-a

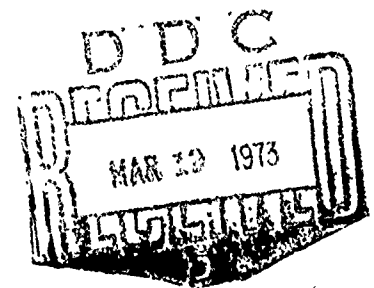
AD-757/62

PROJECT THEMIS REPORT NO. 73-34

**CALCULATION OF THE THREE DIMENSIONAL
PARTICLE TRAJECTORIES IN A ONE AND
ONE-HALF STAGE OF A COMPRESSOR**

M. Fathy Hussein and W. Tabakoff

February 1973



**Approved for public release; distribution
unlimited.**

**This work was supported by the U.S. Army
Research Office - Durham under Project
Themis Contract Number DAHC04-69-C-0016.**

**Reproduced by
NATIONAL TECHNICAL
INFORMATION SERVICE
U S Department of Commerce
Springfield VA 22151**

DEPARTMENT OF AEROSPACE ENGINEERING

University of Cincinnati, Cincinnati, Ohio 45221

TABLE OF CONTENTS

	<u>Page</u>
LIST OF ILLUSTRATIONS.	ii
NOMENCLATURE	ix
ABSTRACT	xii
INTRODUCTION	1
Equations of Motion of Solid Particles Suspended by the Gas Flow in a Rotating Cascade.	2
PARTICLES DYNAMIC BEHAVIOR IN A ONE AND ONE-HALF STAGE OF A COMPRESSOR.	6
Effect of Particles Mean Diameter on Their Dynamic Behavior.	7
Effect of Particles Material Density on Their Dynamic Behavior.	8
Effect of Particles and Gas Initial Velocities on Particles Dynamic Behavior.	8
Effect of Compressor Rotor Rotational Speed on the Dynamic Behavior of the Solid Particles (Compressor Off-Design Conditions	8
CONCLUSION	10
REFERENCES	11

LIST OF ILLUSTRATIONS

<u>Figure</u>		<u>Page</u>
1	12
2	12
3	13
4	Nondimensional Angle of Rebound	14
5	Drop in Particle Relative Velocity Due to Collision (Restitution Ratio)	14
6	Compressor Stage Dimensions	15
7	Combined Gas Velocity Diagram (Compressor Stage)	15
8	Mesh Points for Compressor Blading.	16
9	Axial and Tangential Components of Particle Trajectories	17
10	Axial and Tangential Components of Particle Trajectories Relative to the Rotor Blades.	17
11	Axial and Radial Components of Particle Trajectories.	18
12	Particle Nondimensional Absolute Velocities	18
13	Axial and Tangential Components of Particle Trajectories	19
14	Axial and Tangential Components of Particle Tra- jectories Relative to the Rotor Blades.	19
15	Axial and Radial Components of Particle Trajectories.	20
16	Particle Nondimensional Absolute Velocities	20
17	Axial and Tangential Components of Particle Trajectories.	21
18	Axial and Tangential Components of Particle Trajector- ies Relative to the Rotor Blades.	21
19	Axial and Radial Components of Particle Trajectories.	22
20	Particle Nondimensional Absolute Velocities	22
21	Axial and Tangential Components of Particle Trajectories.	23
22	Axial and Tangential Components of Particle Trajectories Relative to the Rotor Blades	23
23	Axial and Radial Components of Particle Trajectories.	24
24	Particle Nondimensional Absolute Velocities	24
25	Axial and Tangential Components of Particle Trajectories (Effect of d_p)	25
26	Axial and Tangential Components of Particle Trajector- ies Relative to the Rotor Blades (Effect of d_p)	25

<u>Figure</u>		<u>Page</u>
27	Axial and Radial Components of Particle Trajectories.	26
28	Particle Nondimensional Absolute Velocities (Effect of d_p).	26
29	Particle Velocity Diagram	26
30	Axial and Tangential Components of Particle Trajectories (Effect of d_p)	27
31	Axial and Tangential Components of Particle Trajectories Relative to the Rotor Blades (Effect of d_p).	27
32	Axial and Radial Components of Particle Trajectories.	28
33	Particle Nondimensional Absolute Velocities (Effect of d_p).	28
34	Particle Velocity Diagram	28
35	Axial and Tangential Components of Particle Trajectories (Effect of d_p)	29
36	Axial and Tangential Components of Particle Trajectories Relative to the Rotor Blades (Effect of d_p).	29
37	Axial and Radial Components of Particle Trajectories.	30
38	Particle Nondimensional Absolute Velocities (Effect of d_p).	30
39	Particle Velocity Diagram	30
40	Axial and Tangential Components of Particle Trajectories (Effect of d_p)	31
41	Axial and Tangential Components of Particle Trajectories Relative to the Rotor Blades (Effect of d_p).	31
42	Axial and Radial Components of Particle Trajectories.	32
43	Particle Nondimensional Absolute Velocities (Effect of d_p).	32
44	Particle Velocity Diagram	32
45	Axial and Tangential Components of Particle Trajectories (Effect of ρ_p)	33
46	Axial and Tangential Components of Particle Trajectories Relative to the Rotor Blades (Effect of ρ_p).	33
47	Axial and Radial Components of Particle Trajectories.	34

<u>Figure</u>		<u>Page</u>
48	Particle Nondimensional Absolute Velocities (Effect of ρ_p)	34
49	Axial and Tangential Components of Particle Trajectories (Effect of ρ_p)	35
50	Axial and Tangential Components of Particle Trajectories Relative to the Rotor Blades (Effect of ρ_p)	35
51	Axial and Radial Components of Particle Trajectories.	36
52	Particle Nondimensional Absolute Velocities (Effect of ρ_p)	36
53	Axial and Tangential Components of Particle Trajectories (Effect of ρ_p)	37
54	Axial and Tangential Components of Particle Trajectories Relative to the Rotor Blades (Effect of ρ_p)	37
55	Axial and Radial Components of Particle Trajectories.	38
56	Particle Nondimensional Absolute Velocities (Effect of ρ_p)	38
57	Axial and Tangential Components of Particle Trajectories (Effect of ρ_p)	39
58	Axial and Tangential Components of Particle Trajectories Relative to the Rotor Blades (Effect of ρ_p)	39
59	Axial and Radial Components of Particle Trajectories.	40
60	Particle Nondimensional Absolute Velocities (Effect of ρ_p)	40
61	Axial and Tangential Components of Particle Trajectories (Effect of C_{p_i}/C_{g_i})	41
62	Axial and Tangential Components of Particle Trajectories Relative to the Rotor Blades (Effect of C_{p_i}/C_{g_i})	41
63	Axial and Radial Components of Particle Trajectories.	42
64	Particle Nondimensional Absolute Velocities (Effect of C_{p_i}/C_{g_i})	42
65	Axial and Tangential Components of Particle Trajectories (Effect of C_{p_i}/C_{g_i})	43
66	Axial and Tangential Components of Particle Trajectories Relative to the Rotor Blades (Effect of C_{p_i}/C_{g_i})	43

<u>Figure</u>		<u>Page</u>
67	Axial and Radial Components of Particle Trajectories.	44
68	Particle Nondimensional Absolute Velocities (Effect of C_{p_i}/C_{g_i})	44
69	Axial and Tangential Components of Particle Trajectories (Effect of C_{p_i}/C_{g_i})	45
70	Axial and Tangential Components of Particle Trajectories Relative to the Rotor Blades (Effect of C_{p_i}/C_{g_i})	45
71	Axial and Radial Components of Particle Trajectories.	46
72	Particle Nondimensional Absolute Velocities (Effect of C_{p_i}/C_{g_i})	46
73	Axial and Tangential Components of Particle Trajectories (Effect of C_{p_i}/C_{g_i})	47
74	Axial and Tangential Components of Particle Trajectories Relative to the Rotor Blades (Effect of C_{p_i}/C_{g_i})	47
75	Axial and Radial Components of Particle Trajectories.	48
76	Particle Nondimensional Absolute Velocities (Effect of C_{p_i}/C_{g_i})	48
77	Combined Gas Velocity Diagram for Design and Off-Design Blade Angular Velocity (Compressor Stage).	49
78	Axial and Tangential Components of Particle Trajectories (Effect of ω/ω_d)	50
79	Axial and Tangential Components of Particle Trajectories Relative to the Rotor Blades (Effect of ω/ω_d)	50
80	Axial and Radial Components of Particle Trajectories.	51
81	Particle Nondimensional Absolute Velocities (Effect of ω/ω_d)	51
82	Axial and Tangential Components of Particle Trajectories (Effect of ω/ω_d)	52
83	Axial and Tangential Components of Particle Trajectories Relative to the Rotor Blades (Effect of ω/ω_d)	52
84	Axial and Radial Components of Particle Trajectories.	53
85	Particle Nondimensional Absolute Velocities (Effect of ω/ω_d)	53

<u>Figure</u>		<u>Page</u>
86	Axial and Tangential Components of Particle Trajectories (Effect of ω/ω_d)	54
87	Axial and Tangential Components of Particle Trajectories Relative to the Rotor Blades (Effect of ω/ω_d)	54
88	Axial and Radial Components of Particle Trajectories.	55
89	Particle Nondimensional Absolute Velocities (Effect of ω/ω_d)	55
90	Axial and Tangential Components of Particle Trajectories (Effect of ω/ω_d)	56
91	Axial and Tangential Components of Particle Trajectories Relative to the Rotor Blades (Effect of ω/ω_d)	56
92	Axial and Radial Components of Particle Trajectories.	57
93	Particle Nondimensional Absolute Velocities (Effect of ω/ω_d)	57
94	Axial and Tangential Components of Particle Trajectories (Effect of ω/ω_d)	58
95	Axial and Tangential Components of Particle Trajectories Relative to the Rotor Blades (Effect of ω/ω_d)	58
96	Axial and Radial Components of Particle Trajectories.	59
97	Particle Nondimensional Absolute Velocities (Effect of ω/ω_d)	59
98	Axial and Tangential Components of Particle Trajectories (Effect of ω/ω_d)	60
99	Axial and Tangential Components of Particle Trajectories Relative to the Rotor Blades (Effect of ω/ω_d)	60
100	Axial and Radial Components of Particle Trajectories.	61
101	Particle Nondimensional Absolute Velocities (Effect of ω/ω_d)	61
102	Axial and Tangential Components of Particle Trajectories Relative to the Rotor Blades (Effect of ω/ω_d)	62
103	Axial and Tangential Components of Particle Trajectories (Effect of ω/ω_d)	62
104	Axial and Radial Components of Particle Trajectories.	63

<u>Figure</u>		<u>Page</u>
105	Particle Nondimensional Absolute Velocities (Effect of ω/ω_d)	63
106	Axial and Tangential Component of Particle Trajectories (Effect of ω/ω_d)	64
107	Axial and Tangential Components of Particle Trajectories Relative to the Rotor Blades (Effect of ω/ω_d)	64
108	Axial and Radial Components of Particle Trajectories.	65
109	Particle Nondimensional Absolute Velocities (Effect of ω/ω_d)	65
110	Axial and Tangential Components of Particle Trajectories (Effect of ω/ω_d)	66
111	Axial and Tangential Components of Particle Trajectories Relative to the Rotor Blades (Effect of ω/ω_d)	66
112	Axial and Radial Components of Particle Trajectories.	67
113	Particle Nondimensional Absolute Velocities (Effect of ω/ω_d)	67
114	Axial and Tangential Components of Particle Trajectories (Effect of ω/ω_d)	68
115	Axial and Tangential Components of Particle Trajectories Relative to the Rotor Blades (Effect of ω/ω_d)	68
116	Axial and Radial Components of Particle Trajectories.	69
117	Particle Nondimensional Absolute Velocities (Effect of ω/ω_d)	69
118	Axial and Tangential Components of Particle Trajectories (Effect of ω/ω_d)	70
119	Axial and Tangential Components of Particle Trajectories Relative to the Rotor Blades (Effect of ω/ω_d)	70
120	Axial and Radial Components of Particle Trajectories.	71
121	Particle Nondimensional Absolute Velocities (Effect of ω/ω_d)	71
122	Axial and Tangential Components of Particle Trajectories (Effect of ω/ω_d)	72
123	Axial and Tangential Components of Particle Trajectories Relative to the Rotor Blades (Effect of ω/ω_d)	72

<u>Figure</u>		<u>Page</u>
124	Axial and Radial Components of Particle Trajectories.	73
125	Particle Nondimensional Absolute Velocities (Effect of ω/ω_d)	73
126	Axial and Tangential Components of Particle Trajectories (Effect of ω/ω_d)	74
127	Axial and Tangential Components of Particle Trajectories Relative to the Rotor Blades (Effect of ω/ω_d)	74
128	Axial and Radial Components of Particle Trajectories.	75
129	Particle Nondimensional Absolute Velocities (Effect of ω/ω_d)	75
130	Axial and Tangential Components of Particle Trajectories (Effect of ω/ω_d)	76
131	Axial and Tangential Components of Particle Trajectories Relative to the Rotor Blades (Effect of ω/ω_d)	76
132	Axial and Radial Components of Particle Trajectories.	77
133	Particle Nondimensional Absolute Velocities (Effect of ω/ω_d)	77
134	Axial and Tangential Components of Particle Trajectories (Effect of ω/ω_d)	78
1351	Axial and Tangential Components of Particle Trajectories Relative to the Rotor Blades (Effect of ω/ω_d)	78
136	Axial and Radial Components of Particle Trajectories.	79
137	Particle Nondimensional Absolute Velocities (Effect of ω/ω_d)	79
138	Axial and Tangential Components of Particle Trajectories (Effect of ω/ω_d)	80
139	Axial and Tangential Components of Particle Trajectories Relative to the Rotor Blades (Effect of ω/ω_d)	80
140	Axial and Radial Components of Particle Trajectories.	81
141	Particle Nondimensional Absolute Velocities (Effect of ω/ω_d)	81

NOMENCLATURE

B	frame fixed in blades (Figure 1)
B_o	origin of the frame B (Figure 3)
β	angle between particle relative velocity and tangent to surface
C_g	absolute gas velocity
C_p	absolute particle velocity
C'_g	gas absolute velocity component in the x, θ plane
C'_p	particles absolute velocity component in the x, θ plane
C_{Pg}	specific heat of gas at constant pressure
ψ	modified stream function (Equation (13))
d_p	particle mean diameter
Δx	spacing between adjacent points in the meridional direction Figure 8
$\Delta \theta$	spacing between adjacent points in the tangential direction Figure 8
Δt	increment of time
E	frame fixed in the engine (Figure 1)
E_o	origin of E (Figure 1)
G	coefficient inversely proportional with the particle characteristics time (Equation (4))
$g(Re)$	Reynolds number dependent function (Equation (5))
h	normal stream channel thickness (blade height) (Figure 2)
λ	angle between meridional streamline and engine axis
μ_g	gas viscosity
$\bar{n}_1, \bar{n}_2, \bar{n}_3$	unit vectors in the direction of the coordinate curves x, θ, z
$\bar{N}_1, \bar{N}_2, \bar{N}_3$	unit vectors in the direction of the axes X, Y, Z
p	pressure at a point
R	blade mean radius (Figures 1 and 2)

Re	Reynolds number (Equation (10))
r	radius from axis of rotation (Equation (12))
ρ_g	gas density
$\bar{\rho}_p$	particle material density
T_g	gas temperature
U	blade speed at the mean radius (Figure 7)
u_g	gas relative velocity component in the x-direction
v_g	gas relative velocity
v_p	particle relative velocity
v'_g	gas relative velocity component in the x, θ plane
v'_p	particle relative velocity component in the x, θ plane
v_g	gas relative velocity component in the tangential direction
W	weight flow rate of mixture per channel
w_p	particle relative velocity component in the radial direction
ω	blade angular velocity
x, θ, z	coordinate axis in the meridional, tangential and radial direction, fixed in B (Figures 1 and 2)
X, Y, Z	axes fixed in engine (Figures 1 and 2)
$\dot{x}, \dot{\theta}, \dot{z}$	particle velocity components measured in B
$\ddot{x}, \ddot{\theta}, \ddot{z}$	particle acceleration components measured in B
$\dot{X}, \dot{Y}, \dot{Z}$	absolute velocity measured in E
$\ddot{X}, \ddot{Y}, \ddot{Z}$	absolute acceleration measured in E
y	distance measured along the tangential direction

Subscripts

a	absolute trajectory
g	gas
i	initial conditions at particles entrance
in	conditions at the boundary AH (Figure 14)

n	normal to surface
o	total conditions
out	after cascade
p	particle
t	tangent to surface
1	before collision
2	after collision

INTRODUCTION

In modern gas turbine engines, solid particles entrained by the gas flow passing through the channels of the compressor impinge with the compressor blades and cause their erosion. The study of the dynamic behavior of the solid particles is important to further understand the blade erosion phenomenon. The fundamental equations, in three dimensions, that govern the motion of the solid particles suspended by the gas flow in a cascade of a turbomachine are given by the authors in References 1 and 2 for the cases of stationary and rotating cascades, respectively. These fundamental equations are solved for the case of particle motion in turbines in Reference 2. Due to the difference in geometry and the function of turbines and compressors, the dynamic behavior of the solid particles in compressor cascades are expected to be different from that for a turbine. In this investigation the solid particles equations of motion of Reference 2 are solved to determine the dynamic behavior of the solid particles in a one and one-half stage of a compressor. The particles are taken to enter the compressor guide vanes uniformly. The compressor cascade pitch, mean radius and speed of rotation of the rotor are taken the same as those for the turbine example of Reference 2, in order to show the fundamental difference in the dynamic characteristics of the solid particles in compressors and turbines. The particles are assumed to be spheres of constant average mean diameter, uniform material density, and small in size. The forces acting on the solid particles causing their motion in the gas flow are assumed to be mainly the drag forces that the gas exerts on them. It is further assumed that the presence of the solid particles in the flow does not alter the gas properties from that for the nonparticulate gas flow passing through the same cascade. This assumption is valid for small particle concentrations and high particle material densities.

The computer program given by the authors in Reference 3 is used to compute and plot the particle dynamic behavior, namely, the particle absolute and relative three dimensional paths, their velocity distributions, and overall velocity diagrams. The results of the investigation of the impact and rebound phenomenon of the solid particles with the blades given in Reference 1 gives the restitution and rebound to incidence angle ratios of the particles. These ratios define the particle condition after impact and are used in solving the equations of motion of the solid particles in the compressor. Particle collision and rebound from both compressor blades and casing are considered. The gas properties anywhere in the cascade channel are calculated by solving the fundamental equations of motion for a gas in a cascade.

The equations of motion of the particles are formulated with respect to axes fixed in the blades at the entrance of the cascade row. With the impact and rebound phenomenon well described, and the drag coefficient and gas properties known, the equations of motion of the particles may be solved. One row of blades is considered at a time. The particles enter the row with known initial conditions, hit the walls and rebound (perhaps several times), until they leave the nozzle. The particles outlet conditions constitute the initial condition for the successive row. The equations of motion of the particles with respect to a new frame of axes using the known initial conditions are then solved using the corresponding gas properties in the new cascade row and so on. The particles positions

may be referred to the initial axes by a simple transformation. Repeated solution of equations of motion of the particles for all successive cascade rows gives the particles dynamic behavior through the compressor stages. This study showed the effects of the flow main parameters such as the particles mean diameter, solid particles material density, particle and gas initial velocities, and compressor rotor rotational speed on the dynamic behavior of the solid particles.

Examination of the particles trajectories showed the areas on the blades of the compressor guide vanes, both rotor and stator, which are subjected to more particle impacts. This made it possible to predict the blades portions that are likely to erode and predict solutions to minimize blade erosion.

Equations of Motion of Solid Particles Suspended By the Gas Flow in a Rotating Cascade

Referring to Figure 1 and Figure 2, the frame B, is fixed in an arbitrary blade of the rotating cascade with \bar{i}_1 , \bar{n}_2 , and \bar{n}_3 a set of nonparallel, noncoplaner, right-handed unit vectors in the direction of the coordinate curves x , θ and z , respectively. The point B_0 is the origin of the frame B, which is taken at the intersection of the plane tangent to the blade row at the entrance and the blade axial chord in the mid-stream surface of revolution of radius R that passes through the middle of the blade height. The coordinate curves, x , θ and z are in the axial or meridional direction, the tangential, and the radial directions, respectively. Further, it is assumed that the frame B, fixed in the blade row, moves with a constant angular velocity ω , equal to the angular speed of the rotor in a reference frame E fixed in the engine. In the reference frame E, \bar{N}_1 , \bar{N}_2 and \bar{N}_3 are unit vectors in the direction of the mutually perpendicular set of axes X , Y and Z , and are fixed in the engine at a point E_0 . Point E_0 is the intersection of the engine axis with the plane tangent to the blade row at the entrance. The coordinate axis X is in the axial direction, while Y and Z are axes normal to the X axis in the plane tangent to the blade row at the entrance, as shown in Figures 1 and 2.

Referring to Figure 3, the coordinate curves x , θ and z , that rotate with an angular velocity ω , after a time t , are at an angle equal to ωt from the Z axis. The particle p is at any arbitrary position x , θ and z measured from B_0 . According to Newton's laws of motion using a proper transformation between the relative and fixed frames, it is shown (Reference 2) that the three dimensional equations of motion of the solid particles entrained by the gas flow in a rotating cascade are

$$\ddot{\mathbf{x}} = G(\mathbf{u}_g - \dot{\mathbf{x}}) \quad (1)$$

$$\ddot{\theta} = \frac{G}{(R+z)} [\mathbf{v}_g - (R+z)\dot{\theta}] - \frac{2\dot{z}}{(R+z)} (\dot{\theta} + \omega) \quad (2)$$

$$\ddot{z} = -G \dot{z} + (R + z) (\dot{\theta} + \omega)^2 \quad (3)$$

where u_g and v_g are the gas relative velocity components in the axial and tangential directions. Also, x, θ, z and $\dot{x}, \dot{\theta}, \dot{z}$ and $\ddot{x}, \ddot{\theta}, \ddot{z}$ are the particles coordinate curves, velocity and acceleration components in the axial, tangential and radial directions, respectively, measured in the relative frame B. It may be noted that the second term in the right hand side of Equation (2) represents the Coriolis acceleration, while the second term in the right hand side of Equation (3) represents the centrifugal accelerations of a particle moving in curved path in the rotating frame B.

The coefficient G in Equations (1), (2) and (3), which is inversely proportional to particle characteristic time, is given by

$$G = \frac{18 \mu_g}{d_p^2 \frac{\rho_g}{\rho_p}} g(Re) \quad (4)$$

In Equation (4), the Reynolds number dependent function $g(Re)$ is a correction factor to the drag force formula given by Stokes for spherical particles moving at a very small Reynolds number in a gas flow (Reference 1). This function is given by:

$$g(Re) = C_D \frac{Re}{24} = \frac{C_D}{C_{D_0}} \quad (5)$$

where C_{D_0} is the Stokes drag coefficient, and

C_D is the drag coefficient for spherical particle at any Reynolds number.

From Reference 1, this drag coefficient is given by

$$C_D = \frac{24}{Re} \quad 0 < Re \leq 1 \quad (6)$$

$$C_D = \frac{24}{Re} \left(1 + \frac{3}{16} Re\right) \quad 1 \leq Re \leq 4 \quad (7)$$

$$C_D = 21.9416 Re^{-0.718} + 0.3240 \quad 4 \leq Re \leq 2000 \quad (8)$$

$$C_D = 0.4 \quad 2000 \leq Re \leq 3 \times 10^4 \quad (9)$$

The Reynolds number given in Equations (6), (7), (8), and (9) is defined as:

$$Re = \frac{d_p \rho_g}{\mu_g} \sqrt{(u_g - \dot{x})^2 + [v_g - \dot{\theta}(R+z)]^2 + \dot{z}^2} \quad (10)$$

The distance y that a particle travels in the θ direction on the surface of revolution with radius $(R+z)$ is given as a function of the particle relative position vector components z and θ and the cascade mean radius R as

$$y = (R+z)\theta \quad (11)$$

The gas relative velocity components u_g and v_g in Equations (1), (2), and (3) can be computed at every mesh point of a square grid constructed in the cascade channel by solving the gas equations of motion give in Reference 2. The gas equations of motion are:

Combined Momentum and Continuity Equations

$$\begin{aligned} \frac{\partial^2 \psi}{\partial x^2} + \frac{1}{r^2} \frac{\partial^2 \psi}{\partial \theta^2} + \left[\frac{\sin \lambda}{r} - \frac{1}{h \rho_g} \frac{\partial(h \rho_g)}{\partial x} \right] \frac{\partial \psi}{\partial x} \\ - \frac{1}{r^2 \rho_g} \frac{\partial \rho_g}{\partial \theta} \frac{\partial \psi}{\partial \theta} = \frac{2h \rho_g}{W} \omega \sin \lambda \end{aligned} \quad (12)$$

where ψ is a form of the stream function give by

$$\begin{aligned} u_g &= \frac{W}{rh \rho_g} \frac{\partial \psi}{\partial \theta} \\ v_g &= - \frac{W}{h \rho_g} \frac{\partial \psi}{\partial x} \end{aligned} \quad (13)$$

the combined energy and state equation is

$$\frac{\rho_g}{\rho_{g,in}} = \left[1 - \frac{\frac{1}{\gamma-1} |\bar{C}_g|^2}{2 C_{p_g} T_{g,in}} \right] \quad (14)$$

Discussion of the numerical solution of Equations (12), (13) and (14) is reported in Reference 3.

The particle velocity and direction after impact are determined experimentally (Reference 4) for corn cups particles and steel blades. The restitution ratio is shown in Figure 4 while the rebound to incidence angle ratio is given in Figure 5. The restitution ratio data is

represented by the dotted line in Figure 4 and give by the expression:

$$\frac{V_{P2}}{V_{P1}} = \frac{V_{Pn2}}{V_{Pn1}} \cdot \sqrt{\frac{1 + \cot^2 \beta_2}{1 + \cot^2 \beta_1}} \quad (15)$$

also the dotted line in Figure 5 represents the rebound to incidence angle ratio as,

$$\frac{\beta_2}{\beta_1} = \frac{1}{\beta_1} \cot^{-1} \left[\left(\frac{V_{Pt2}}{V_{Pt1}} \cdot \frac{V_{Pn1}}{V_{Pn2}} \right) \cdot \cot \beta_1 \right] \quad (16)$$

In Equations (15) and (16) the ratio between the particle relative velocity components tangent and normal to the blade surface after and before collision [1] are given, respectively, by the equations:

$$V_{Pt2}/V_{Pt1} = 0.95 + 0.00055 \beta_1 \quad (17)$$

$$V_{Pn2}/V_{Pn1} = 1.0 - 0.02108 \beta_1 + 0.0001417 \beta_1^2 \quad (18)$$

Equations (1), (2), and (3) may be solved numerically for every particle entering the cascade in increments of time if the initial conditions are known. The time increment may have a constant value as long as it does not take the particle beyond the walls, thus, at the regular increment nearest the wall the time increment has to be iterated to the exact value that is necessary for the particle to just hit the wall. Solution of the general system of equations of the type of Equations (1), (2), and (3) and a discussion of errors are given in Reference 3. The solution of the particle equations of motion utilizes Equations (6) through (9) to compute the coefficient G of Equation (4), the solution of Equations (12), (13), and (14) to yield the gas properties, and Equations (15) through (18) to give the particle conditions after rebound that can be used as the new initial conditions at the points of discontinuity.

The solution of the equations of motion of the particles, Equations (1), (2), and (3) gives the relative and absolute locations as well as the velocity components of a particle in the rotating cascade row. Successive solution of these equations for every cascade row will give the particles paths throughout the compressor. The computer program of Reference 3 uses the IBM 1130 and the Calcomp plotter to draw the particle trajectories and velocities in the compressor.

PARTICLES DYNAMIC BEHAVIOR IN ONE AND
ONE-HALF STAGE OF A COMPRESSOR

The dimensions of the compressor guide vanes, the rotor, and the stator that constitute the one and one-half stage of a compressor are given in Figure 6. The cascade pitch equals 1.295 inch, the cascade mean radius $R = 7.05$ inches and the cascade height equals 1.5 inch. The diameter of the compressor is taken relatively small so that the centrifugal effects on the particles are pronounced and also in order to give a more general particle path. Reference 5 gives the airfoil data. The rotor blades are assumed to be at the position shown in Figure 6 when the particle is at the guide vane exit. The combined gas velocity diagram for a compressor stage of 43.8% degree of reaction is given in Figure 7. The mesh distribution is shown in Figure 8. The gas conditions at the compressor guide vanes inlet are: gas initial₃ velocity $C_{gi} = 142.64$ ft/sec, initial gas density $\rho_{gin} = 0.076$ lb/ft³, initial gas total temperature $T_{gin} = 60^\circ\text{F}$, and the total mass flow rate per channel $W = 0.123$ lb/sec. The particles enter at the stream surface of revolution of radius 7.05 inches. The cascade design angular speed at the mid-radius R is taken to be $\omega_d = 603.5$ radians per second, which is equivalent to a mid-radius blade velocity of 352.5 ft/sec. The compressor cascade pitch, the design speed of rotation, the radius of the mean surface of revolution, the total flow rate per channel as well as the gas initial condition at inlet to the guide vanes, are taken equal to those of the turbine stage example of Reference 2 in order to notice the fundamental differences between the particle dynamic behavior in turbines and compressors.

A general idea about the dynamic behavior of the solid particles in the given one and one-half compressor stage may be obtained from the figures that give the absolute and relative trajectories, the radial displacement and nondimensional absolute velocity distribution throughout the compressor blades, Figures 9 through 24. These results are given in groups of four figures, each giving the dynamic behavior of twelve particles entering the compressor guide vanes with a uniform speed equal to 30 percent of the gas inlet velocity at a distance upstream of the compressor guide vanes leading edge. These four groups of figures are for particles with mean diameters equal to 1000, 200, 40 and 8 microns, respectively. They all have material density of 68.7 lb/ft³ and $C_{pi}/C_{gi} = 0.3$. In order to show the effect of the particle collision with the guide vanes leading edge, the distance between particles number 1 and 2 and 11 and 12 is taken smaller, due to the smaller leading edge radius of compressor blades as compared to those for turbine blades [2]. The particles are categorized in four different patterns, such as particles number 2, 5, 8 and 11, according to their trajectories in the guide vanes. Figures 9, 13, 17 and 21 show the projection of the particle absolute trajectories y_a versus x in the $x-\theta$ surface. Figures 10, 14, 18 and 22 give particle trajectories relative to the rotor. The particles with smaller d_p tend to follow more closely the gas streamlines in the guide vanes, move close together and become less scattered in the rotor and stator. Larger diameter particles,

however, do not enter the opposite blade channel but scatter in the successive rotor channels (Figures 10 and 22). Unlike the turbine stage example [2], the particles with large diameters of 1000 and 200 microns, do not return to the guide vanes after hitting the compressor rotor. This is a result of the difference in the stage geometry and blade leading edge radius. Since the radial displacement of the particles increase with increased mean diameter (Figures 11, 15, 19, and 23), larger particles tend to reach the casing of the compressor before leaving the one and one-half stage. The particles absolute velocities, nondimensionalized with respect to gas velocity at the inlet to the guide vanes, are given in Figures 12, 16, 20, and 24. Less abrupt changes in the value of the velocity are observed for particles with smaller d_p , but they are more influenced by the changes in gas velocity, especially near the blade surface (Figures 12 and 24). Smaller particles move with higher initial accelerations in the guide vanes. The particle velocity approximately reaches a constant value in the rotor. The higher particle velocities in the rotor indicate that the rotor blades can suffer from severe erosion.

Observations concerning blade erosion may be summarized from Figures 9 through 24. In general, compressor guide vanes and rotor blades may suffer leading edge erosion due to the impingement of all size particles. The pressure side of the guide vanes blade, however, will primarily suffer erosion by particles with higher d_p , since they follow trajectories further from the gas streamlines. As for the compressor rotor, particles of higher d_p tend to hit the lower part of the leading edge, and as d_p decreases the particles are shown to hit at the first half of the rotor pressure side. Less collisions are observed with the rotor blades for particles with $d_p = 8$ microns. This indicates that the first half of the pressure side of the compressor rotor will be eroded severely. The trajectories also show that the pressure side of the compressor stator will be subjected to erosion damage due to the impingement of particles of all sizes. Only particles with higher d_p will cause stator blade leading edge erosion. The blade suction sides will suffer no erosion damage in any cascade row since no particle collisions are observed there. The radial displacement of the particles will cause them to travel toward the blade tip, and after a few stages the blade tips will be eroded by the impingements of all the particles that enter the nozzle at all radii. Erosion of sections closer to the hub is less severe (Reference 6).

Effect of Particles Mean Diameter on Their Dynamic Behavior

The effect of d_p on the dynamic behavior of the four typical particles, namely, particles number 2, 5, 8 and 11 is shown in four groups of five figures each, Figures 25 through 44. Each group of figures consists of the absolute and relative projected particle paths in the stream surface of revolution, its radial displacement, and its nondimensional particle absolute velocity distributions in the one and one-half stage of the compressor. The figures also include particle combined velocity diagrams compared to the gas velocity diagram at the design point. The particles mean diameter takes the values 1000, 200,

40 and 8 microns with constant $\bar{\rho}_p = 68.7 \text{ lb/ft}^3$ and $C_{p_i}/C_{g_i} = 0.3$.

Figures 29, 34, 39 and 44 show the deviation of the particle velocity diagram from that of the gas decreases as d_p decreases. The diagrams give the overall particle velocity at the inlet and the exit of the compressor's first two rows. Similar observations to those given in the preceeding paragraph concerning the effects of varying the particle mean diameter on the particles dynamic behavior may be noticed from Figures 25 through 44.

Effect of Particles Material Density on Their Dynamic Behavior

Figures 45 through 60, illustrate the effect on the particle dynamic behavior for the four typical particles to the changes in $\bar{\rho}_p$. The particle material density, $\bar{\rho}_p$, takes the values of 34, 68.7 and 151 lb/ft^3 , d_p and C_{p_i}/C_{g_i} have constant values of 40 microns and 0.3, respectively. A decrease in $\bar{\rho}_p$ causes less deviation of particle motion from gas streamlines, earlier impingements with the rotor pressure side, and lower velocities in the stator.

Effect of Particles and Gas Initial Velocities on Particles Dynamic Behavior

The effect of changing C_{p_i}/C_{g_i} on the particle dynamic behavior is shown in Figures 61 through 76. Small effects are observed on the particle trajectories, especially the radial displacement component, due to changing C_{p_i}/C_{g_i} . The four typical particles show that the particle velocities tend to reach the same value at the exit from the guide vanes for different C_{p_i}/C_{g_i} . In Figures 61 through 76, C_{p_i}/C_{g_i} take the values 0.15, 0.3 and 0.6, while d_p and $\bar{\rho}_p$ have the constant values; 40 microns and 68.7 lb/ft^3 , respectively.

The effects on the particle dynamic behavior of increasing the gas speed at the inlet to the guide vanes for a certain particle inlet velocity is similar to the effects of decreasing C_{p_i}/C_{g_i} . The particle diameter has the greatest effect on the particle dynamic behavior, while $\bar{\rho}_p$ has a greater effect than C_{p_i}/C_{g_i} .

Effect of Compressor Rotor Rotational Speed on the Dynamic Behavior of the Solid Particles (Compressor Off-Design Conditions)

The combined velocity diagrams for the compressor guide vanes and rotor for different blade rotational speeds are shown in Figure 77. The particular case of the rotor angular velocity equal to 0.8

times its design value is termed the negative off-design condition. Likewise, the positive design condition is the case for which $\omega/\omega_d = 1.2$. Table 1 gives the conditions of gas and particle inlet velocity for the design, negative, and positive off-design conditions. In Table 1, ω/ω_d is the ratio between blade rotational speed at any off-design flow condition and that at design condition, and C_{gi} is the gas velocity at the guide vane inlet.

The effect of ω/ω_d on the dynamic behavior of the solid particles having 1000 microns mean diameter for the four typical particles is shown in groups of four figures each, in Figures 78 through 93. Similar groups of figures for $d_p = 200, 40$ and 8 microns are given in Figures 94 to 109, 110 to 125, and 126 to 141, respectively.

From the above mentioned figures the following observations may be made. The paths of the large particles do not change in the guide vanes with changing ω/ω_d (Figure 78). As the particle mean diameter decreases, slight deviation in the trajectories of particles in the guide vanes is observed (Figure 126). In general, a particle with $d_p = 1000$ microns would enter a different rotor nozzle if ω/ω_d is changed, Figure 79. As d_p decreases the particles tend to enter the same rotor nozzle irrespective of the value of ω/ω_d (Figure 127). The radial displacement does not change with ω/ω_d in the guide vanes. In the rotor, the radial displacement depends to a great extent on particle displacement in the tangential direction, which determines the initial place of collision with the rotor blade (Figures 100 and 104). For particles of all mean diameters, the particle velocity increases more for higher ω/ω_d (Figures 81 and 129). It may be concluded that the change in ω/ω_d causes slight changes in the places of collisions, but the general pattern of the trajectories are maintained. The areas of the blades suffering from erosion damage will remain the same as in the design conditions.

CONCLUSION

The three dimensional dynamic behavior of solid particles entrained by the compressible gas flow in a one and one-half stage of a compressor is determined. The drag forces on the particles are calculated using drag formulas that fit the drag curve of a spherical particle over the practical range of application of the Reynolds numbers. The compressible gas flow properties are computed by solving numerically the gas equations of motion in a blade to blade surface of revolution of a rotating cascade. Experimental investigation is made to study the impact and rebound phenomenon of the particles from the walls, to determine formulas for the restitution ratio, and rebound to incidence angle ratio. These formulas define the particle conditions after collision which are then used to continue the solution of the equations of motion for the particles. These formulas have to be determined experimentally for every particle-target material combination once the turbomachine operating condition is known.

The study showed that in general, solid particle paths are deviated from gas streamlines. This deviation increases with increased particle mean diameter, material density, particle initial velocity or decreased initial gas velocity. The particle mean diameter has the greatest effect on the dynamic behavior of the particles, while the particle material density has a lesser effect and the particle initial velocity has the least effect. Changing rotational speed of the cascade does not effect either the patterns of the trajectories of the particles or the cascade eroded parts.

The compressor stator and rotor will be eroded from the leading edges and pressure sides, especially due to impacts of bigger particles. The study shows that particles tend to displace radially, especially in the rotors, as they move through the compressor. After a few stages the particles will be moving at the tip stream surface of revolution causing severe damage to blade tips and less erosion to blade sections further from the tips.

Turbomachines may be designed to both minimize erosion as well as optimizing aerodynamic characteristics using the results of this investigation. Means may be introduced to collect or deviate some of the particles, especially those that contribute most to erosion, away from the blades, and hence, reduce their erosion damage.

REFERENCES

1. Hussein, M. Fathy, and Tabakoff, W. "Calculations of Particle Trajectories in a Stationary Two-Dimensional Cascade," Project Themis Report No. 72-27, University of Cincinnati, Cincinnati, Ohio, June 1972.
2. Hussein, M. Fathy and Tabakoff, W., "Calculation of the Three-Dimensional Particle Trajectories in a Turbine Stage," Project Themis Report No. 72-33, University of Cincinnati, Cincinnati, Ohio, October 1972.
3. Hussein, M. Fathy and Tabakoff, W., "Computer Program to Calculate and Plot the Dynamic Behavior of Solid Particles Suspended by Fluid Flow in a Rotating Cascade," Project Themis Report, University of Cincinnati, Cincinnati, Ohio, to be published.
4. Hussein, M. Fathy, "The Dynamic Characteristics of Solid Particles in Particulate Flow in Rotating Turbomachinery," Ph.D. Dissertation, University of Cincinnati, Cincinnati, Ohio, 1972.
5. Emery, J.C., Herrig, L.J., Erwin, J.R., and Felix, A.R., "Systematic Two-Dimensional Cascade Tests of NACA 65-Series Compressor Blades at Low Speeds," NACA Report No. 1368. 1958.
6. Wood, R.M., "Study Correlation of Aerodynamic Parameters with Compressor Erosion Final Report," Allison Division, General Motors, Report No. EDR 6092, Indianapolis, February 1969.

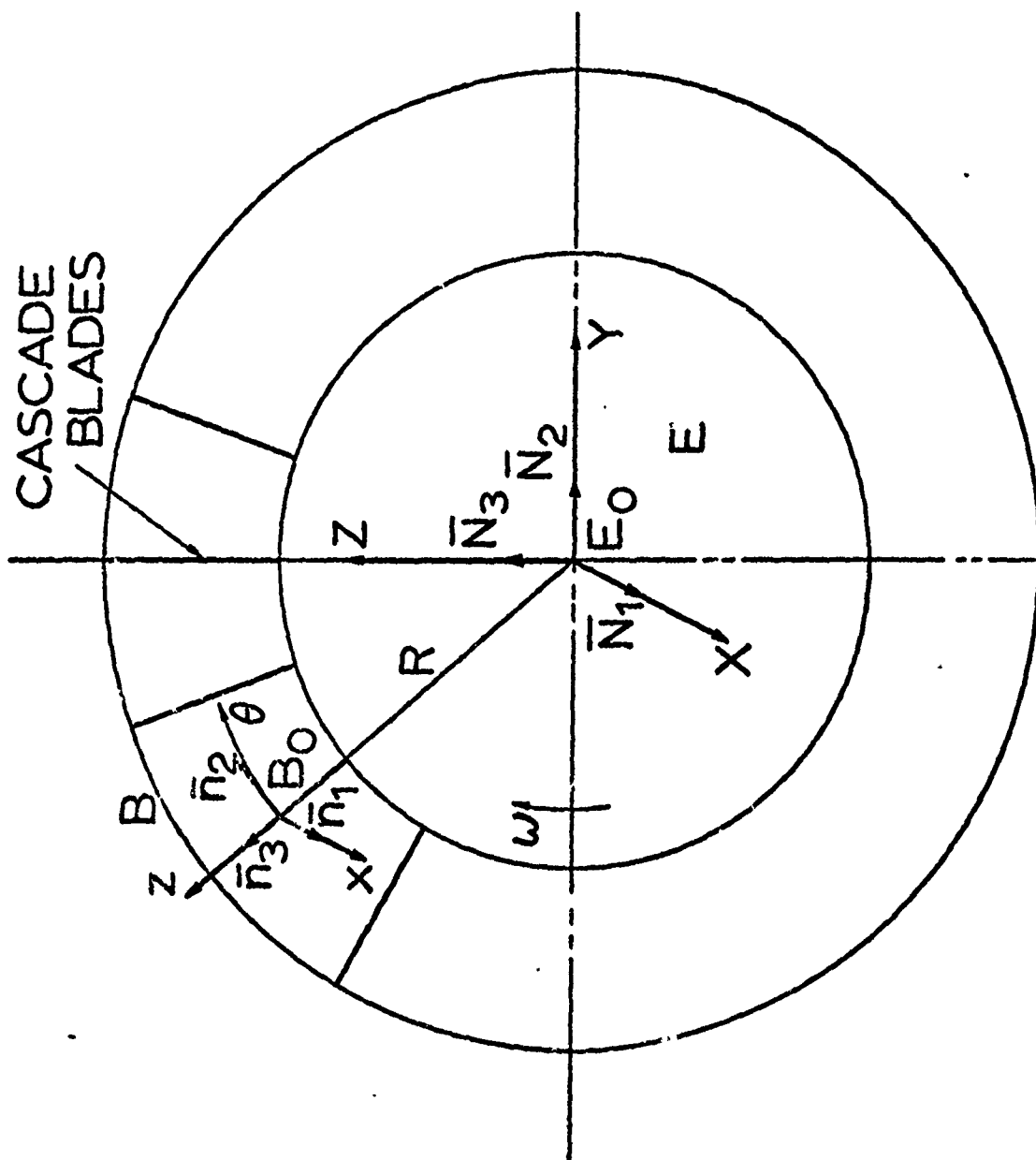


FIGURE 1

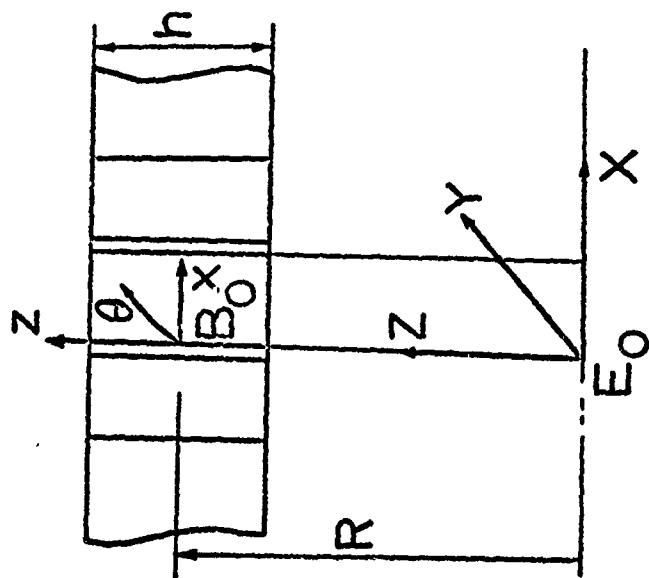


FIGURE 2

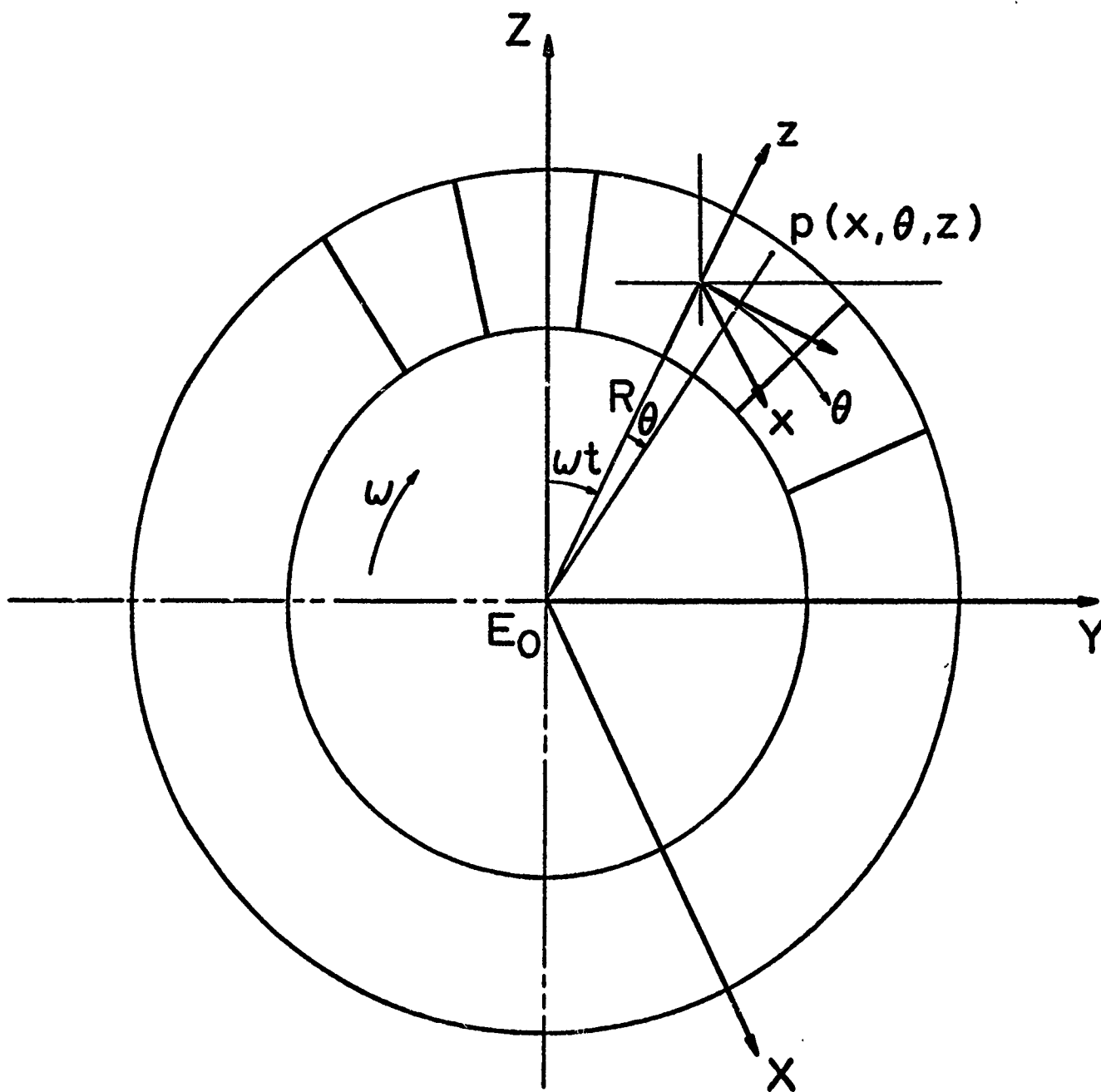


FIGURE 3

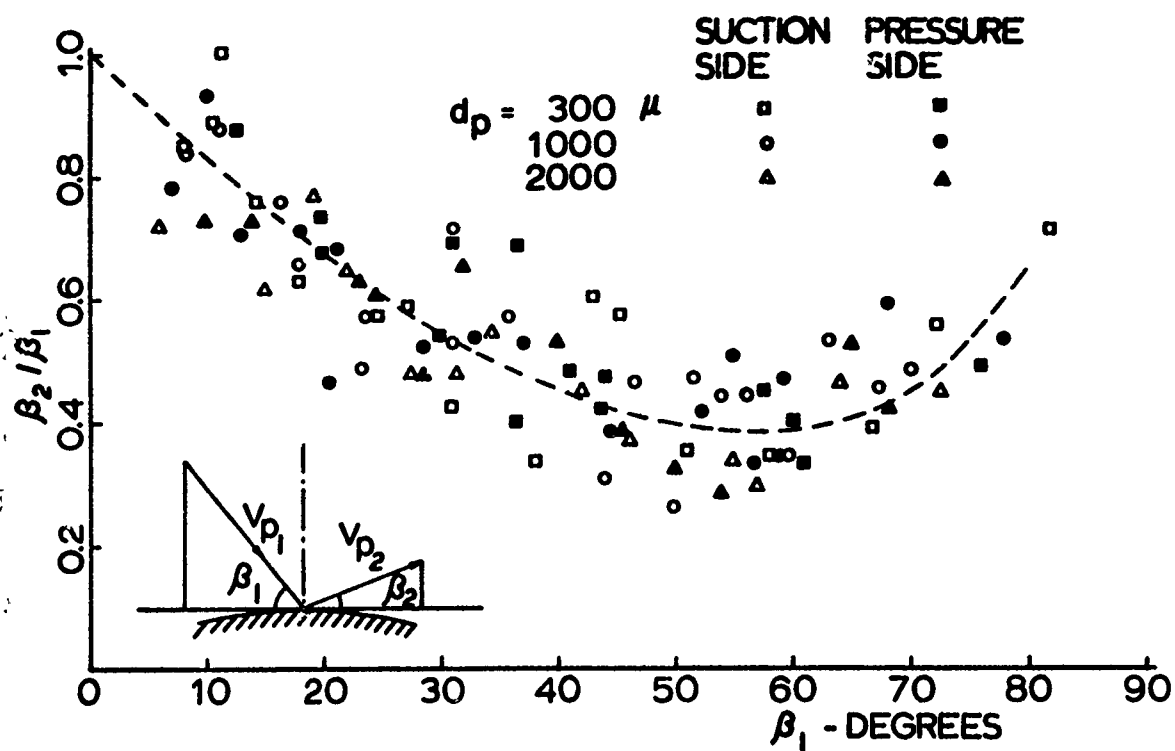


FIG. 4 NONDIMENSIONAL ANGLE OF REBOUND

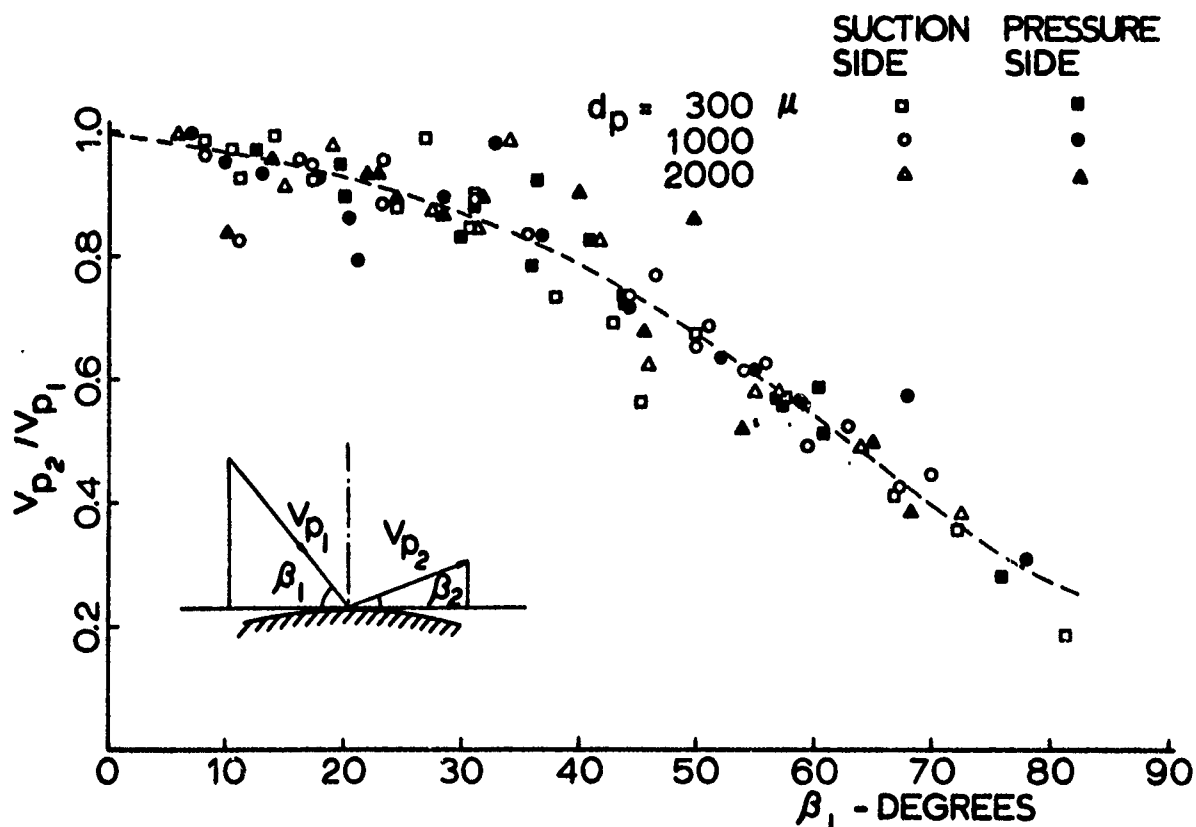


FIG. 5 DROP IN PARTICLE RELATIVE VELOCITY DUE TO COLLISION (RESTITUTION RATIO)

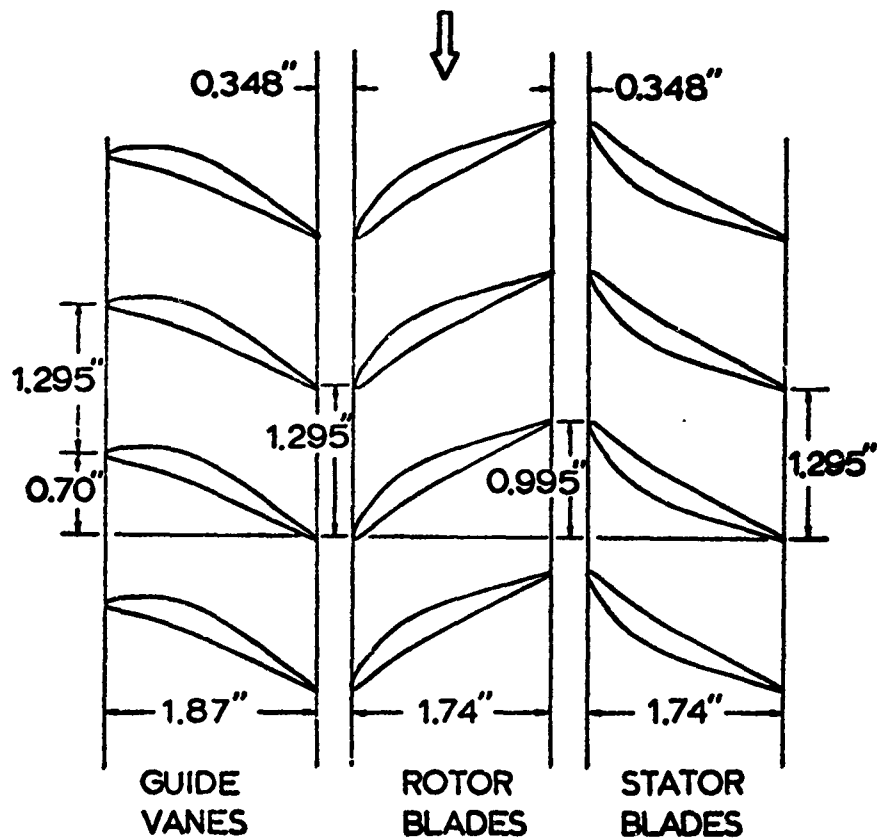


FIGURE 6 COMPRESSOR STAGE DIMENSIONS

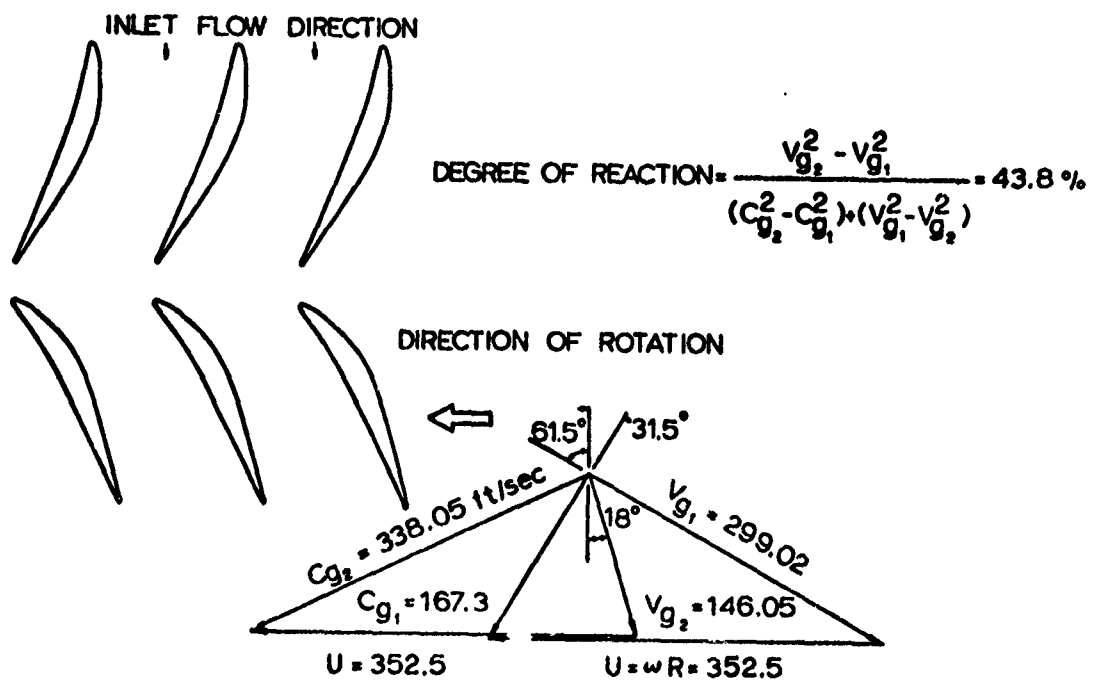


FIGURE 7 COMBINED GAS VELOCITY DIAGRAM
(COMPRESSOR STAGE)

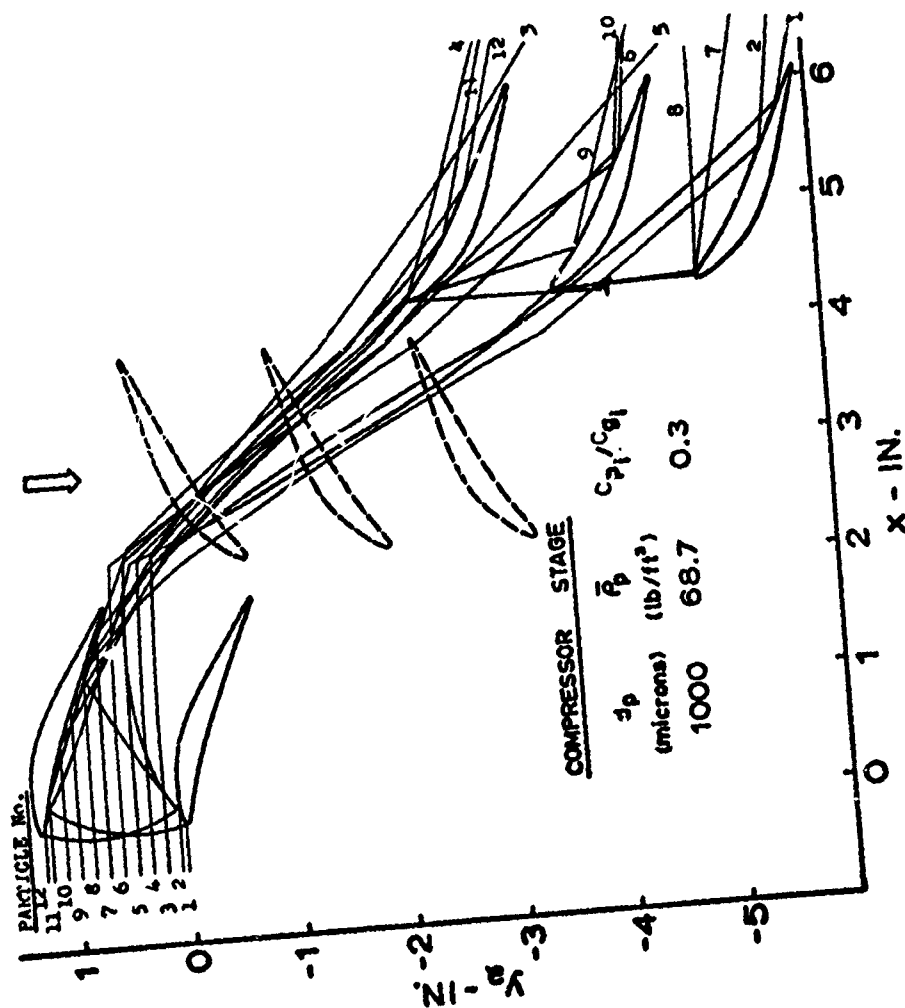


FIGURE 9 AXIAL AND TANGENTIAL COMPONENTS OF PARTICLE TRAJECTORIES

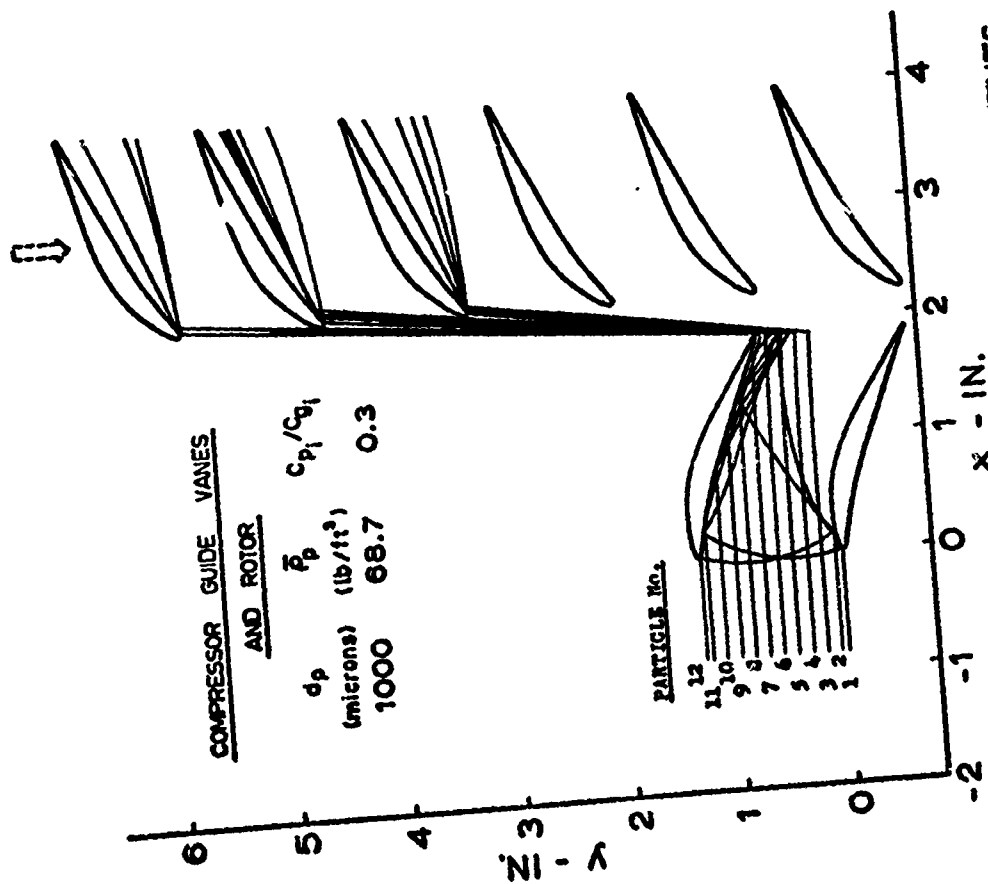


FIGURE 10 AXIAL AND TANGENTIAL COMPONENTS OF PARTICLE TRAJECTORIES RELATIVE TO THE ROTOR BLADES

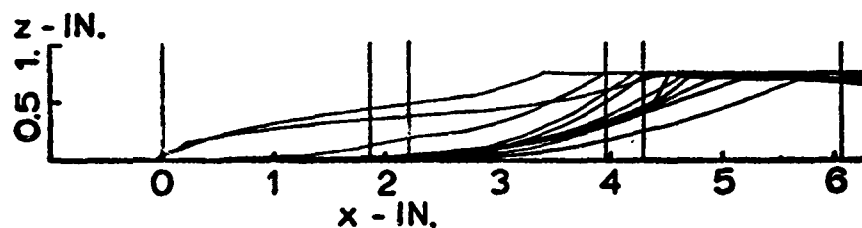


FIGURE 11 AXIAL AND RADIAL COMPONENTS OF PARTICLE TRAJECTORIES

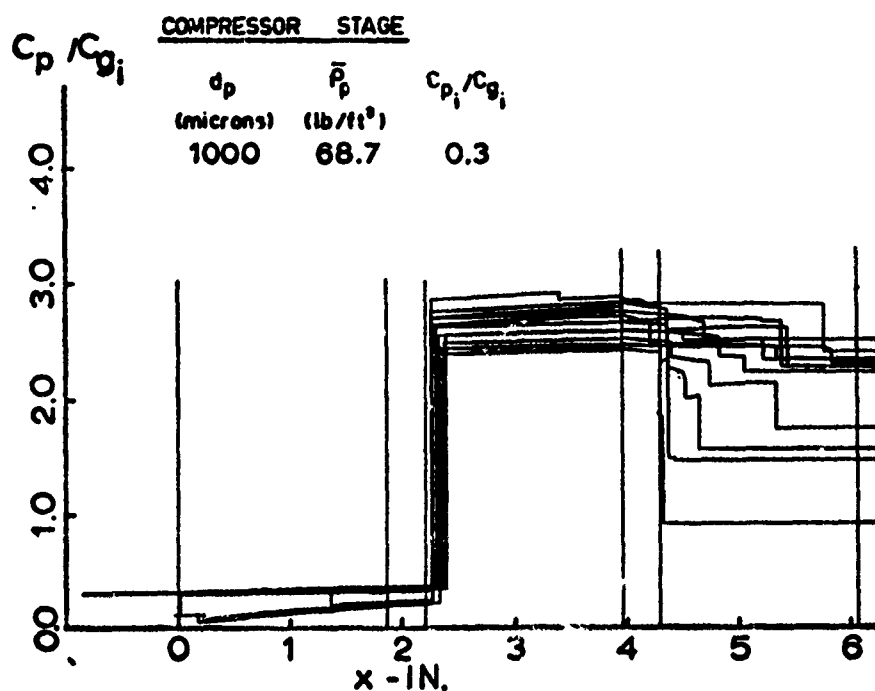


FIGURE 12 PARTICLE NONDIMENSIONAL ABSOLUTE VELOCITIES

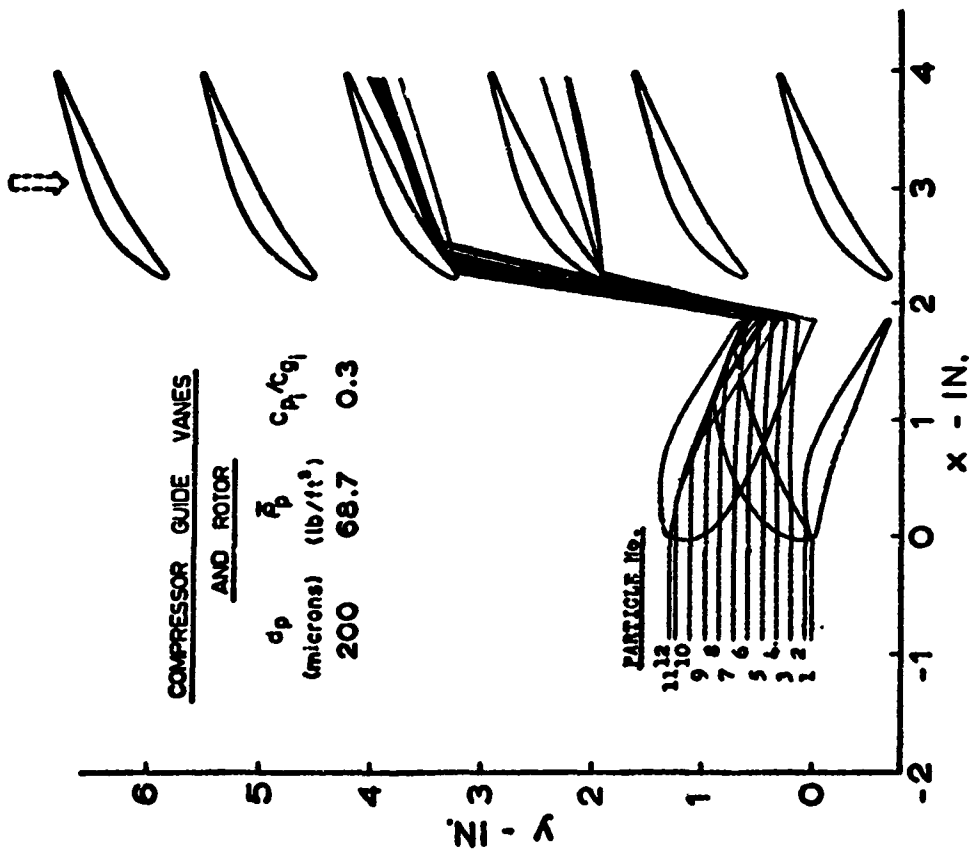


FIGURE 13 AXIAL AND TANGENTIAL COMPONENTS OF PARTICLE TRAJECTORIES

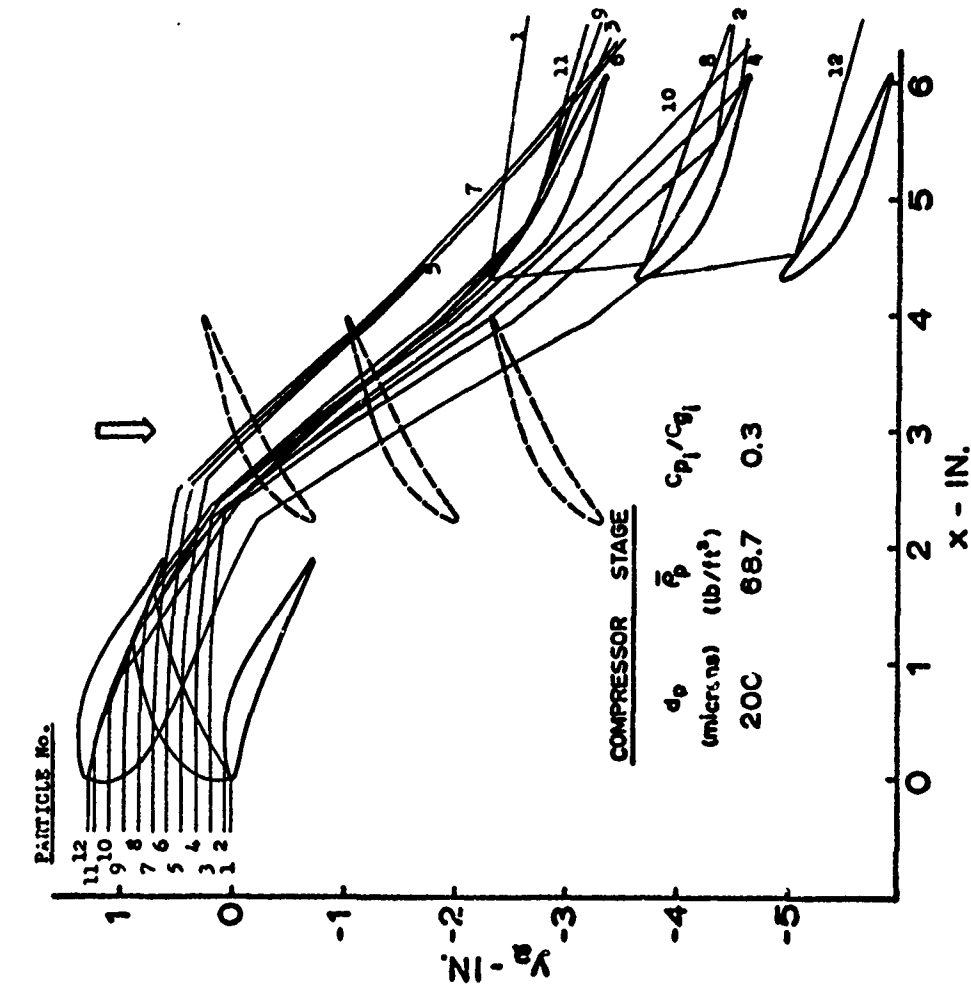


FIGURE 14 AXIAL AND TANGENTIAL COMPONENTS OF PARTICLE TRAJECTORIES RELATIVE TO THE ROTOR BLADES

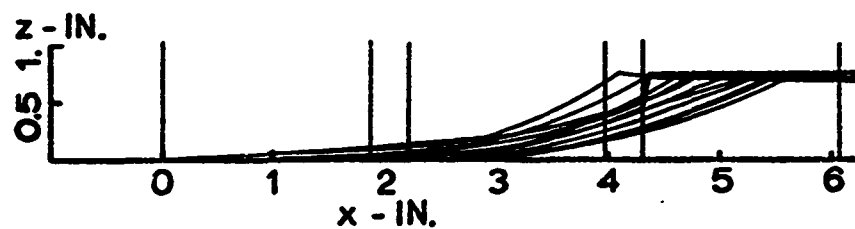


FIGURE 15 AXIAL AND RADIAL COMPONENTS OF PARTICLE TRAJECTORIES

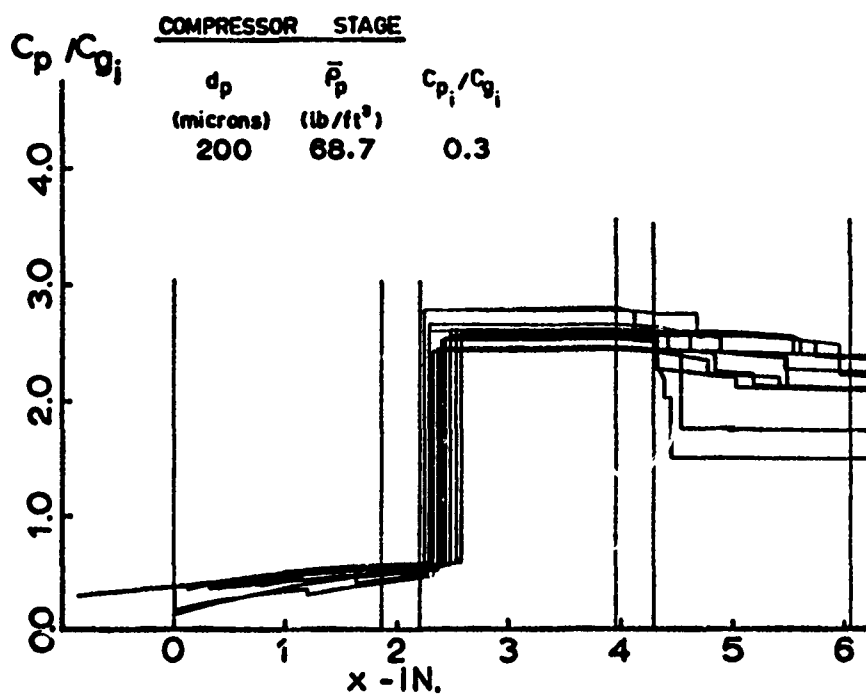


FIGURE 16 PARTICLE NONDIMENSIONAL ABSOLUTE VELOCITIES

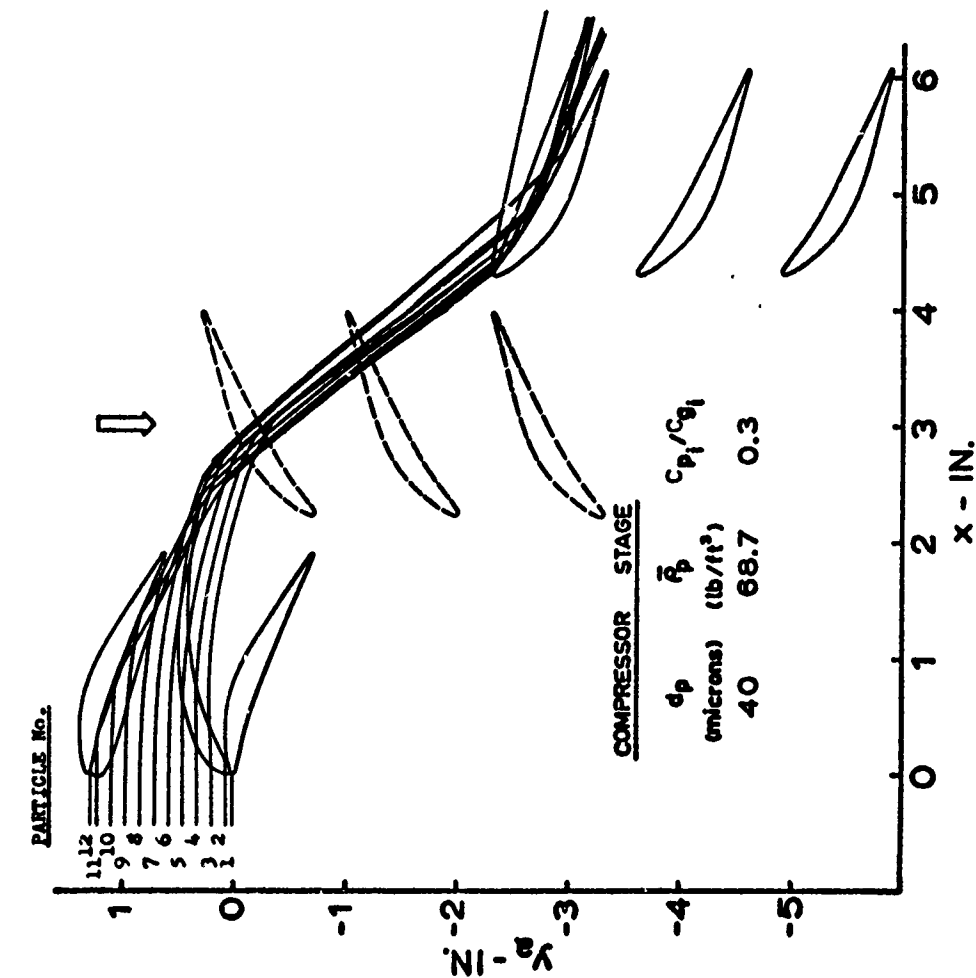


FIGURE 17 AXIAL AND TANGENTIAL COMPONENTS OF PARTICLE TRAJECTORIES

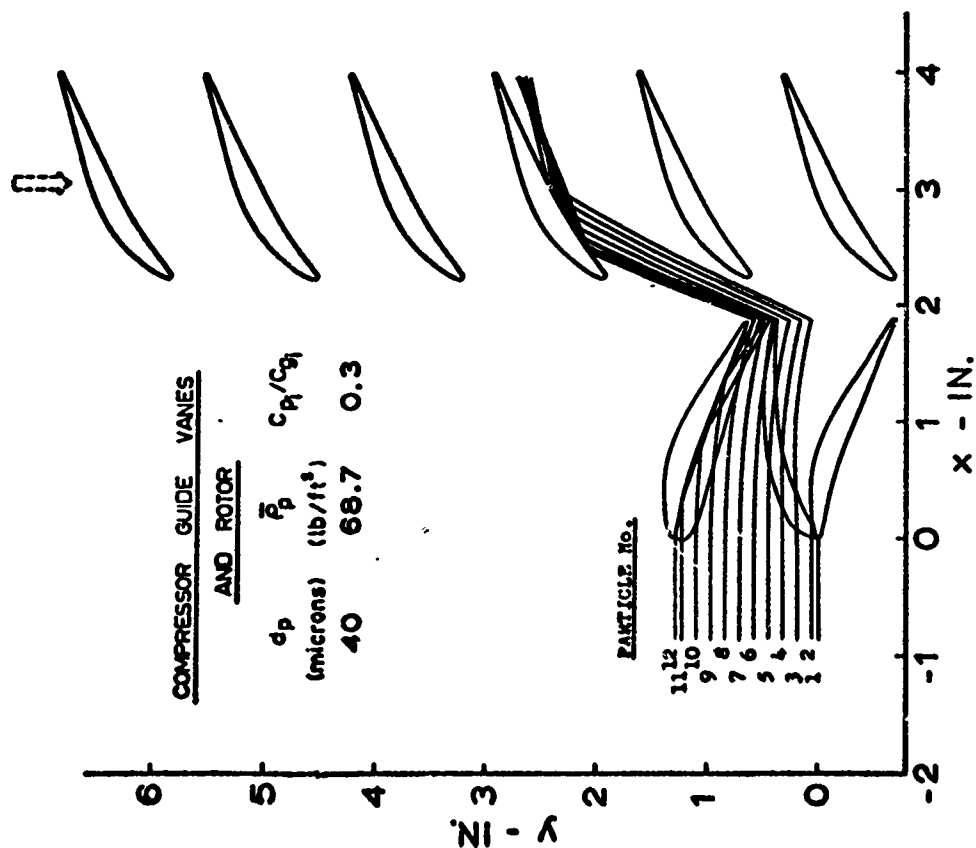


FIGURE 18 AXIAL AND TANGENTIAL COMPONENTS OF PARTICLE TRAJECTORIES RELATIVE TO THE ROTOR BLADES

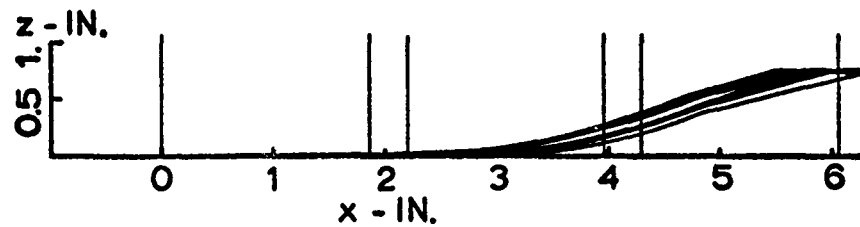


FIGURE 19 AXIAL AND RADIAL COMPONENTS OF PARTICLE TRAJECTORIES

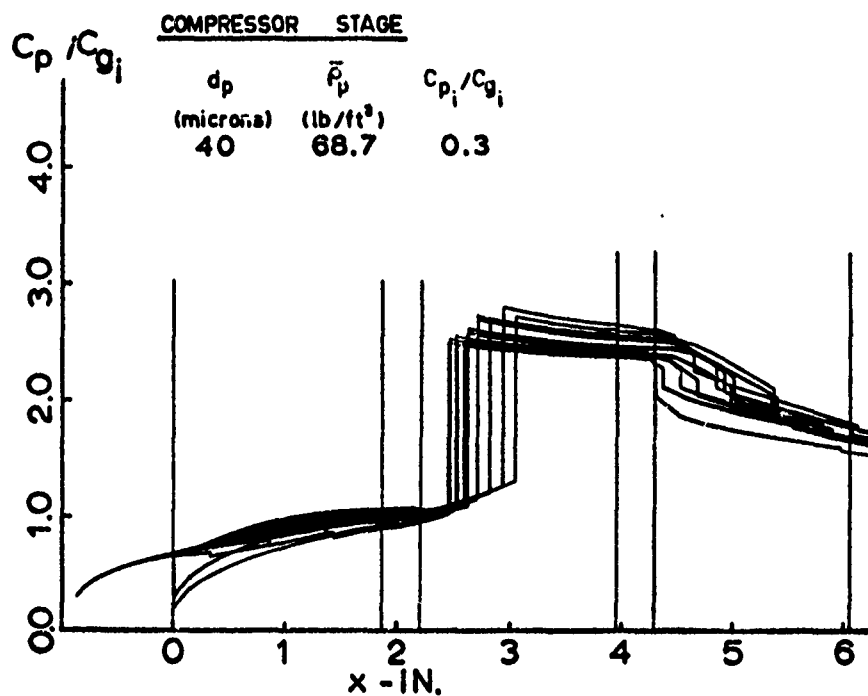


FIGURE 20 PARTICLE NONDIMENSIONAL ABSOLUTE VELOCITIES

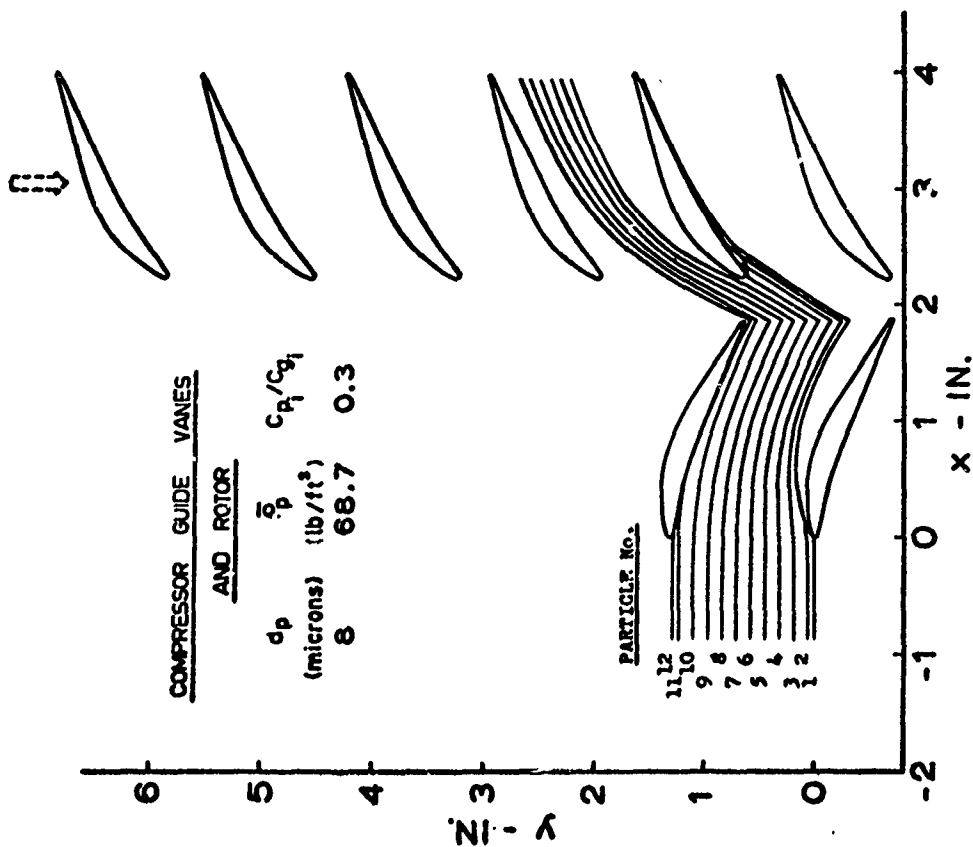


FIGURE 21 AXIAL AND TANGENTIAL COMPONENTS OF PARTICLE TRAJECTORIES

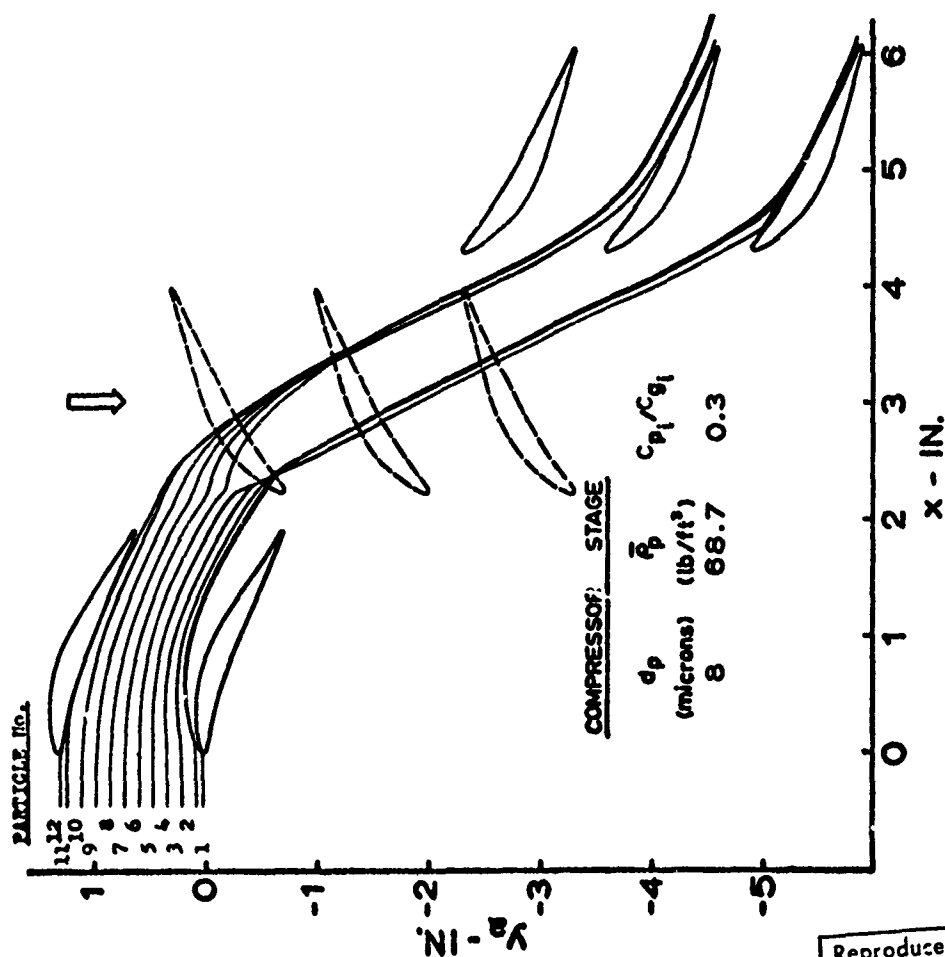


FIGURE 22 AXIAL AND TANGENTIAL COMPONENTS OF PARTICLE TRAJECTORIES RELATIVE TO THE ROTOR BLADES

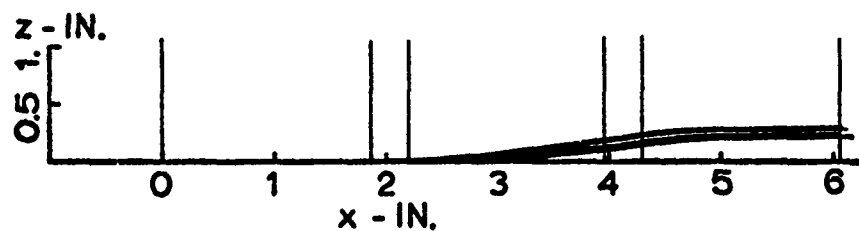


FIGURE 23 AXIAL AND RADIAL COMPONENTS OF PARTICLE TRAJECTORIES

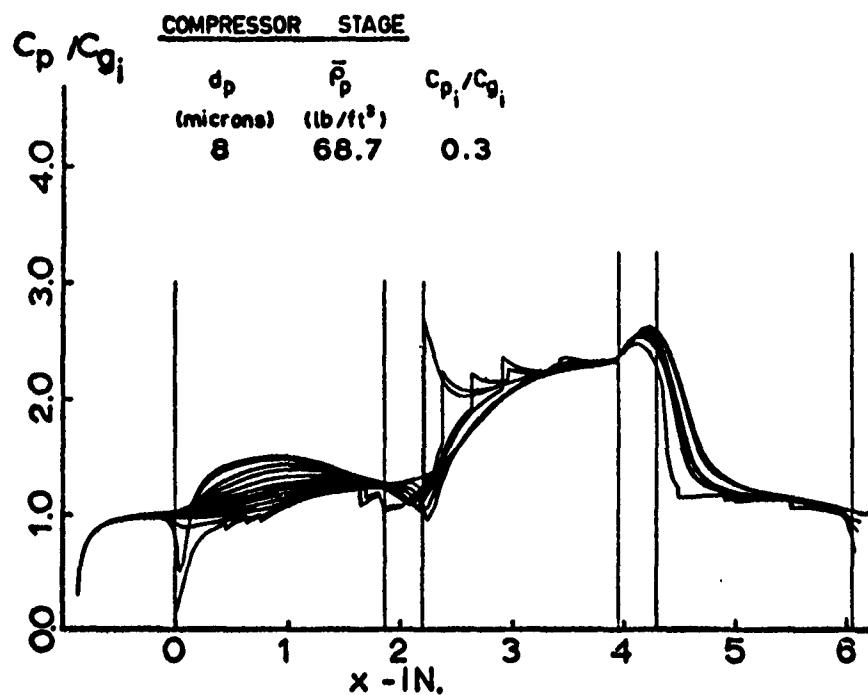


FIGURE 24 PARTICLE NONDIMENSIONAL ABSOLUTE VELOCITIES

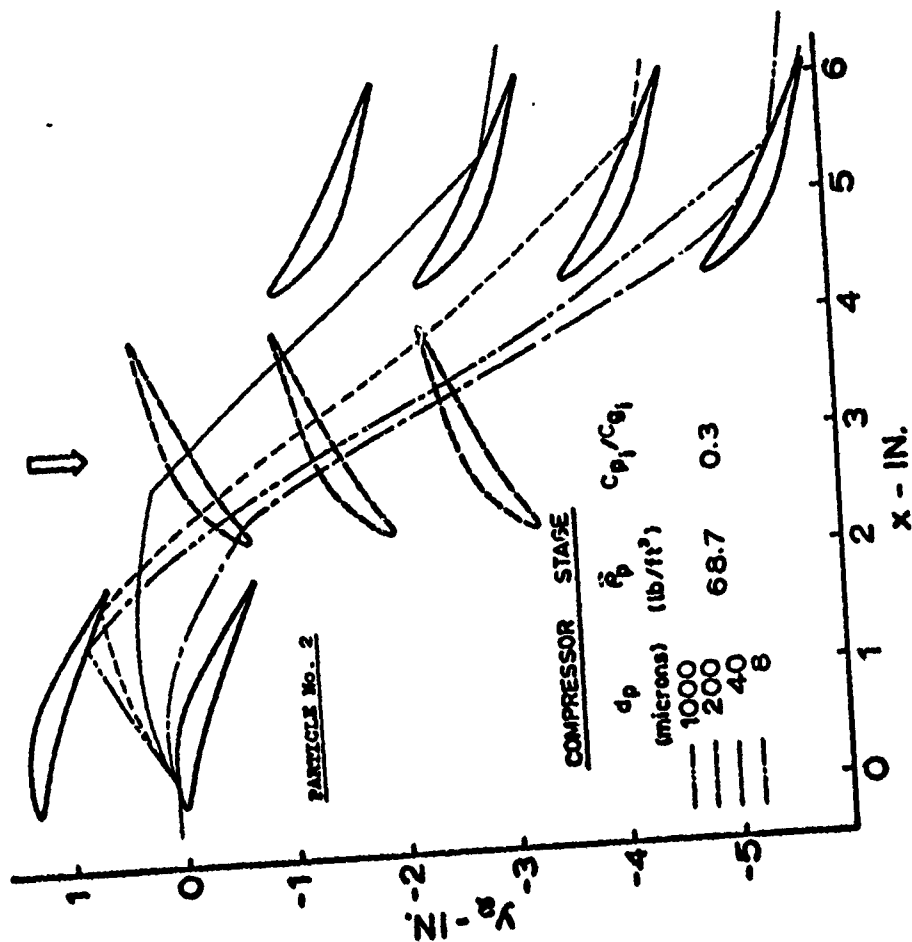


FIGURE 25 AXIAL AND TANGENTIAL COMPONENTS OF PARTICLE TRAJECTORIES (EFFECT OF d_p)

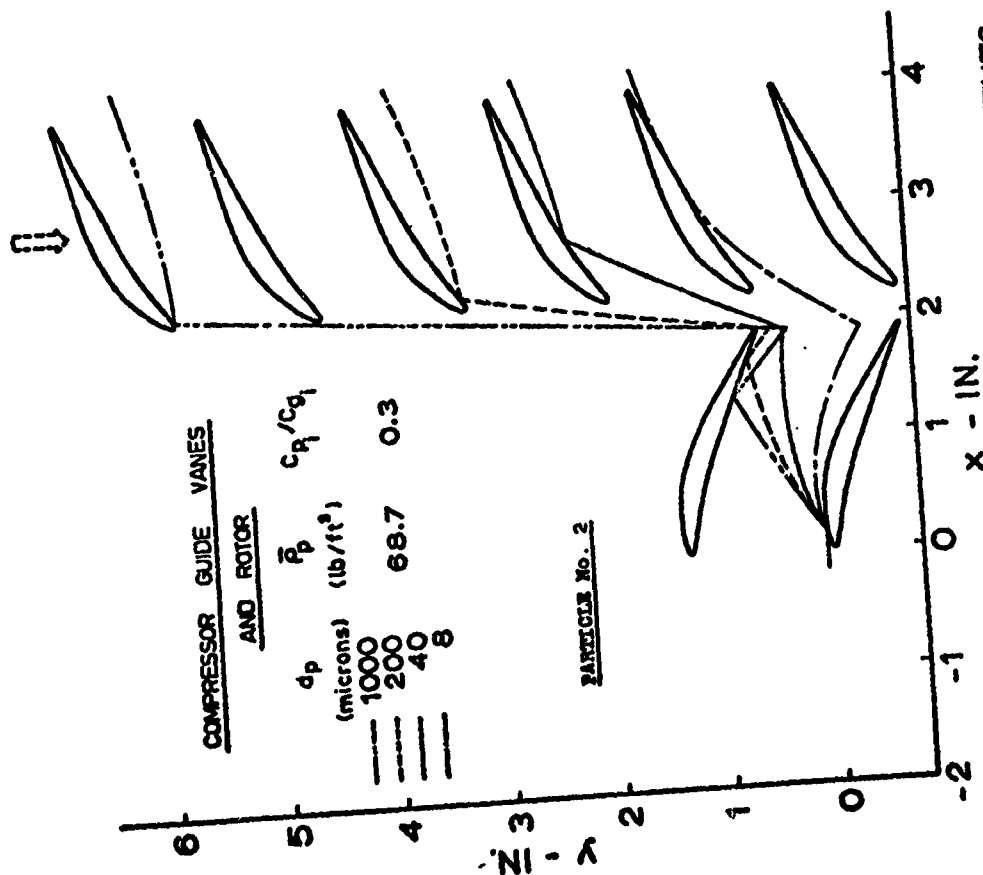


FIGURE 26 AXIAL AND TANGENTIAL COMPONENTS OF PARTICLE TRAJECTORIES RELATIVE TO THE ROTOR BLADES (EFFECT OF d_p)

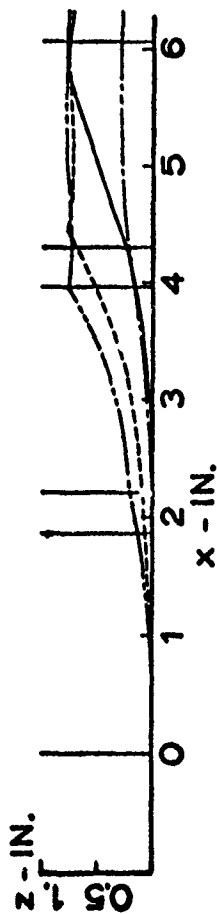


FIGURE 27 AXIAL AND RADIAL COMPONENTS OF PARTICLE TRAJECTORIES

COMPRESSOR STAGE		
d_p (microns)	\bar{P}_p (lb/ft ²)	C_{p_i}/C_{g_i}
1000	68.7	0.3
200		
40		
8		

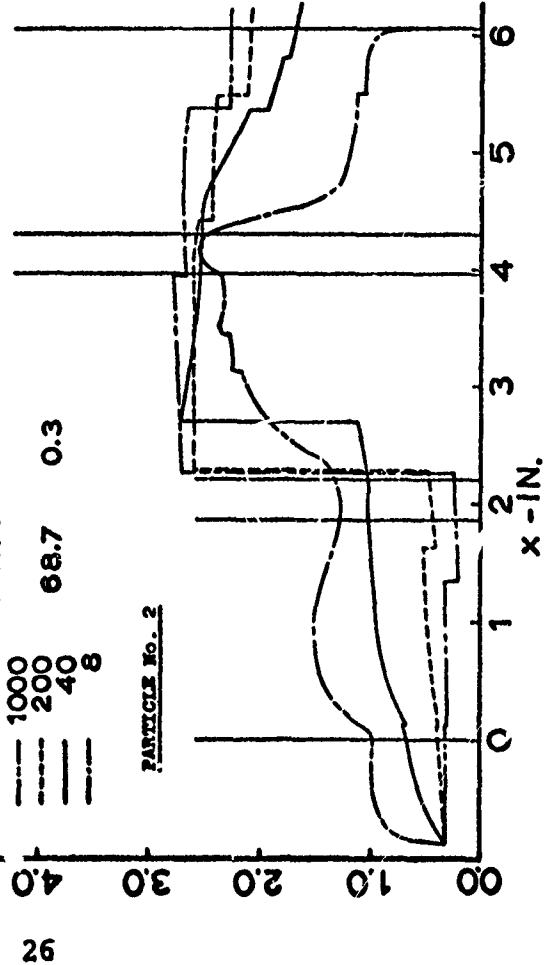


FIGURE 28 PARTICLE NONDIMENSIONAL ABSOLUTE VELOCITIES (EFFECT OF d_p)

COMPRESSOR STAGE		
d_p (microns)	\bar{P}_p (lb/ft ²)	C_{p_i}/C_{g_i}
1000	68.7	0.3
200		
40		
8		

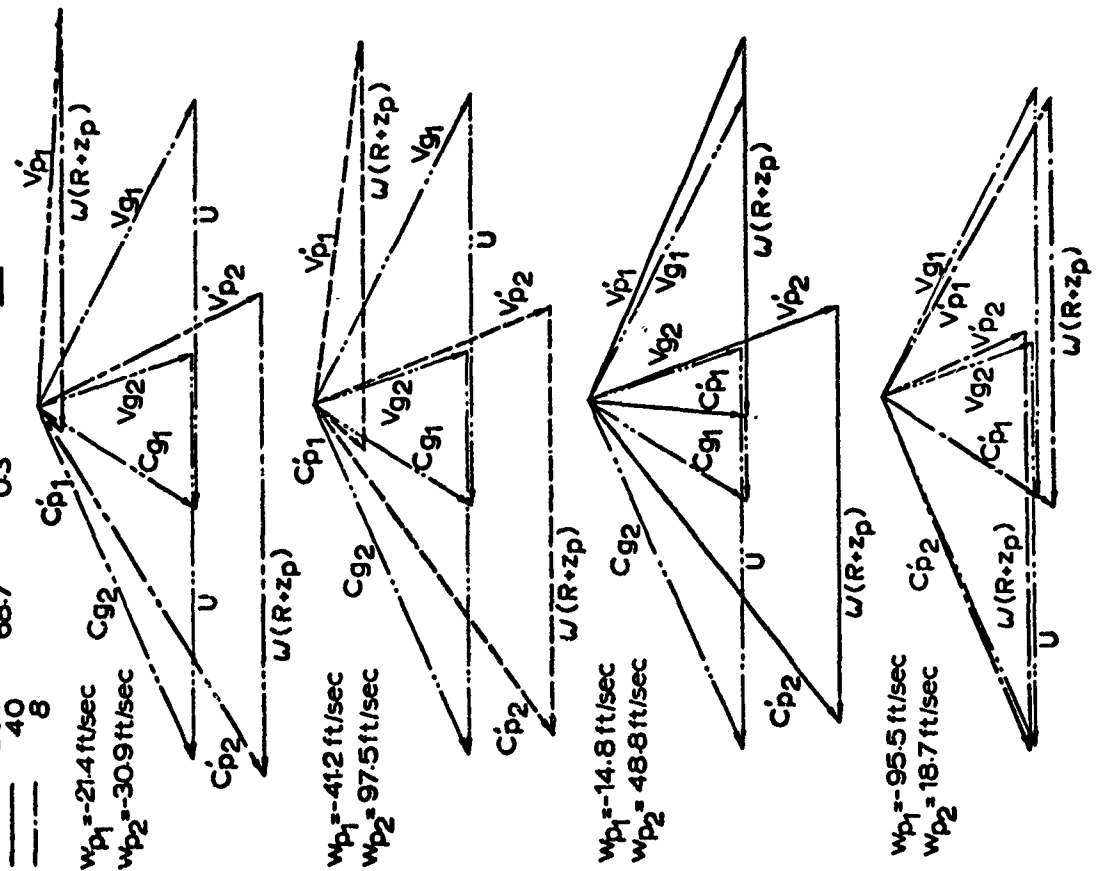


FIGURE 29 PARTICLE VELOCITY DIAGRAM

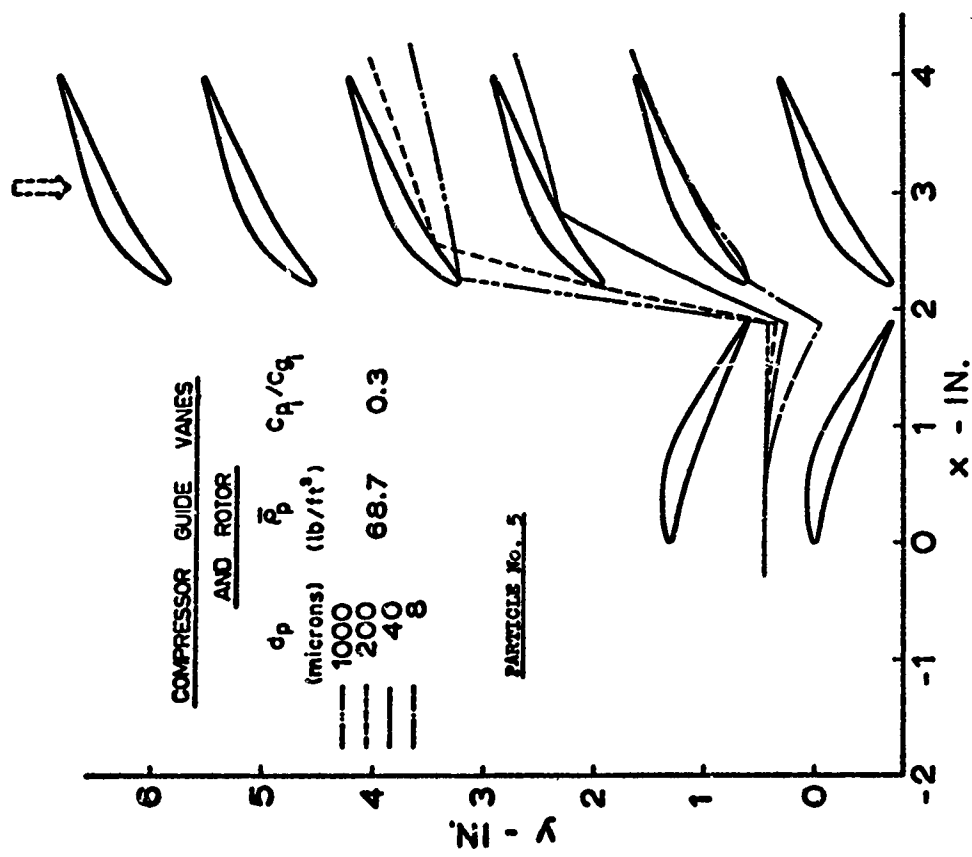


FIGURE 30 AXIAL AND TANGENTIAL COMPONENTS OF PARTICLE TRAJECTORIES RELATIVE TO THE ROTOR BLADES (EFFECT OF d_p)

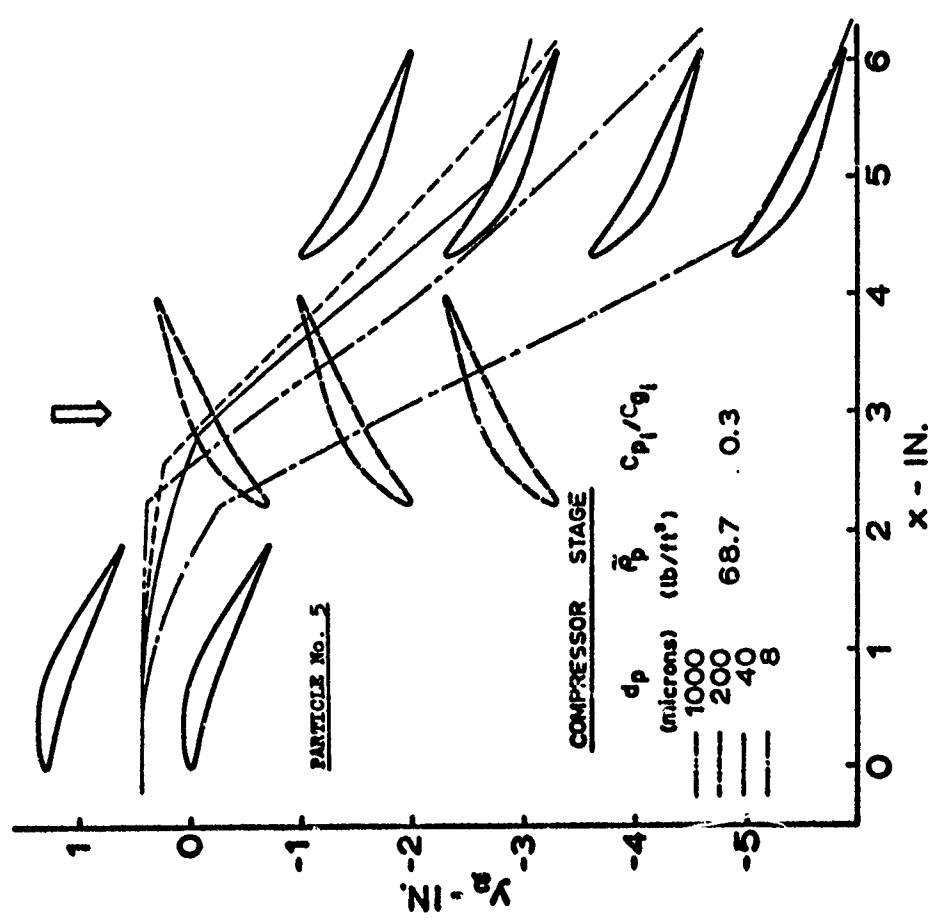


FIGURE 31 AXIAL AND TANGENTIAL COMPONENTS OF PARTICLE TRAJECTORIES RELATIVE TO THE ROTOR BLADES (EFFECT OF d_p)

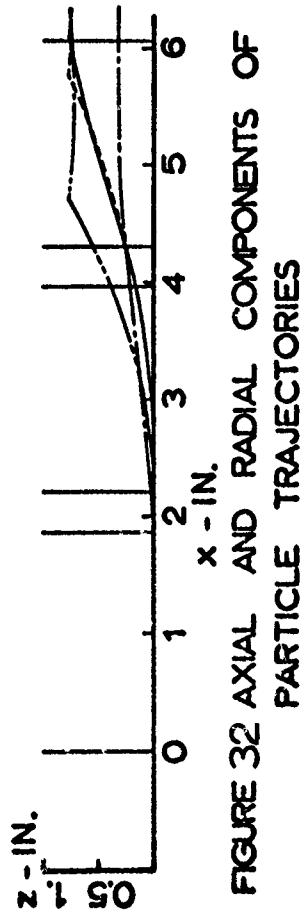


FIGURE 32 AXIAL AND RADIAL COMPONENTS OF PARTICLE TRAJECTORIES

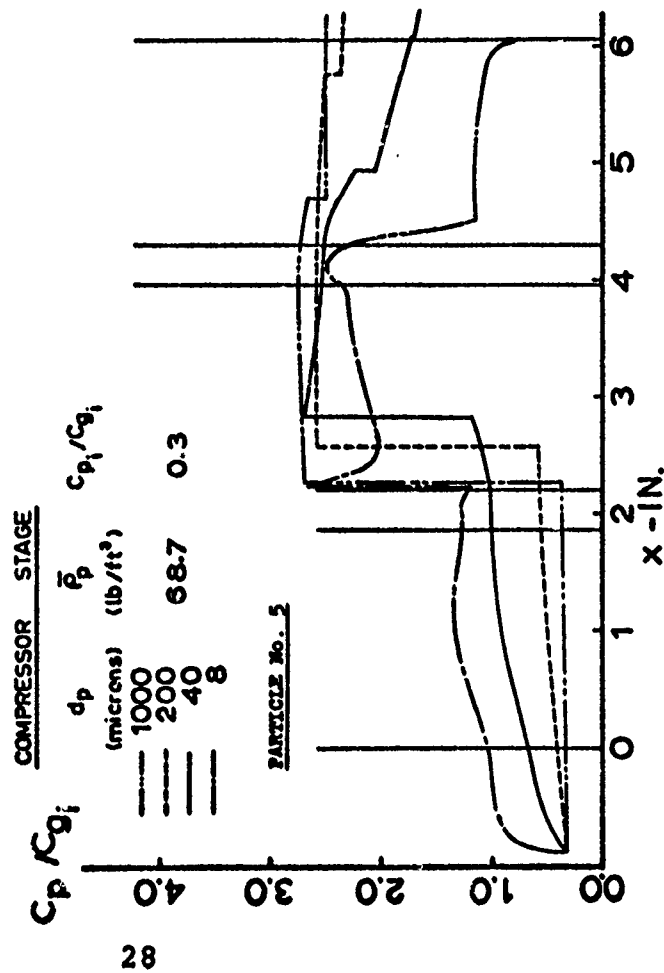


FIGURE 33 PARTICLE NONDIMENSIONAL ABSOLUTE VELOCITIES (EFFECT OF d_p)

COMPRESSOR STAGE

d_p (microns)	$\bar{\rho}_p$ (lb/ft ³)	C_{p1}/C_{g1}
1000	68.7	0.3
200		
40		
8		

PARTICLE NO. 5

100 ft/sec

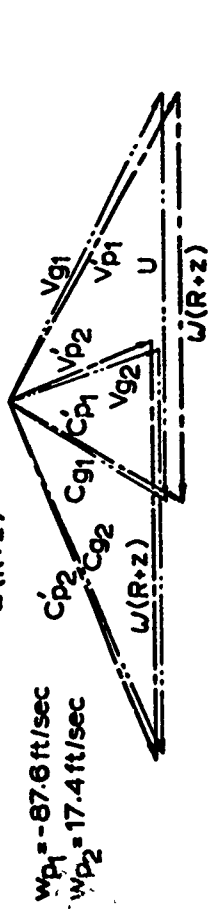
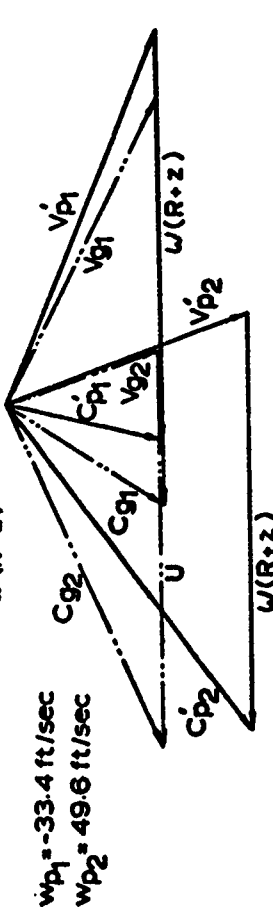
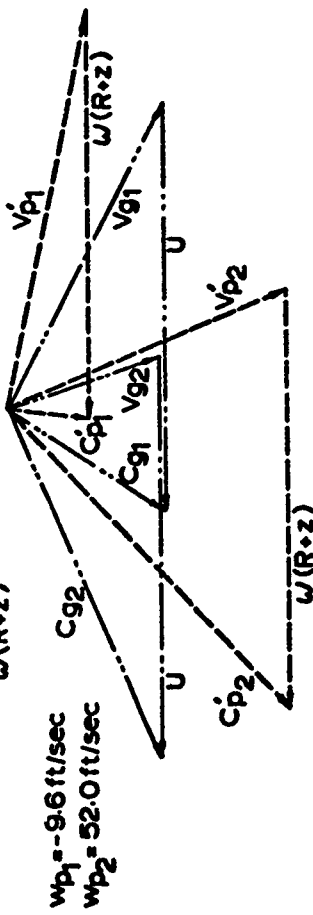
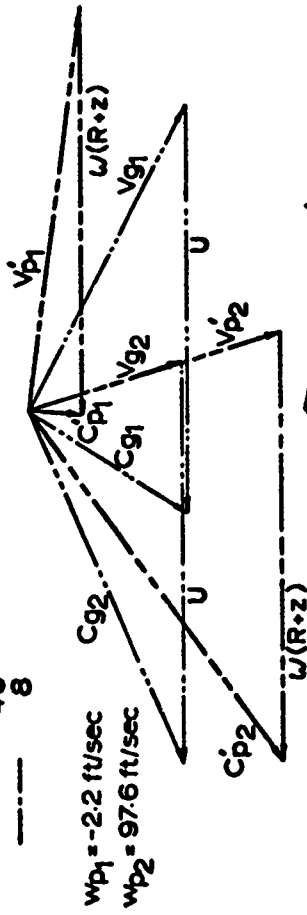


FIGURE 34 PARTICLE VELOCITY DIAGRAM

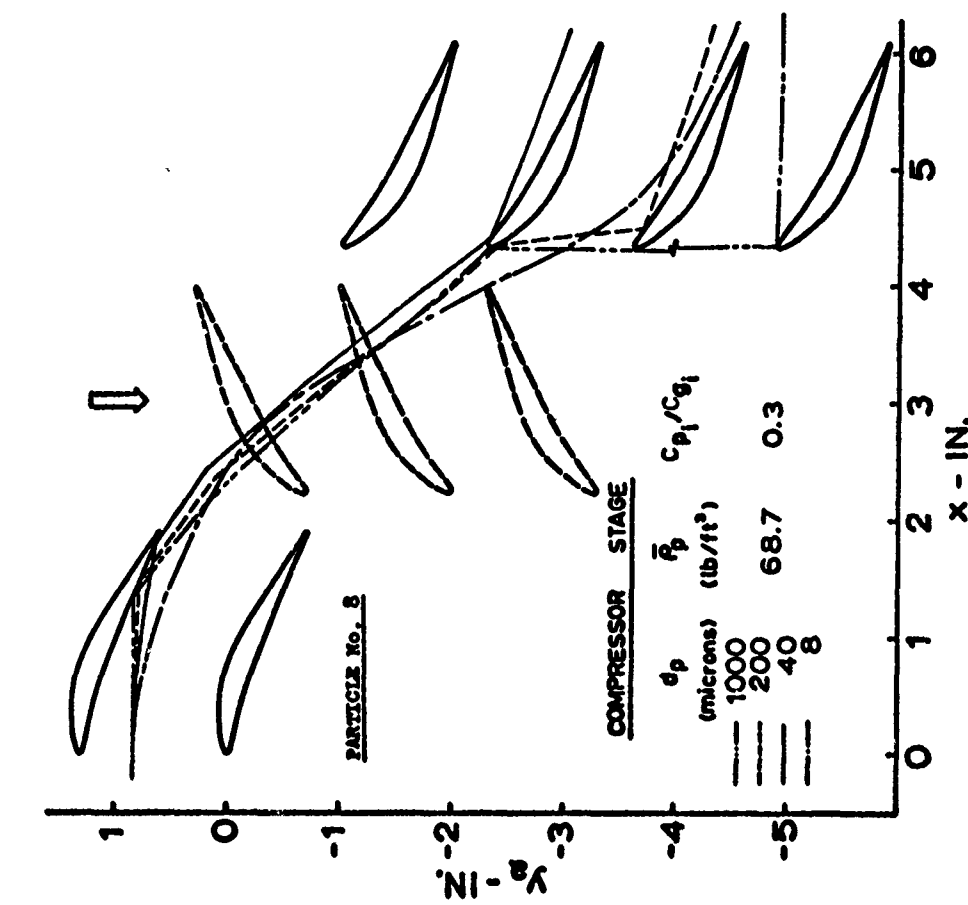


FIGURE 35 AXIAL AND TANGENTIAL COMPONENTS OF PARTICLE TRAJECTORIES (EFFECT OF d_p)

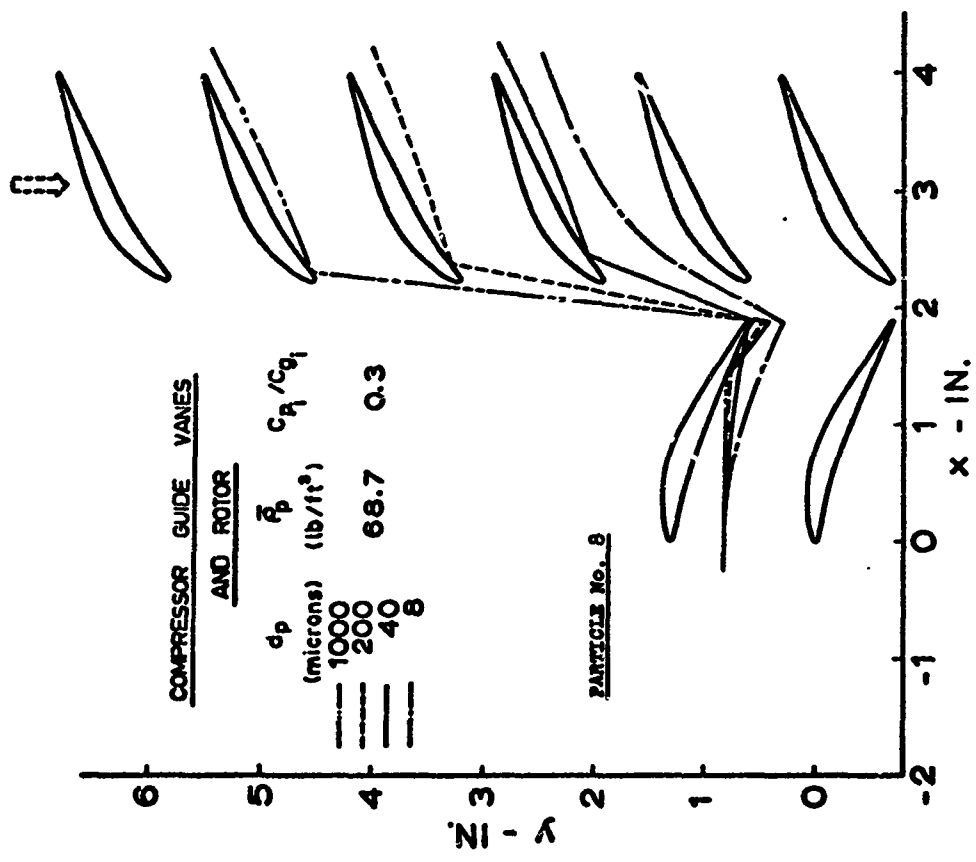


FIGURE 36 AXIAL AND TANGENTIAL COMPONENTS OF PARTICLE TRAJECTORIES RELATIVE TO THE ROTOR BLADES (EFFECT OF d_p)

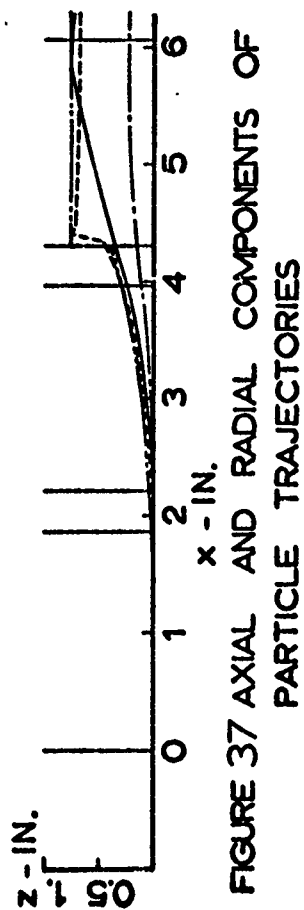


FIGURE 37 AXIAL AND RADIAL COMPONENTS OF PARTICLE TRAJECTORIES

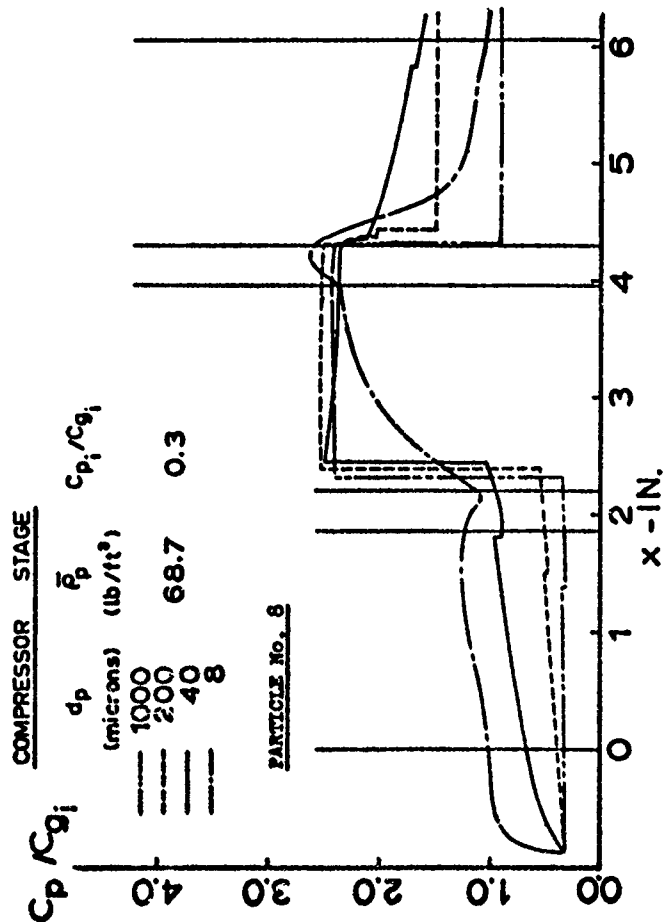


FIGURE 38 PARTICLE NONDIMENSIONAL ABSOLUTE VELOCITIES (EFFECT OF d_p)

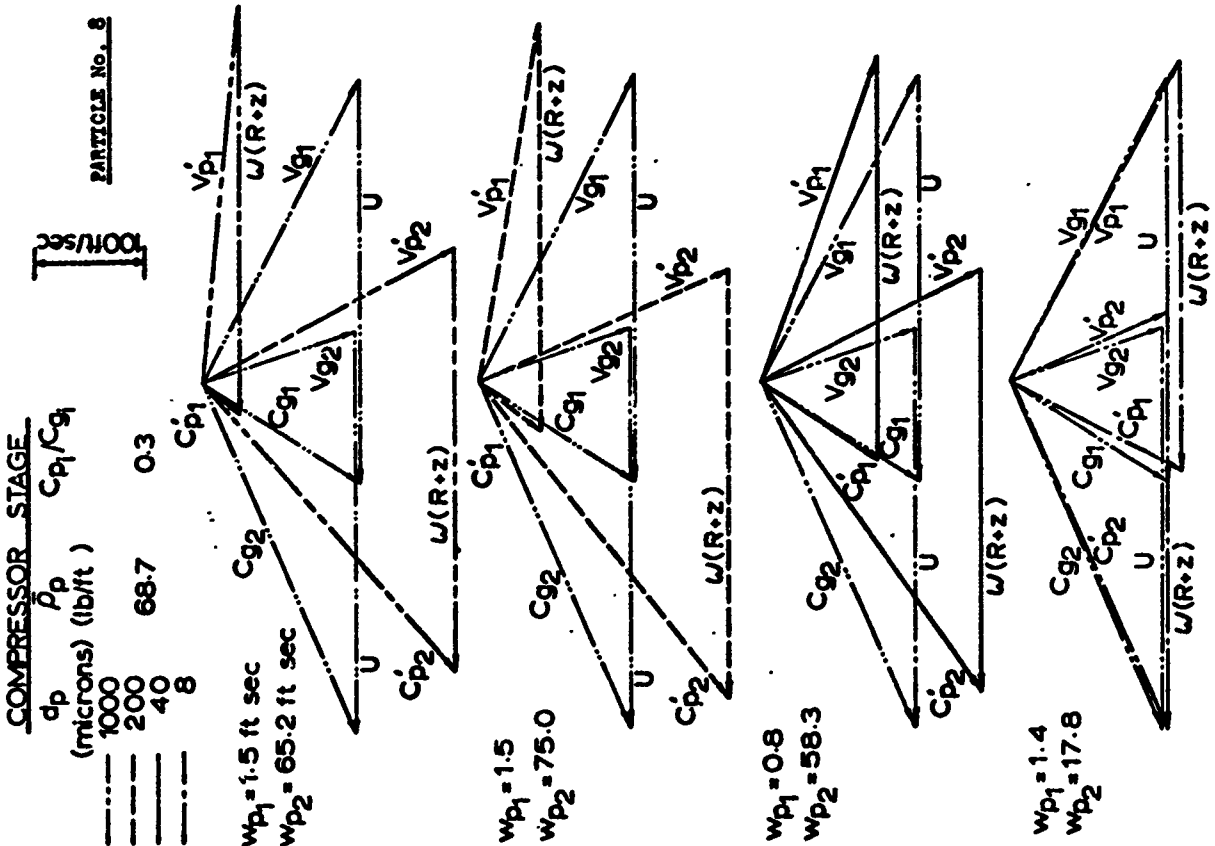


FIGURE 39 PARTICLE VELOCITY DIAGRAM

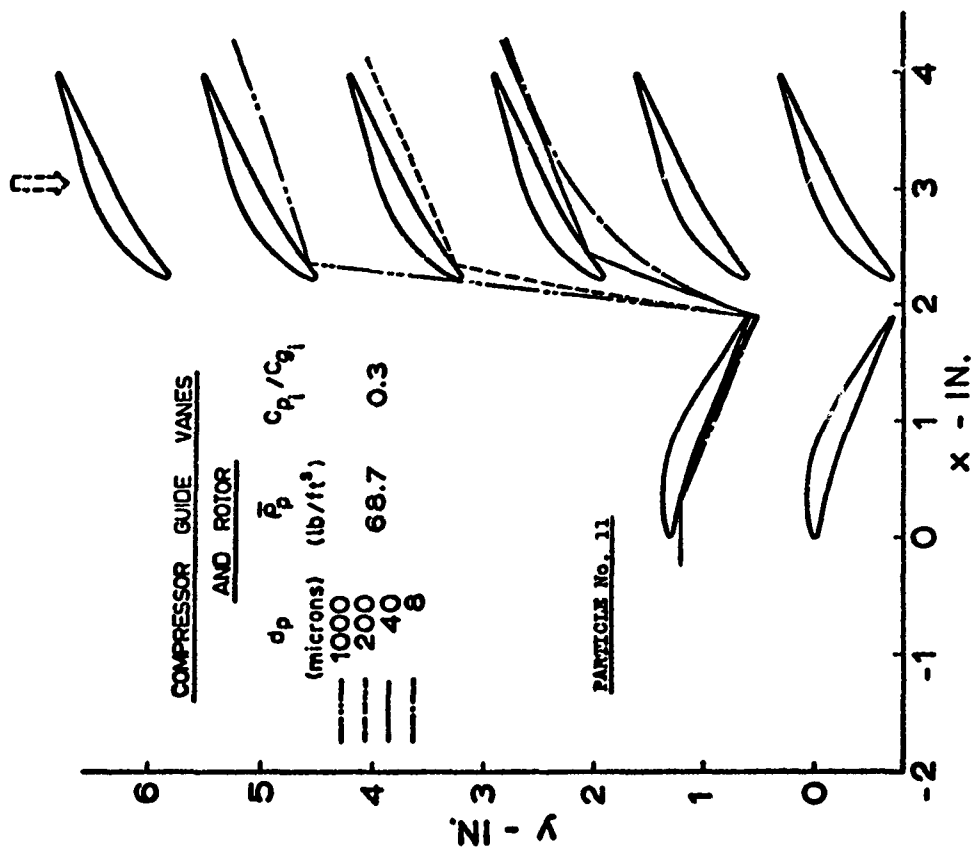


FIGURE 40 AXIAL AND TANGENTIAL COMPONENTS OF PARTICLE TRAJECTORIES (EFFECT OF d_p)

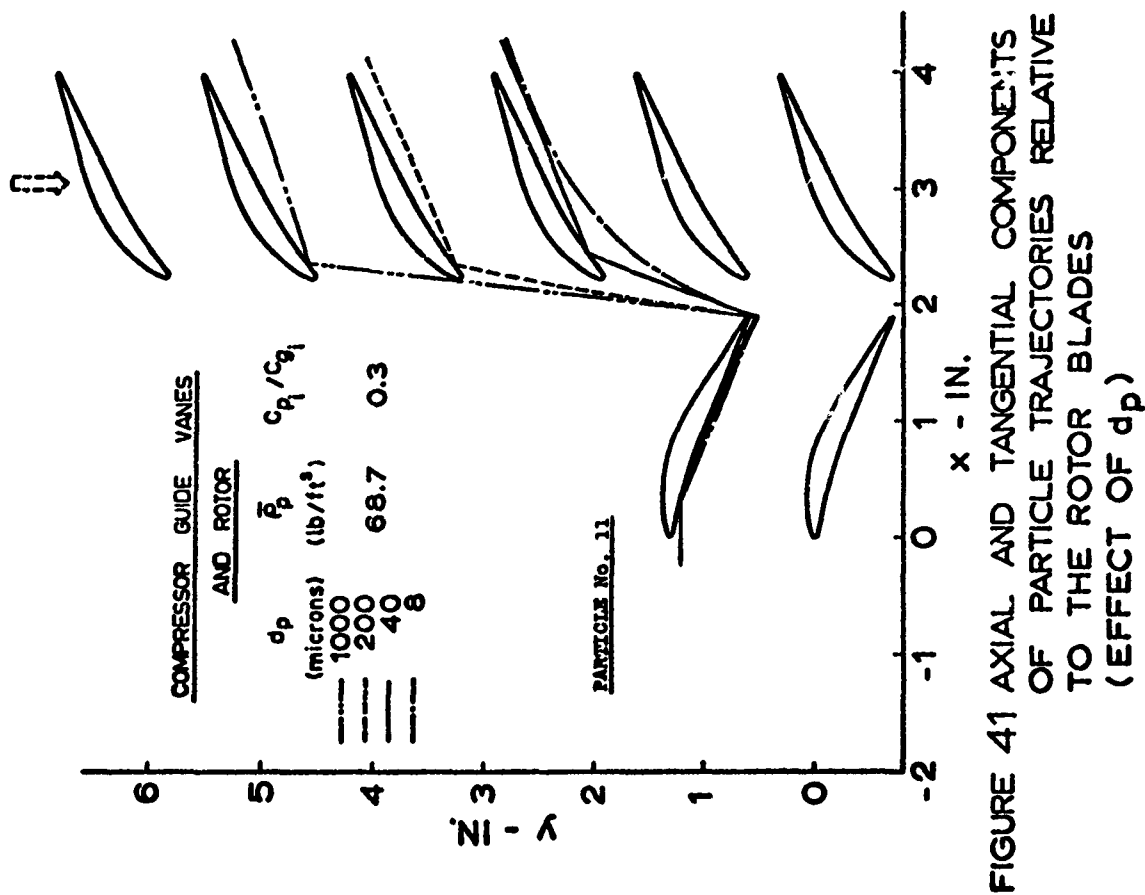


FIGURE 41 AXIAL AND TANGENTIAL COMPONENTS OF PARTICLE TRAJECTORIES RELATIVE TO THE ROTOR BLADES (EFFECT OF d_p)

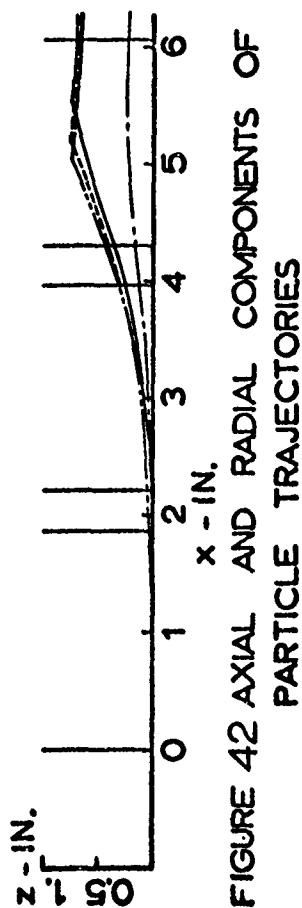


FIGURE 42 AXIAL AND RADIAL COMPONENTS OF PARTICLE TRAJECTORIES

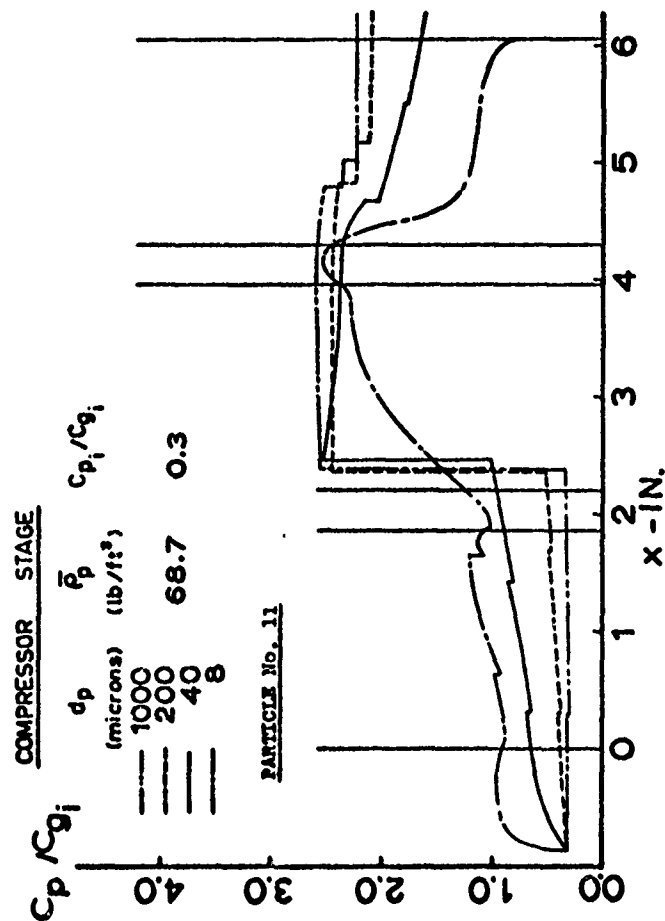


FIGURE 43 PARTICLE NONDIMENSIONAL ABSOLUTE VELOCITIES (EFFECT OF d_p)

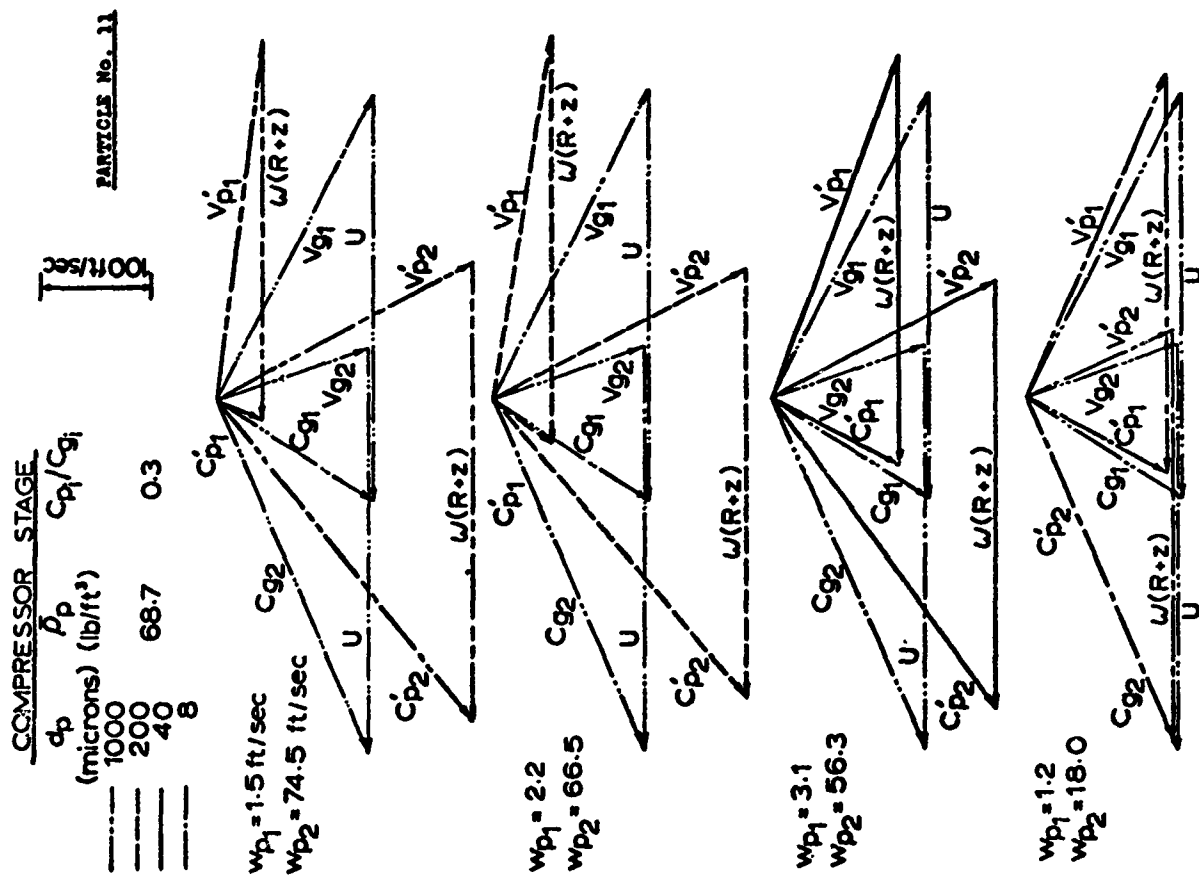


FIGURE 44 PARTICLE VELOCITY DIAGRAM

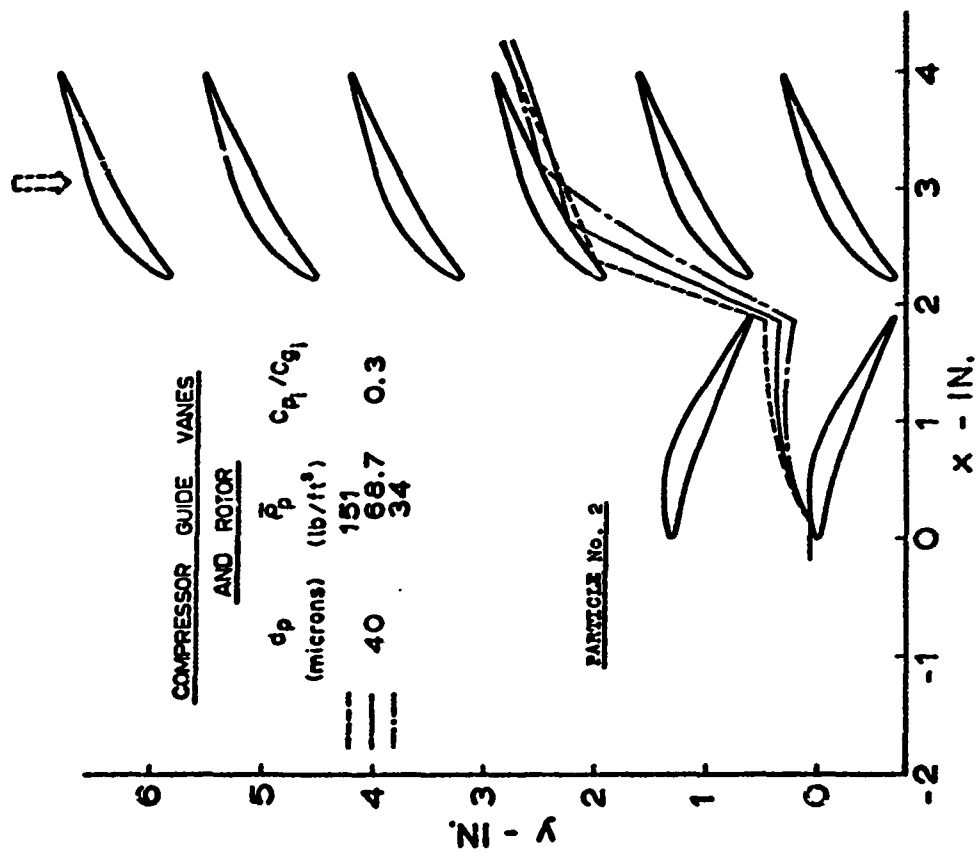


FIGURE 45 AXIAL AND TANGENTIAL COMPONENTS OF PARTICLE TRAJECTORIES (EFFECT OF \bar{p}_p)

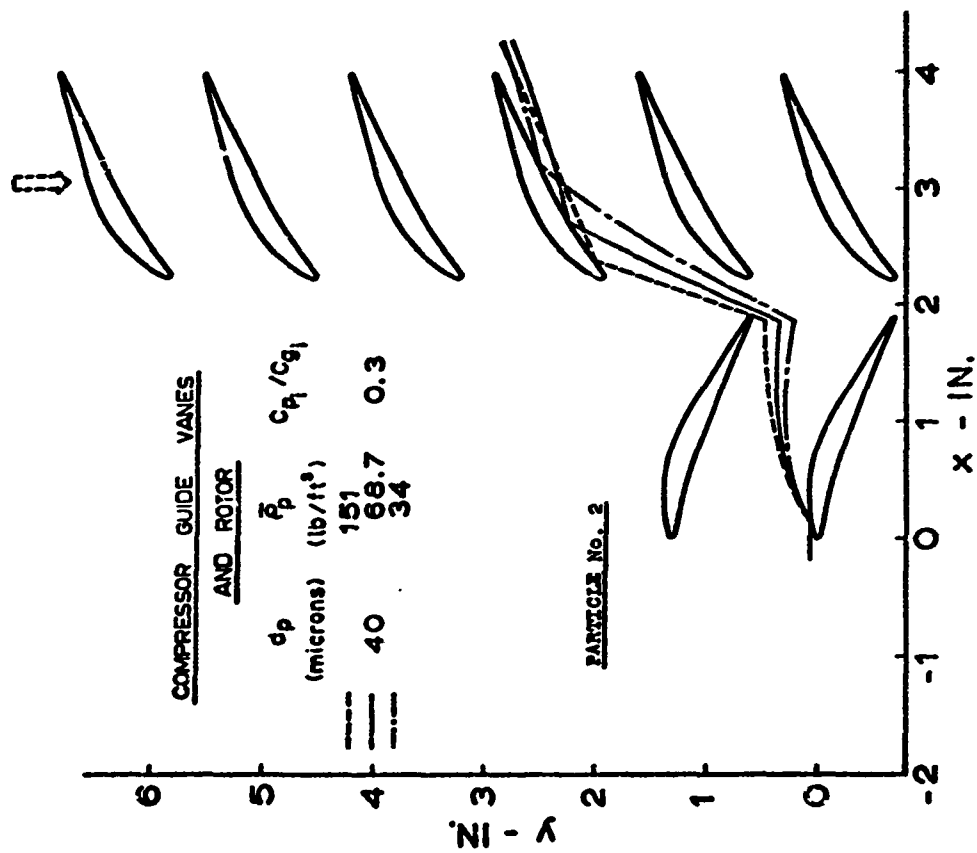


FIGURE 46 AXIAL AND TANGENTIAL COMPONENTS OF PARTICLE TRAJECTORIES RELATIVE TO THE ROTOR BLADES (EFFECT OF \bar{p}_p)

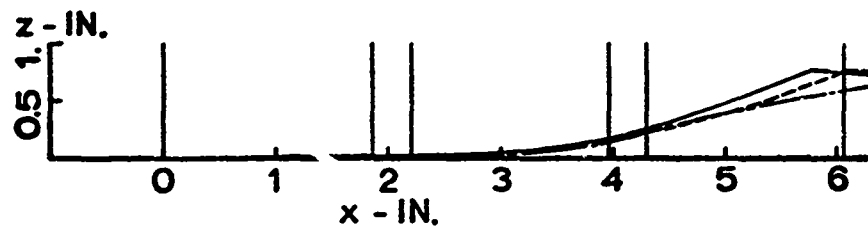


FIGURE 47 AXIAL AND RADIAL COMPONENTS OF PARTICLE TRAJECTORIES

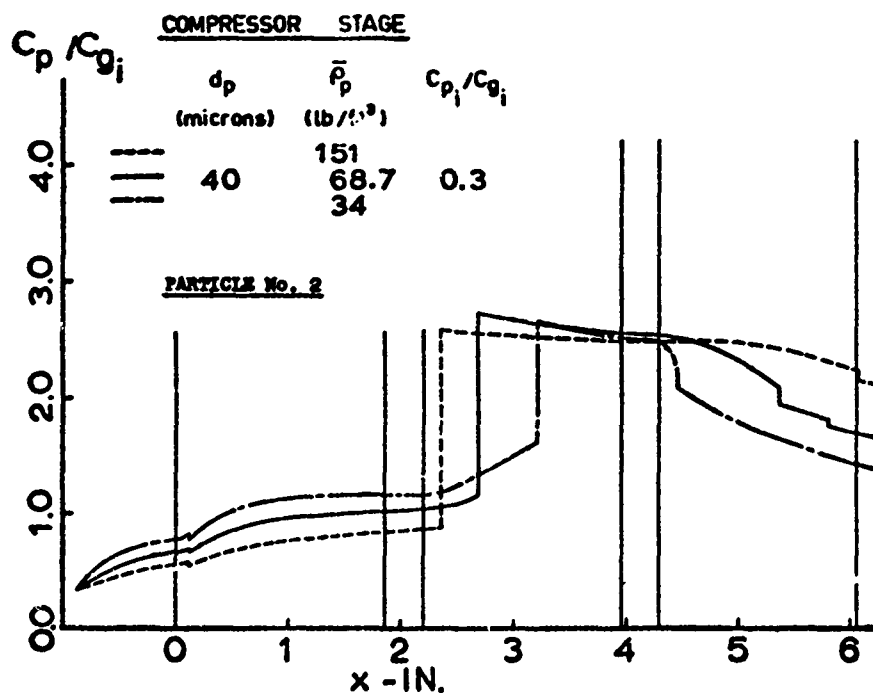


FIGURE 48 PARTICLE NONDIMENSIONAL ABSOLUTE VELOCITIES (EFFECT OF $\bar{\rho}_p$)

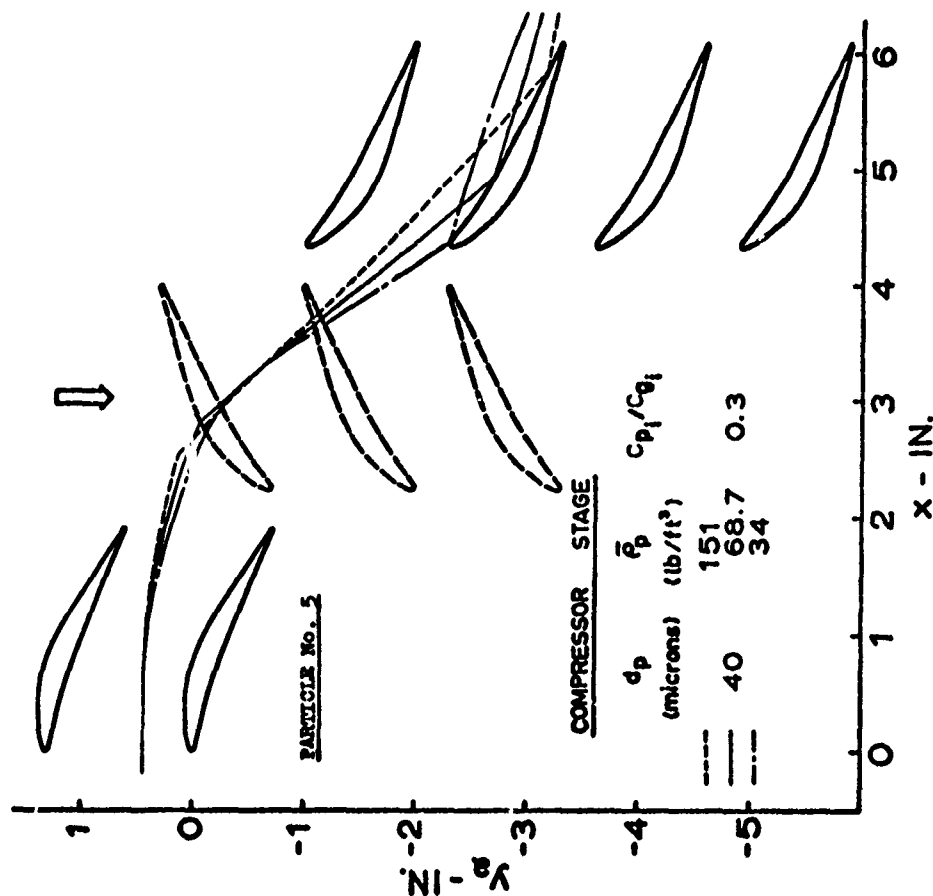


FIGURE 49 AXIAL AND TANGENTIAL COMPONENTS OF PARTICLE TRAJECTORIES (EFFECT OF $\bar{\rho}_p$)

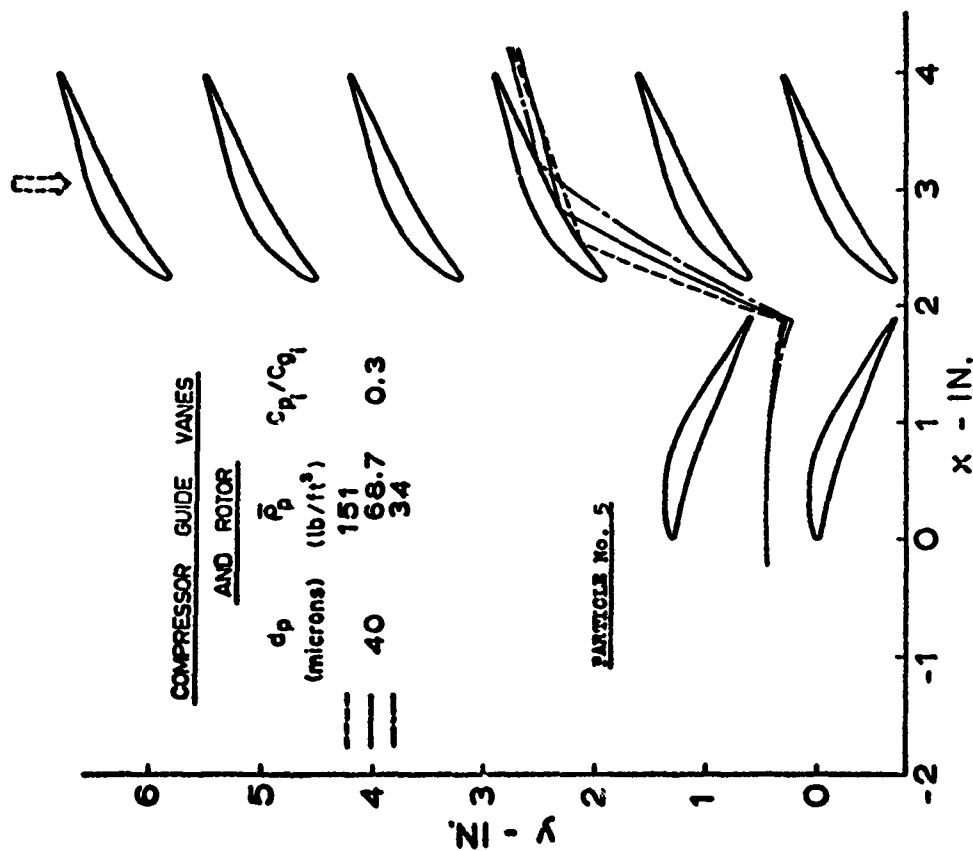


FIGURE 50 AXIAL AND TANGENTIAL COMPONENTS OF PARTICLE TRAJECTORIES RELATIVE TO THE ROTOR BLADES (EFFECT OF $\bar{\rho}_p$)

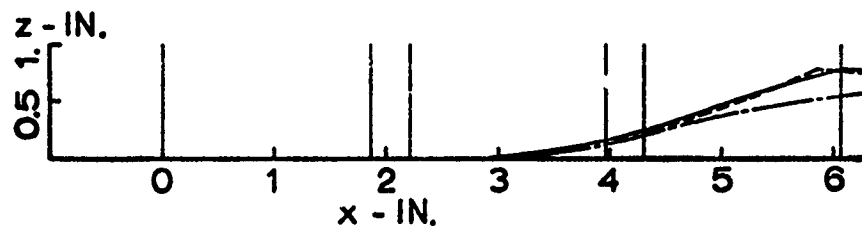


FIGURE 51 AXIAL AND RADIAL COMPONENTS OF PARTICLE TRAJECTORIES

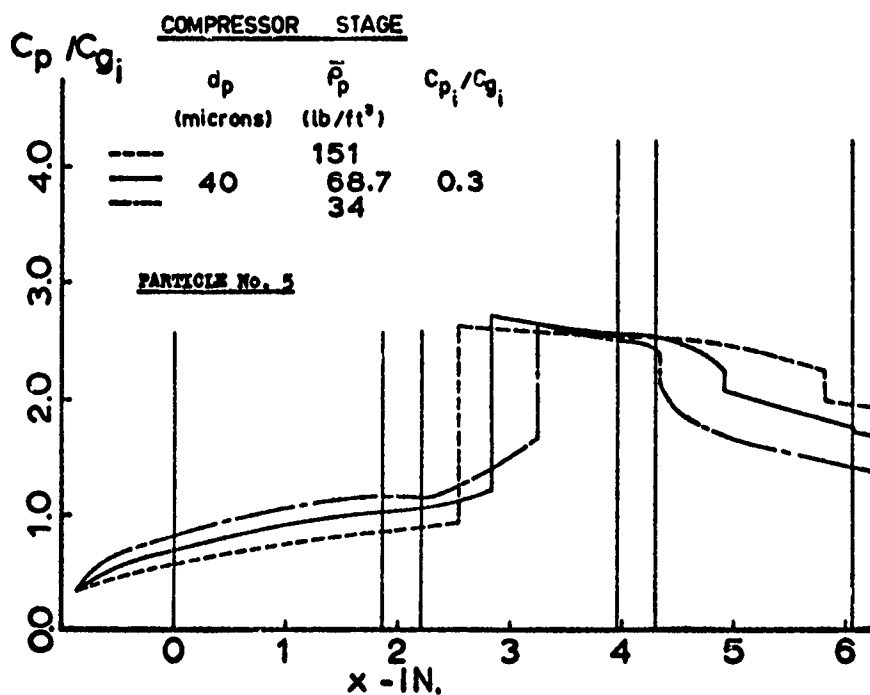


FIGURE 52 PARTICLE NONDIMENSIONAL ABSOLUTE VELOCITIES (EFFECT OF \bar{p}_p)

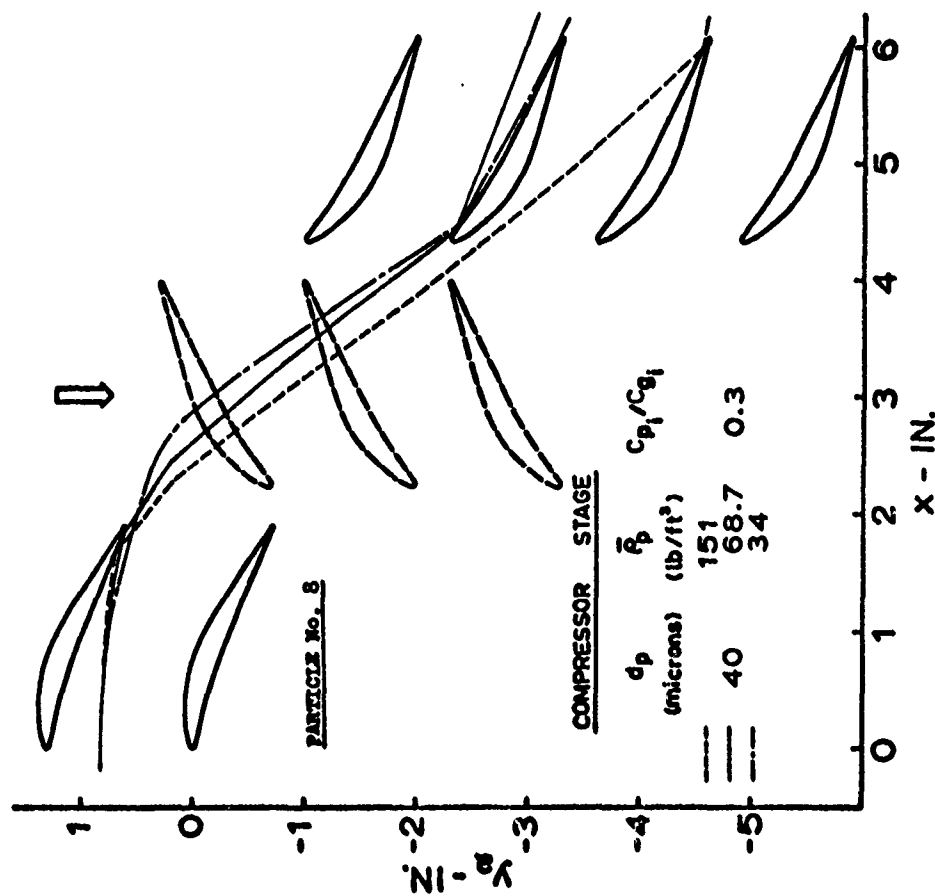


FIGURE 53 AXIAL AND TANGENTIAL COMPONENTS OF PARTICLE TRAJECTORIES (EFFECT OF $\bar{\rho}_p$)

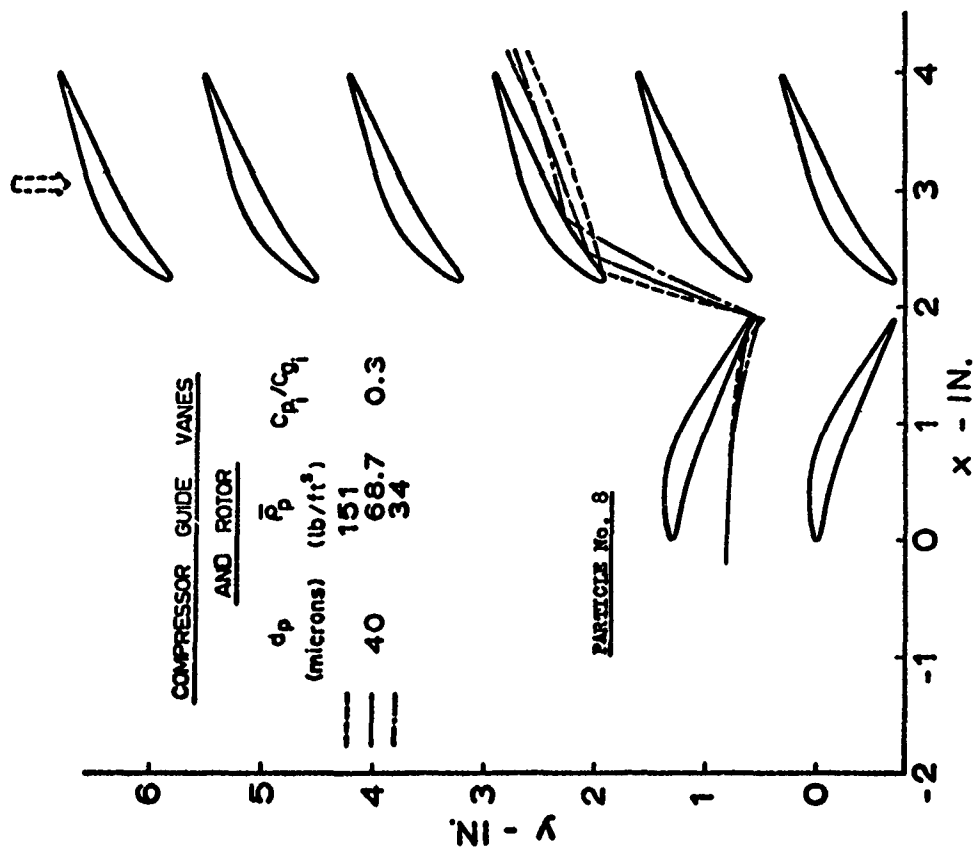


FIGURE 54 AXIAL AND TANGENTIAL COMPONENTS OF PARTICLE TRAJECTORIES RELATIVE TO THE ROTOR BLADES (EFFECT OF $\bar{\rho}_p$)

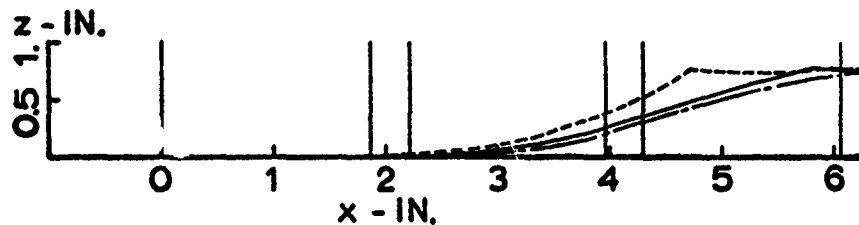


FIGURE 55 AXIAL AND RADIAL COMPONENTS OF PARTICLE TRAJECTORIES

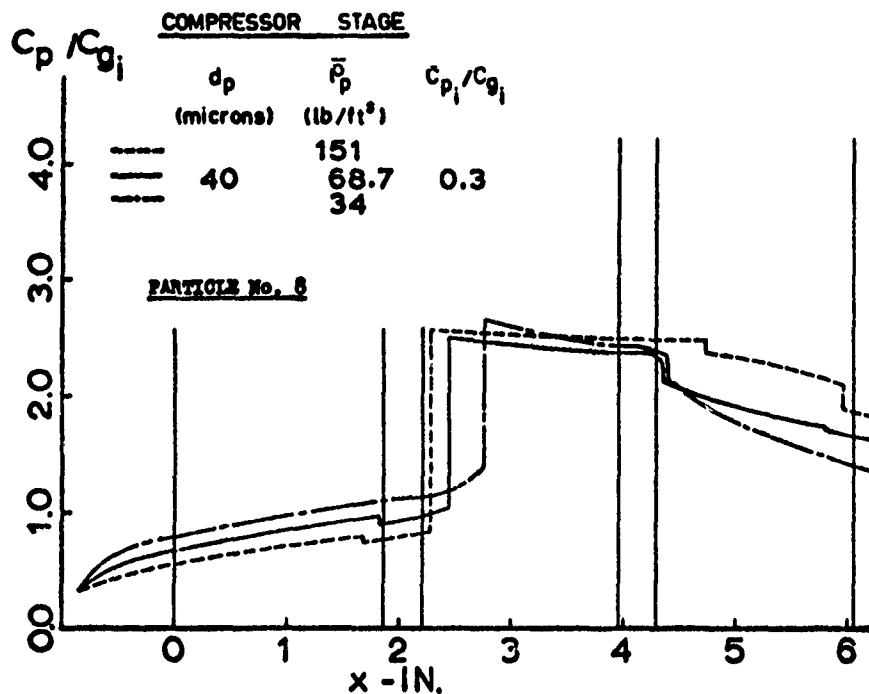


FIGURE 56 PARTICLE NONDIMENSIONAL ABSOLUTE VELOCITIES (EFFECT OF \bar{p}_p)

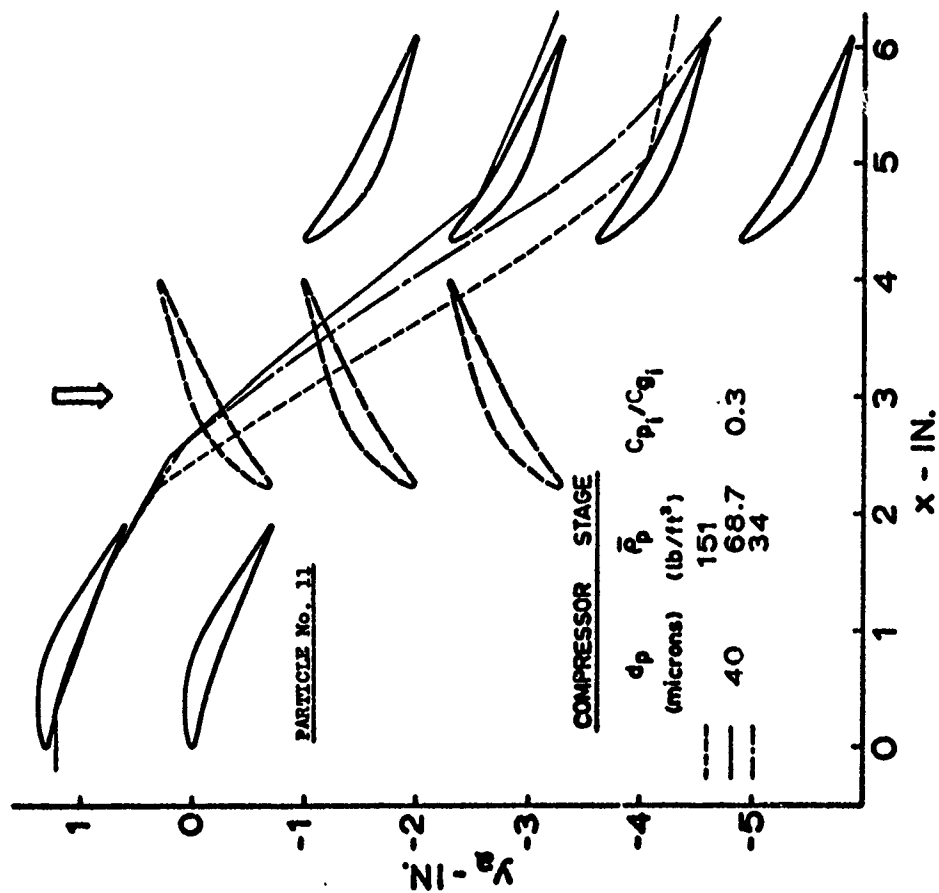


FIGURE 57 AXIAL AND TANGENTIAL COMPONENTS OF PARTICLE TRAJECTORIES (EFFECT OF \bar{p}_p)

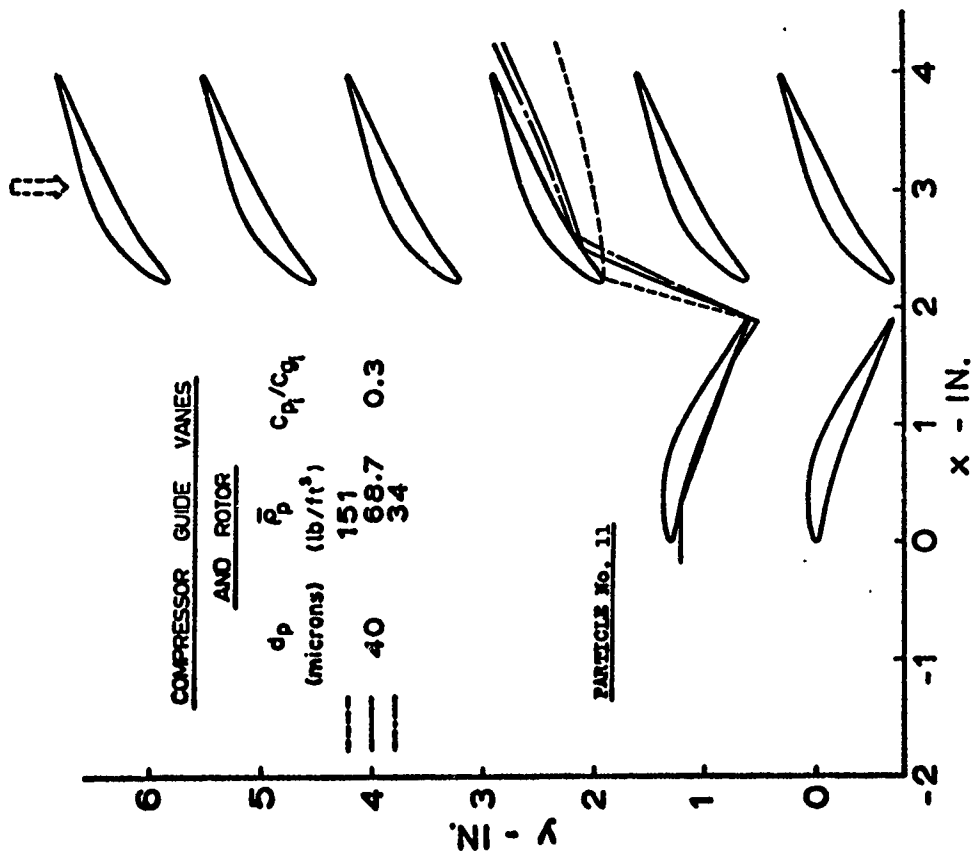


FIGURE 58 AXIAL AND TANGENTIAL COMPONENTS OF PARTICLE TRAJECTORIES RELATIVE TO THE ROTOR BLADES (EFFECT OF \bar{p}_p)

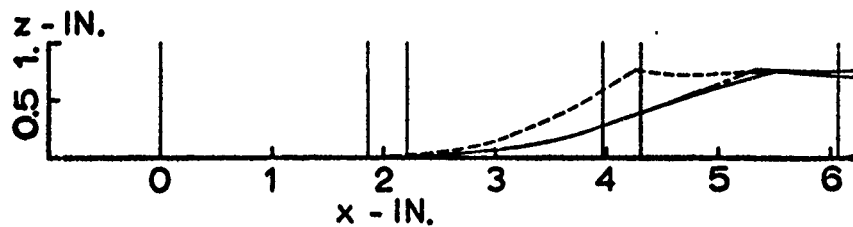


FIGURE 59 AXIAL AND RADIAL COMPONENTS OF PARTICLE TRAJECTORIES

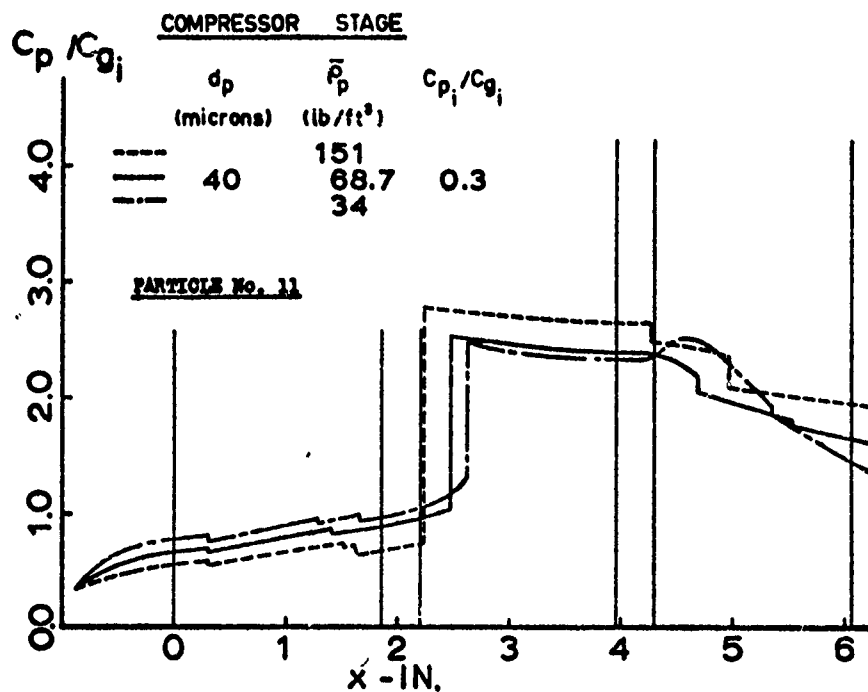


FIGURE 60 PARTICLE NONDIMENSIONAL ABSOLUTE VELOCITIES (EFFECT OF $\bar{\rho}_p$)

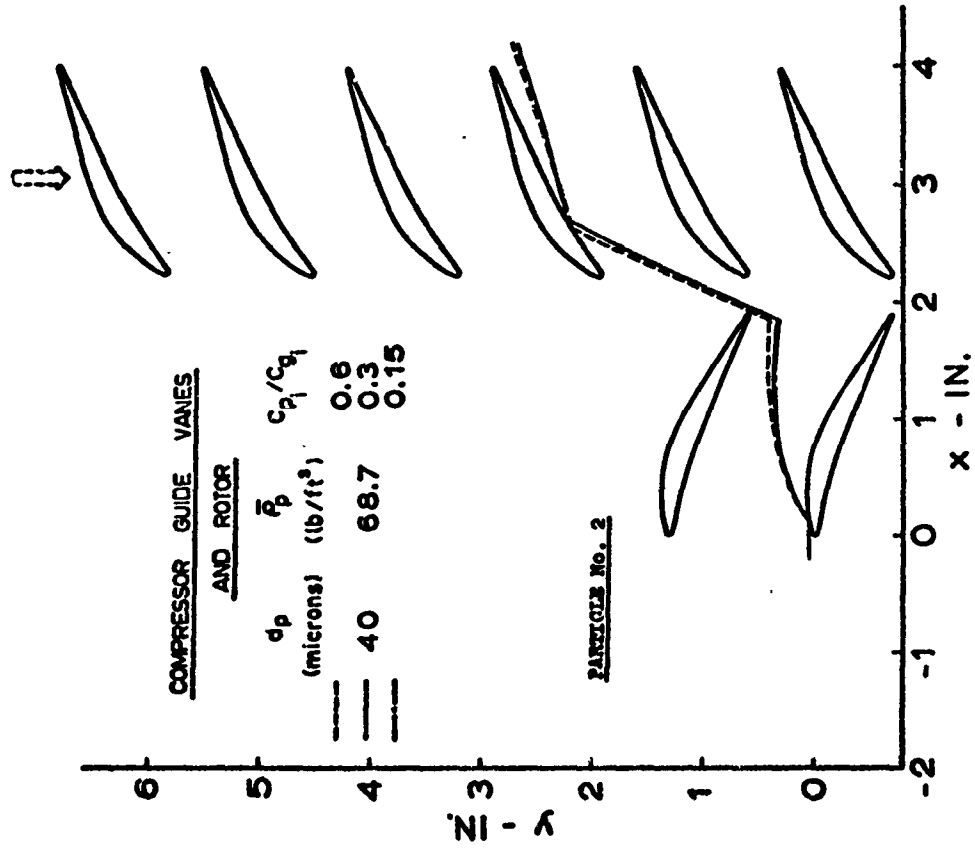


FIGURE 61 AXIAL AND TANGENTIAL COMPONENTS OF PARTICLE TRAJECTORIES (EFFECT OF c_{p1}/c_{g1})

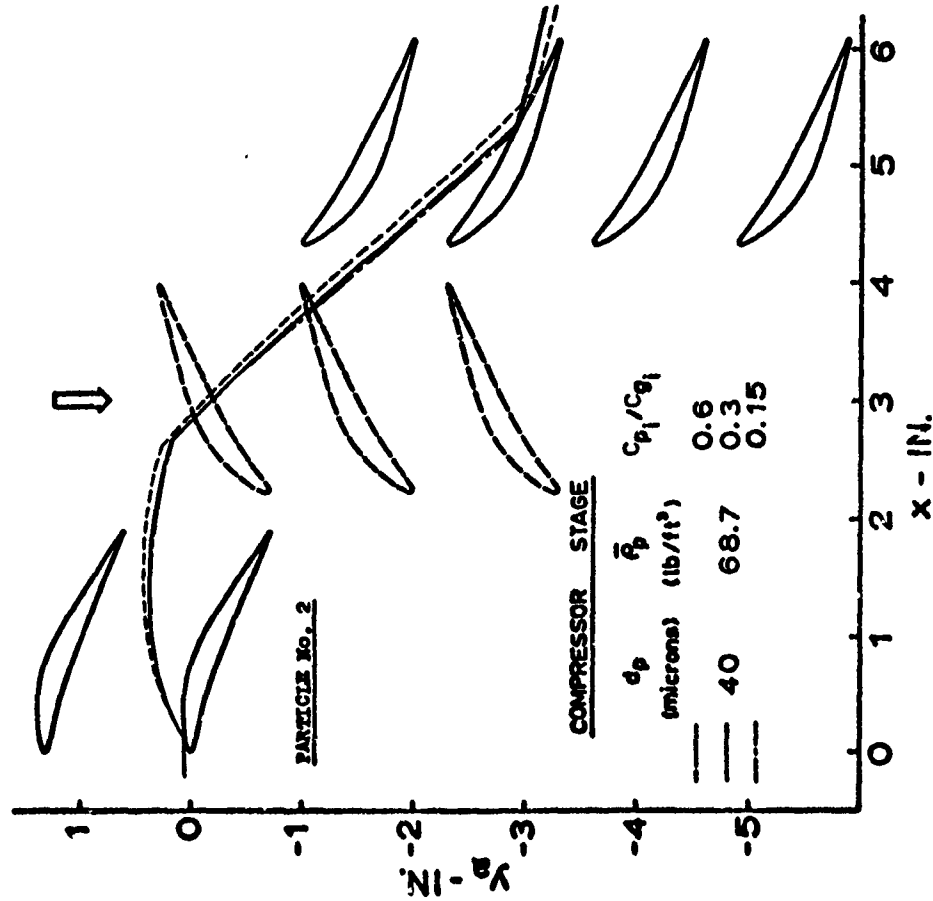


FIGURE 62 AXIAL AND TANGENTIAL COMPONENTS OF PARTICLE TRAJECTORIES (EFFECT OF c_{p1}/c_{g1})

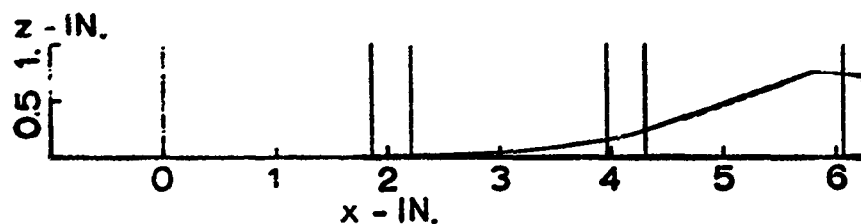


FIGURE 63 AXIAL AND RADIAL COMPONENTS OF PARTICLE TRAJECTORIES

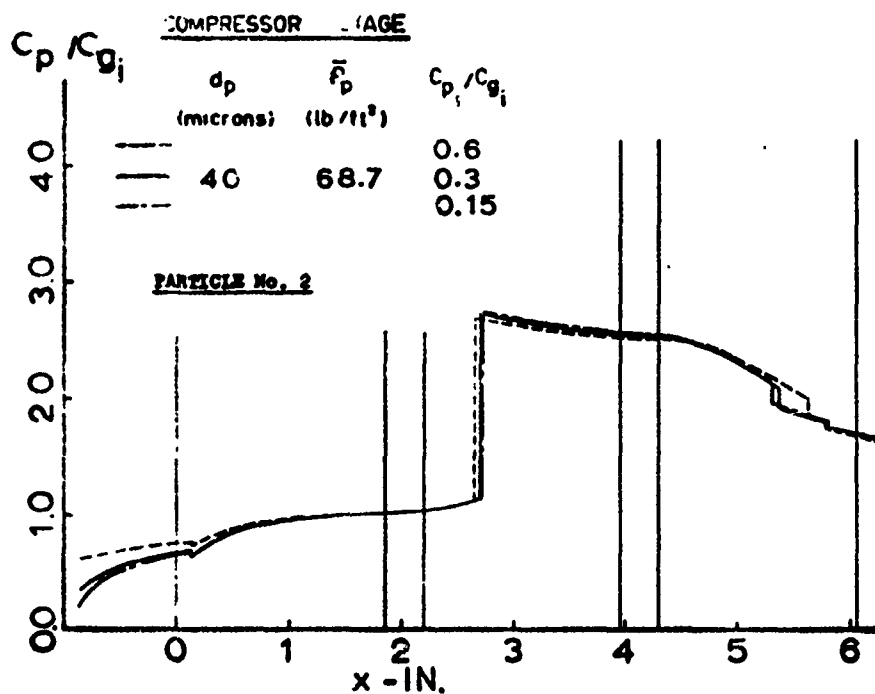


FIGURE 64 PARTICLE NONDIMENSIONAL ABSOLUTE VELOCITIES (EFFECT OF C_{p_i}/C_{g_i})

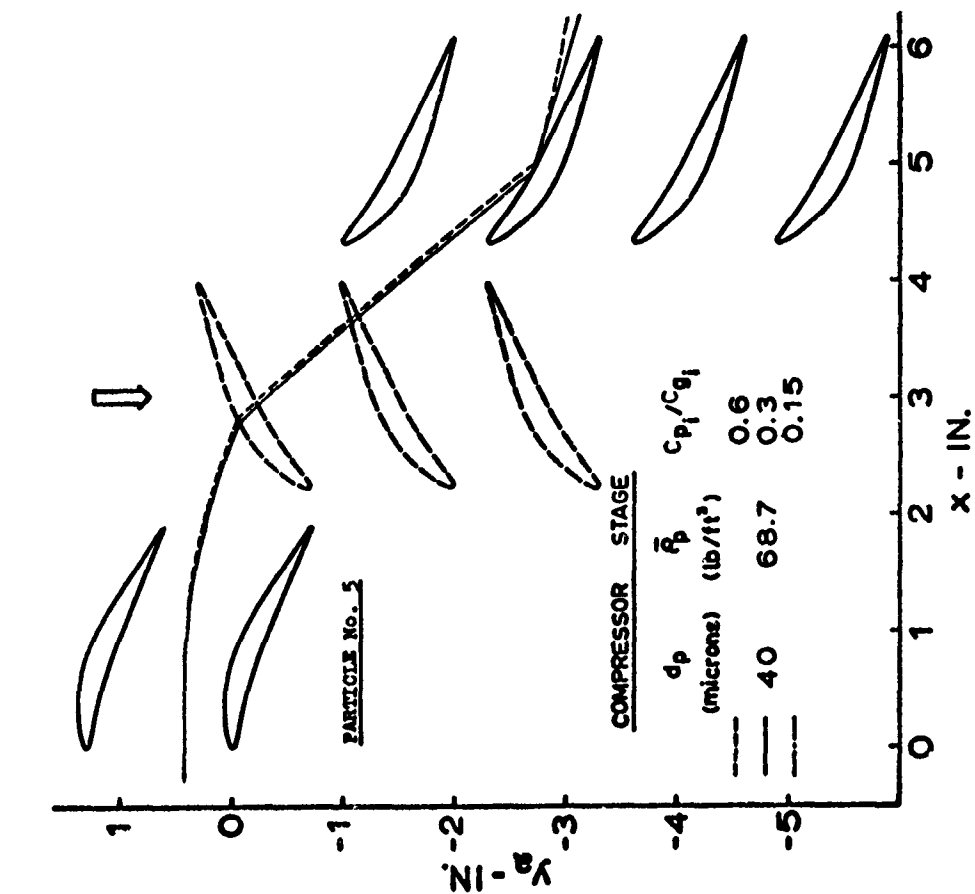


FIGURE 65 AXIAL AND TANGENTIAL COMPONENTS OF PARTICLE TRAJECTORIES (EFFECT OF C_{p1}/C_{g1})

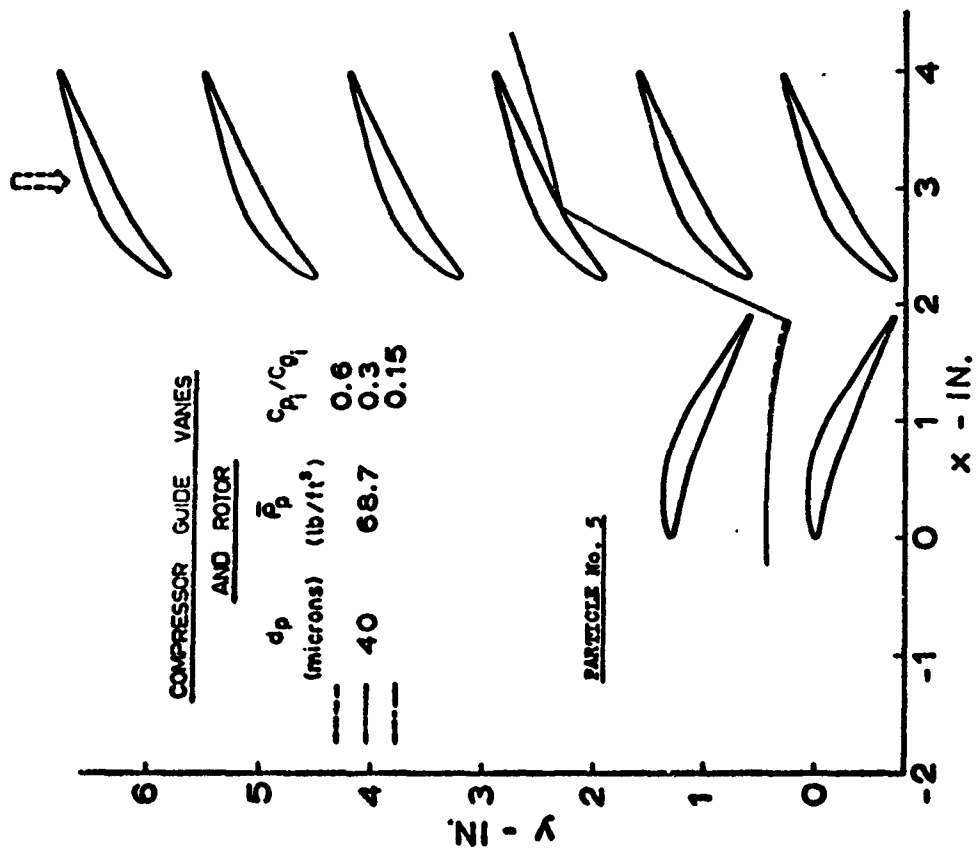


FIGURE 66 AXIAL AND TANGENTIAL COMPONENTS OF PARTICLE TRAJECTORIES RELATIVE TO THE ROTOR BLADES (EFFECT OF C_{p1}/C_{g1})

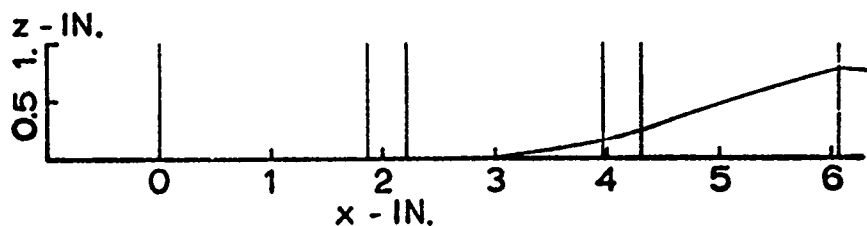


FIGURE 67 AXIAL AND RADIAL COMPONENTS OF PARTICLE TRAJECTORIES

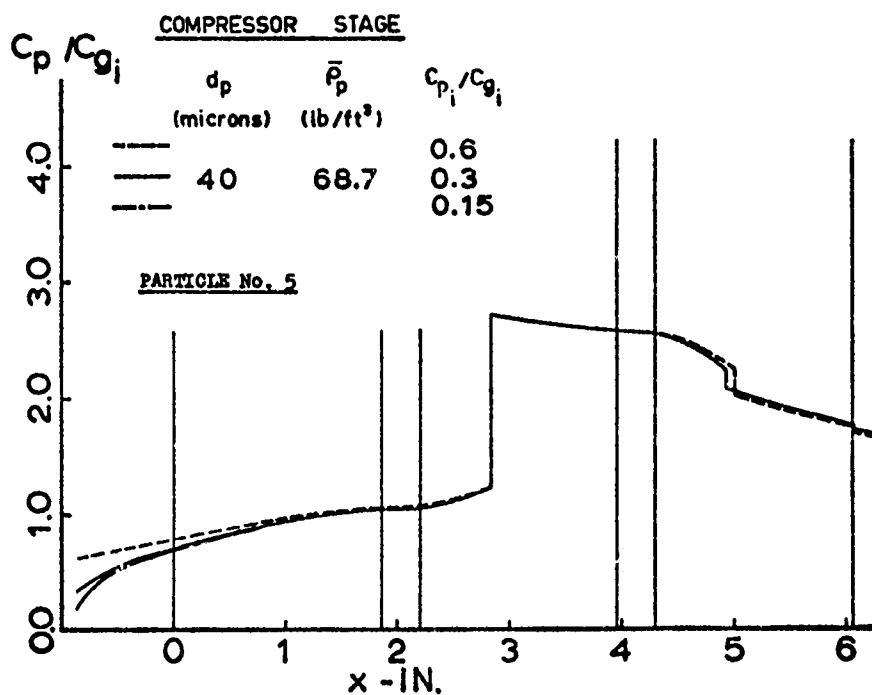


FIGURE 68 PARTICLE NONDIMENSIONAL ABSOLUTE VELOCITIES (EFFECT OF C_{p_i} / C_{g_i})

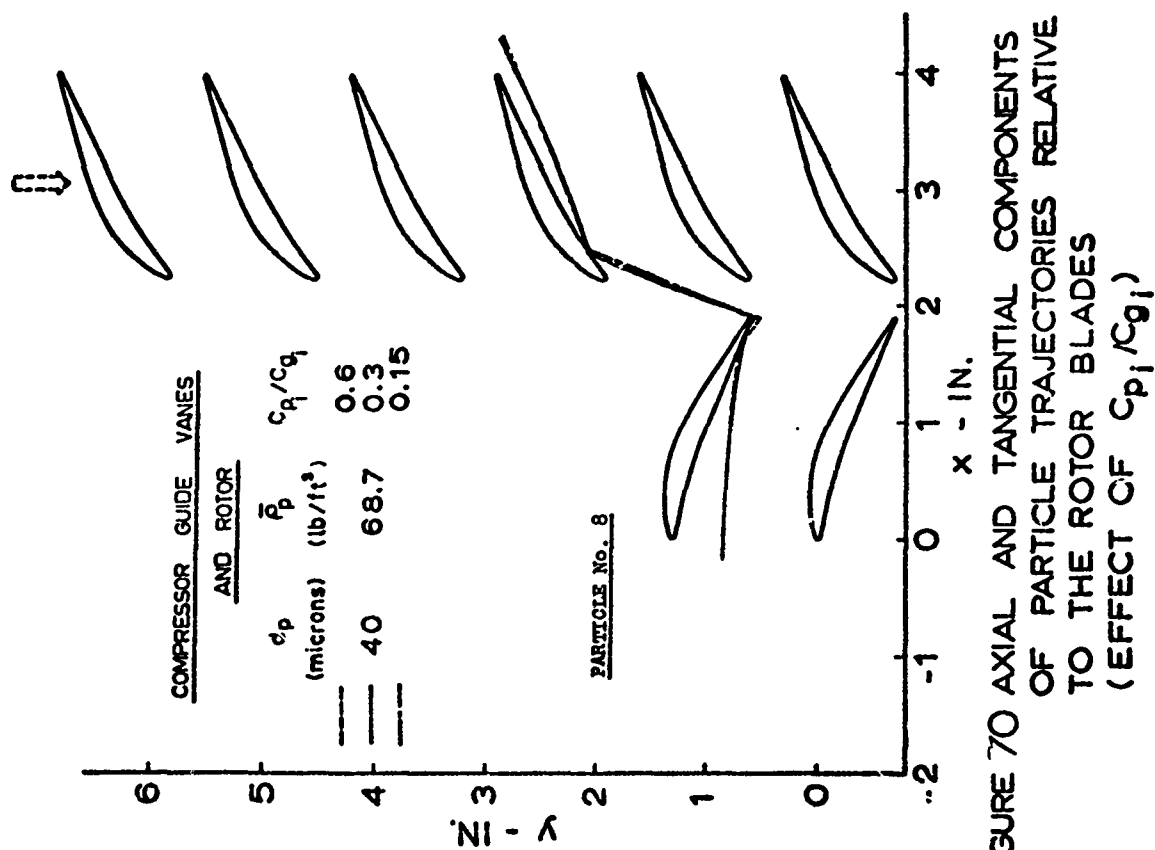


FIGURE 69 AXIAL AND TANGENTIAL COMPONENTS OF PARTICLE TRAJECTORIES RELATIVE TO THE ROTOR BLADES (EFFECT OF C_{p1}/C_{g1})

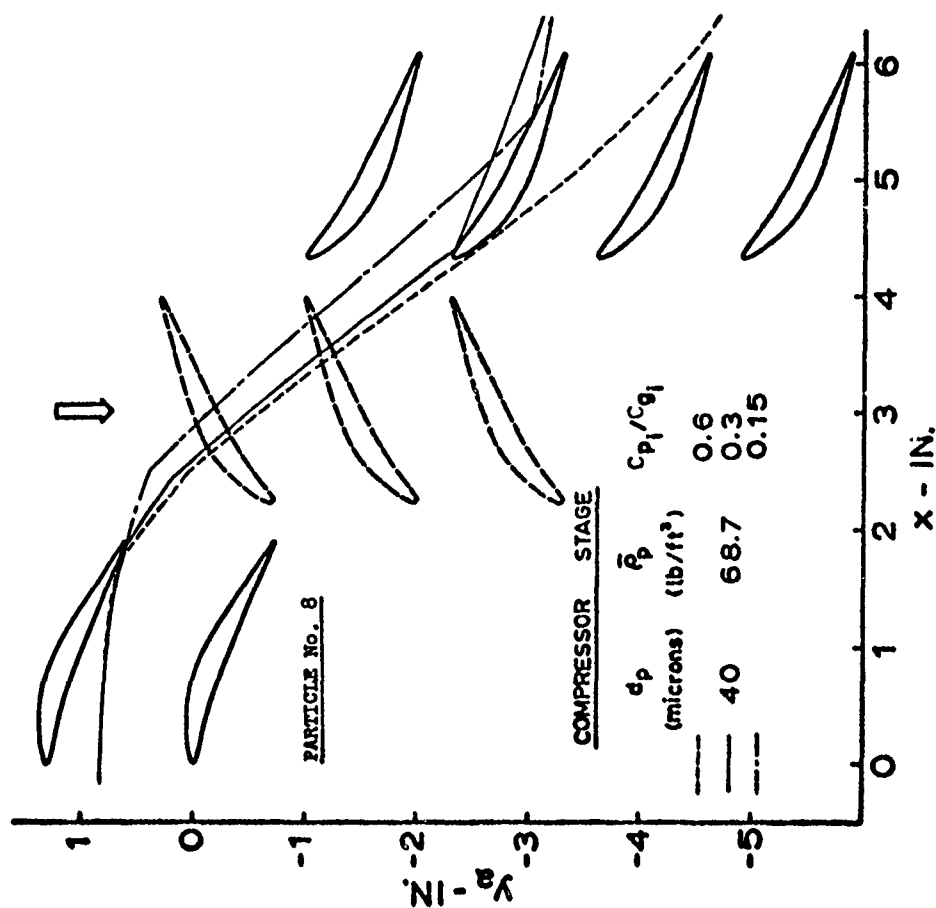


FIGURE 70 AXIAL AND TANGENTIAL COMPONENTS OF PARTICLE TRAJECTORIES RELATIVE TO THE ROTOR BLADES (EFFECT OF C_{p1}/C_{g1})

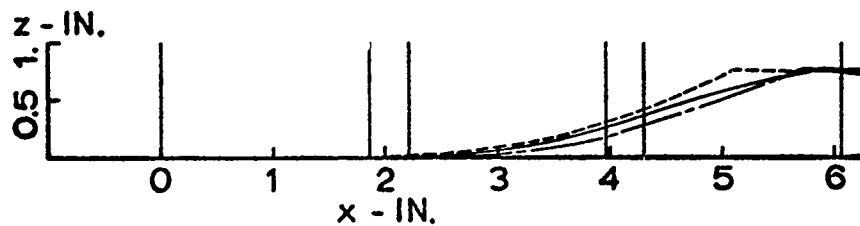


FIGURE 71 AXIAL AND RADIAL COMPONENTS OF PARTICLE TRAJECTORIES

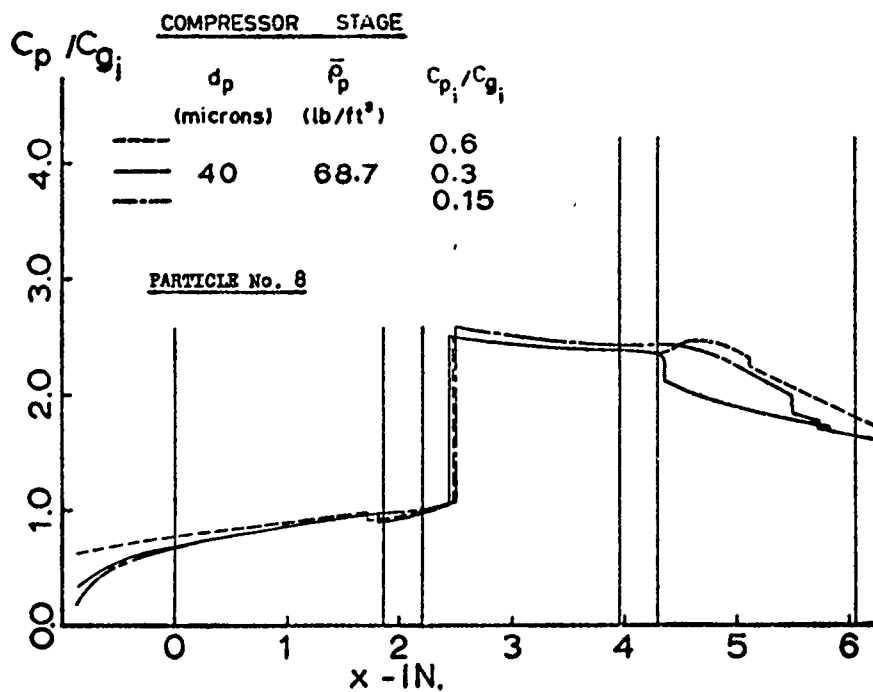


FIGURE 72 PARTICLE NONDIMENSIONAL ABSOLUTE VELOCITIES (EFFECT OF C_{p_i}/C_{g_i})

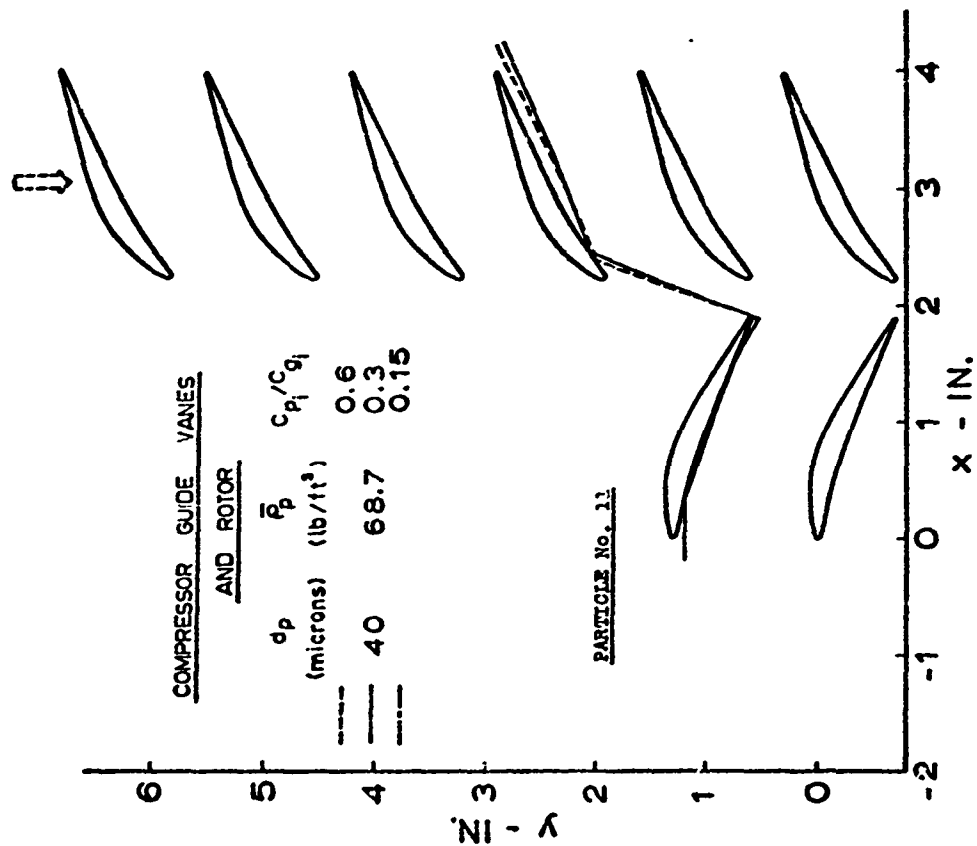


FIGURE 73 AXIAL AND TANGENTIAL COMPONENTS OF PARTICLE TRAJECTORIES RELATIVE TO THE ROTOR BLADES (EFFECT OF C_{p1}/C_{g1})

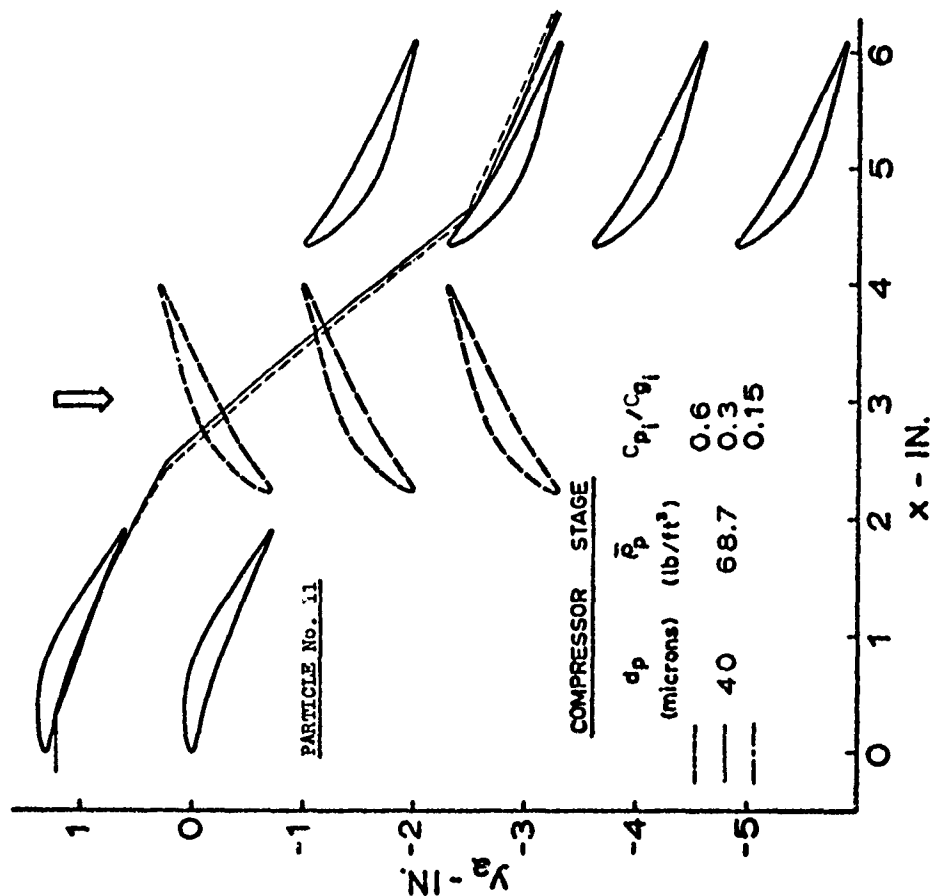


FIGURE 74 AXIAL AND TANGENTIAL COMPONENTS OF PARTICLE TRAJECTORIES RELATIVE TO THE ROTOR BLADES (EFFECT OF C_{p1}/C_{g1})

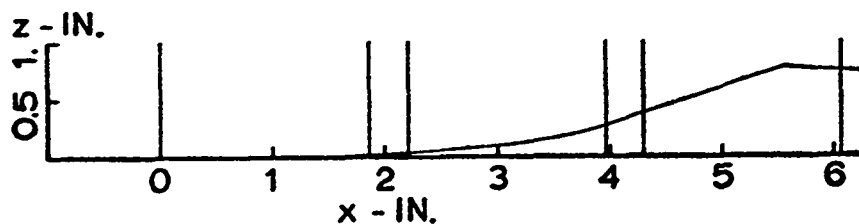


FIGURE 75 AXIAL AND RADIAL COMPONENTS OF PARTICLE TRAJECTORIES

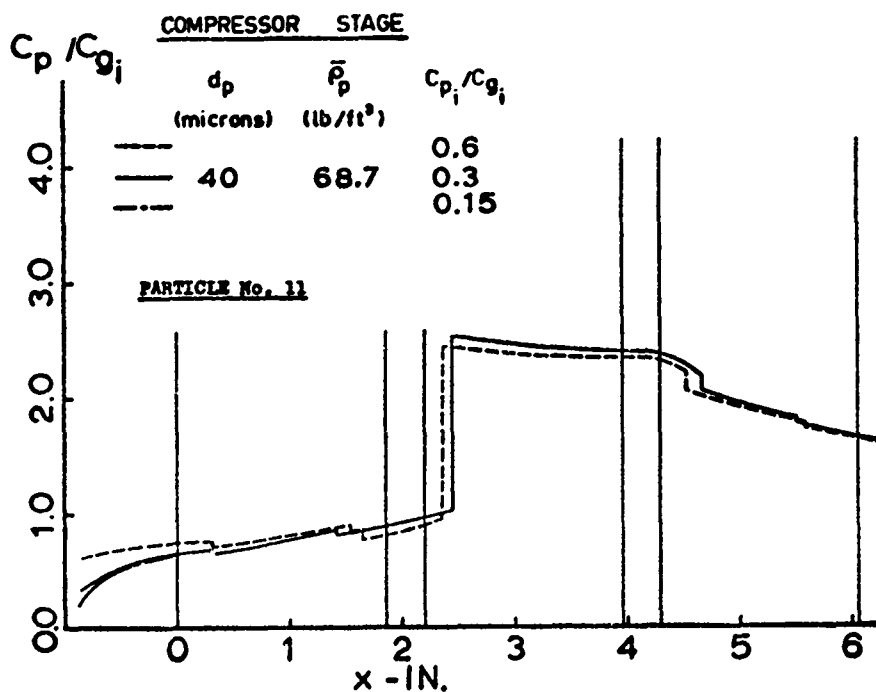


FIGURE 76 PARTICLE NONDIMENSIONAL ABSOLUTE VELOCITIES (EFFECT OF C_{p_i}/C_{g_i})

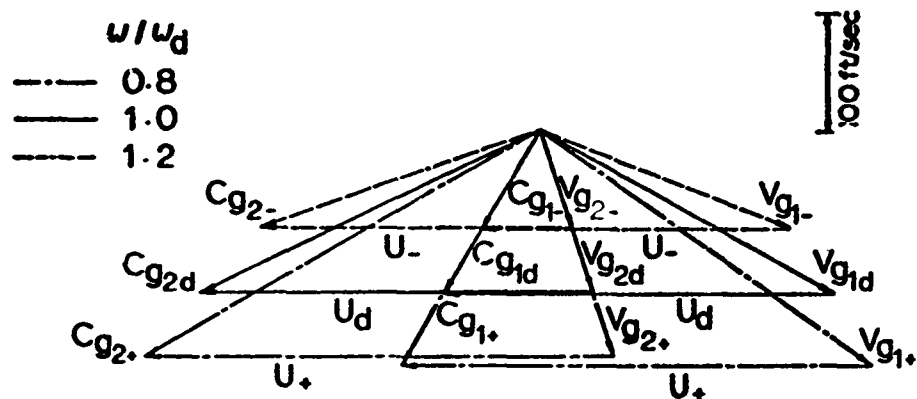


FIGURE 77 COMBINED GAS VELOCITY DIAGRAM FOR DESIGN AND OFF DESIGN BLADE ANGULAR VELOCITY (COMPRESSOR STAGE)

	NEGATIVE OFF- DESIGN CONDITION	DESIGN CONDITION	POSITIVE OFF- DESIGN CONDITION
ω (radian/sec)	482.8	603.5	724.2
ω / ω_d	0.8	1.0	1.2
C_{g1} (ft/sec)	114.11	142.64	171.17
ρ_{g1} (lb/ft ³)	0.076	0.076	0.076
w_1 (lb/sec/channel)	0.074	0.123	0.172
C_{p1}/C_{g1}	0.3	0.3	0.3
C_{p1} (ft/sec)	34.2	42.8	51.4

TABLE 1

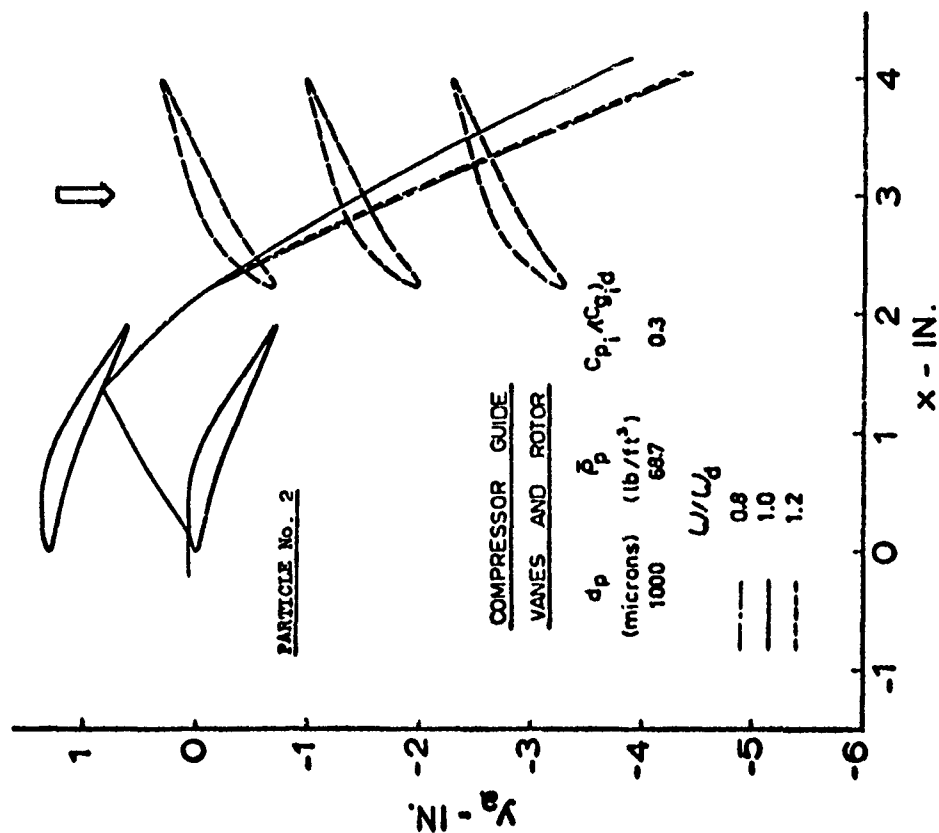


FIGURE 78 AXIAL AND TANGENTIAL COMPONENTS OF PARTICLE TRAJECTORIES (EFFECT OF U/U_d)

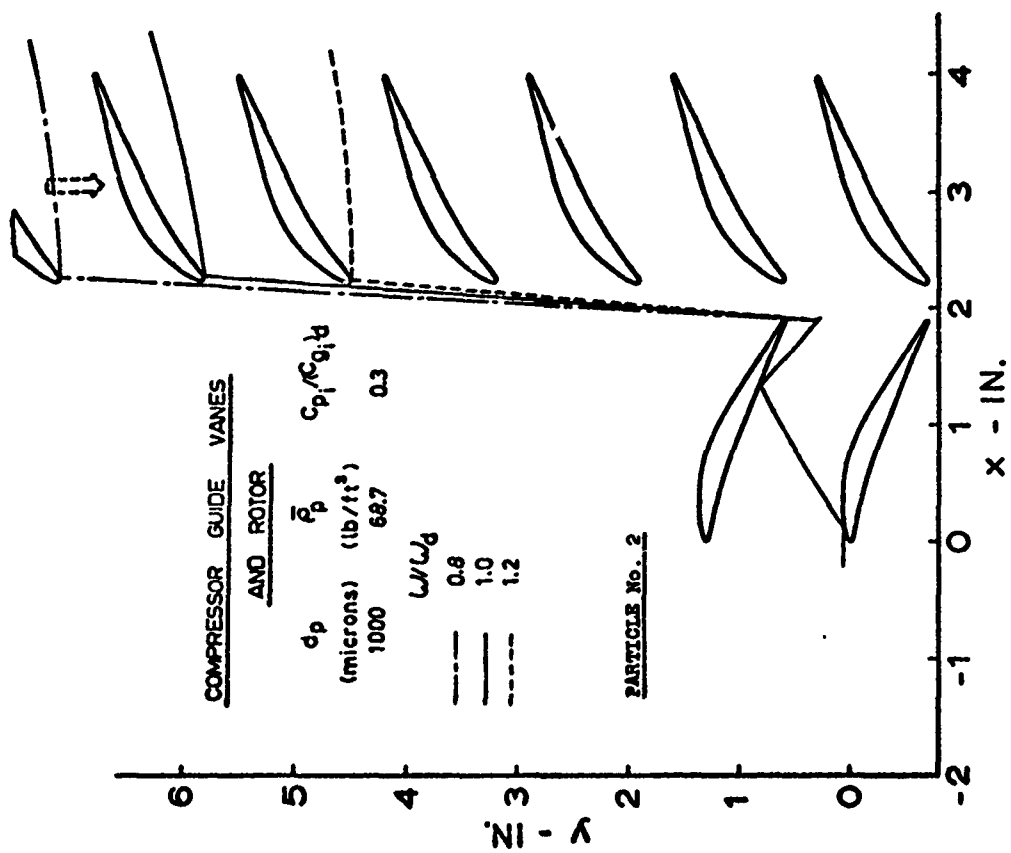


FIGURE 79 AXIAL AND TANGENTIAL COMPONENTS OF PARTICLE TRAJECTORIES RELATIVE TO THE ROTOR BLADES (EFFECT OF U/U_d)

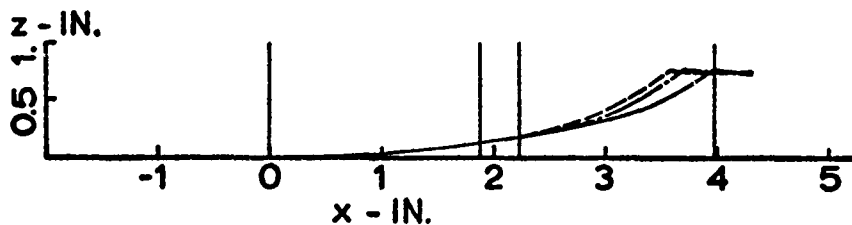


FIGURE 80 AXIAL AND RADIAL COMPONENTS OF PARTICLE TRAJECTORIES

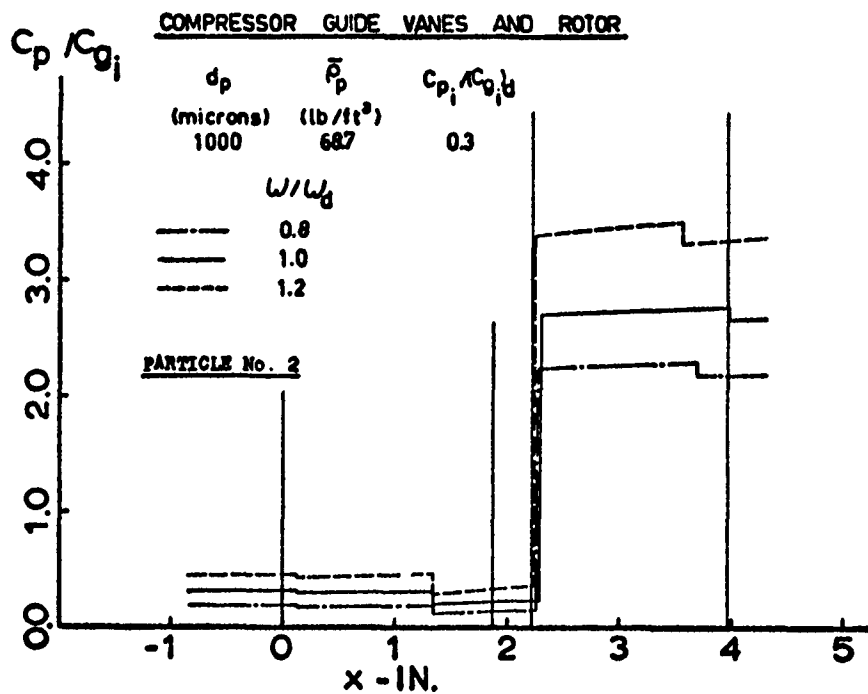


FIGURE 81 PARTICLE NONDIMENSIONAL ABSOLUTE VELOCITIES (EFFECT OF w/w_g)

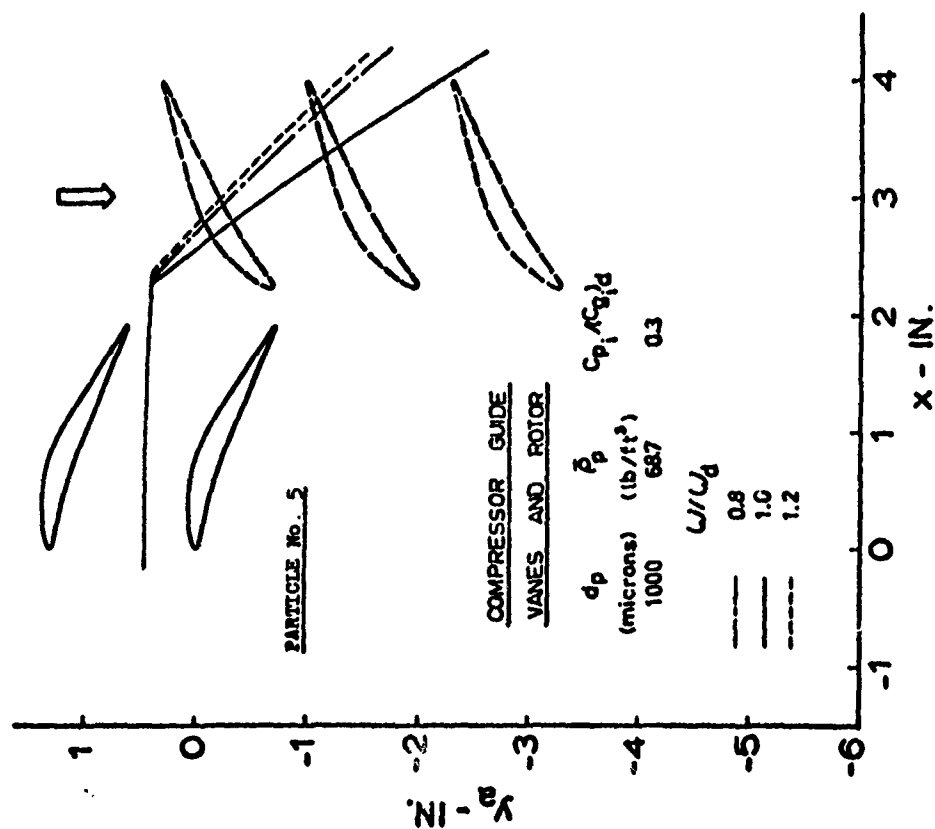


FIGURE 82 AXIAL AND TANGENTIAL COMPONENTS OF PARTICLE TRAJECTORIES (EFFECT OF w/w_d)

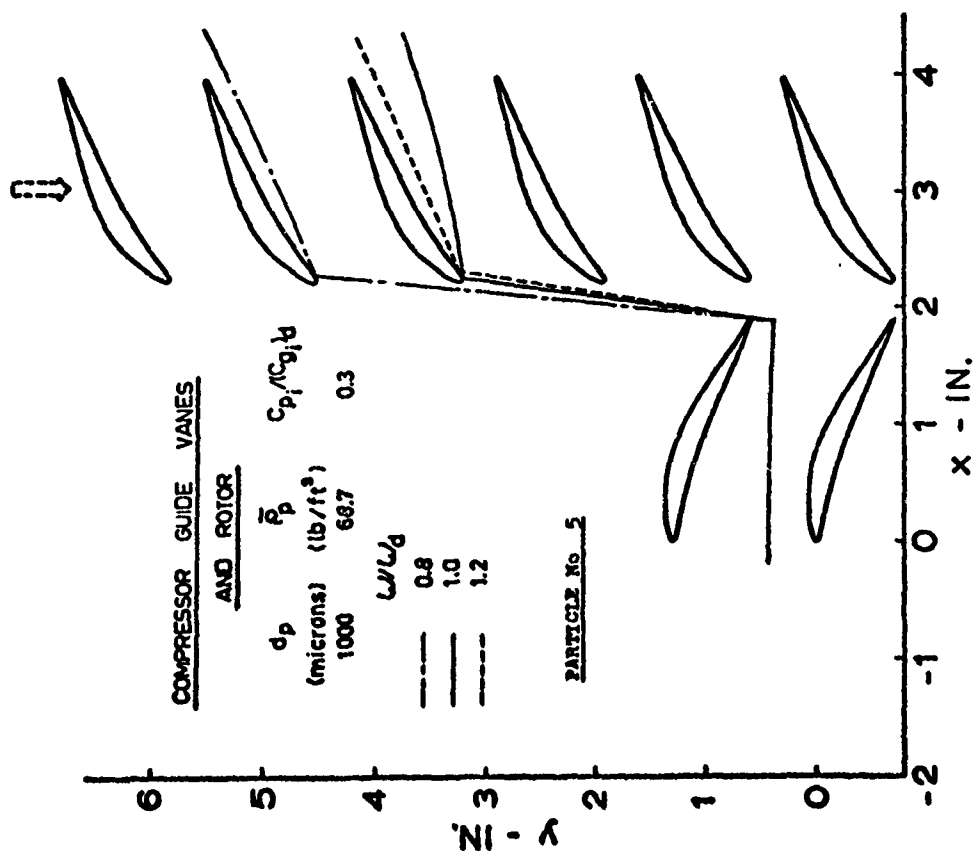


FIGURE 83 AXIAL AND TANGENTIAL COMPONENTS OF PARTICLE TRAJECTORIES RELATIVE TO THE ROTOR BLADES (EFFECT OF w/w_d)

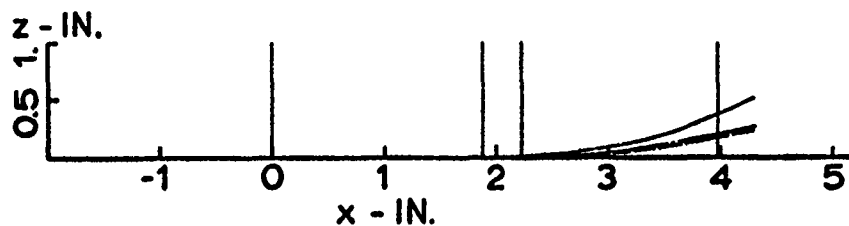


FIGURE 84 AXIAL AND RADIAL COMPONENTS OF PARTICLE TRAJECTORIES

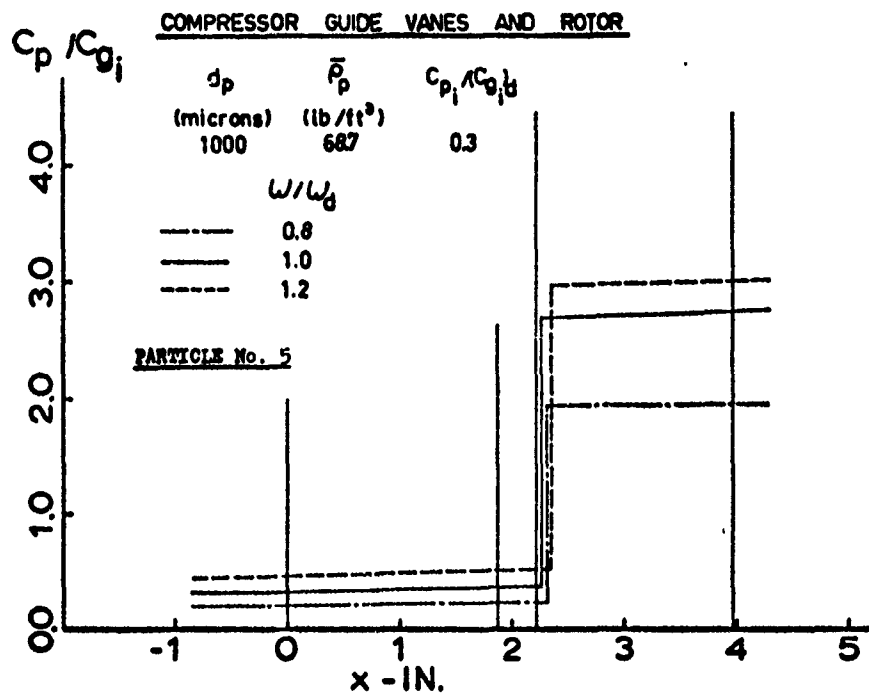


FIGURE 85 PARTICLE NONDIMENSIONAL ABSOLUTE VELOCITIES (EFFECT OF W/W_d)

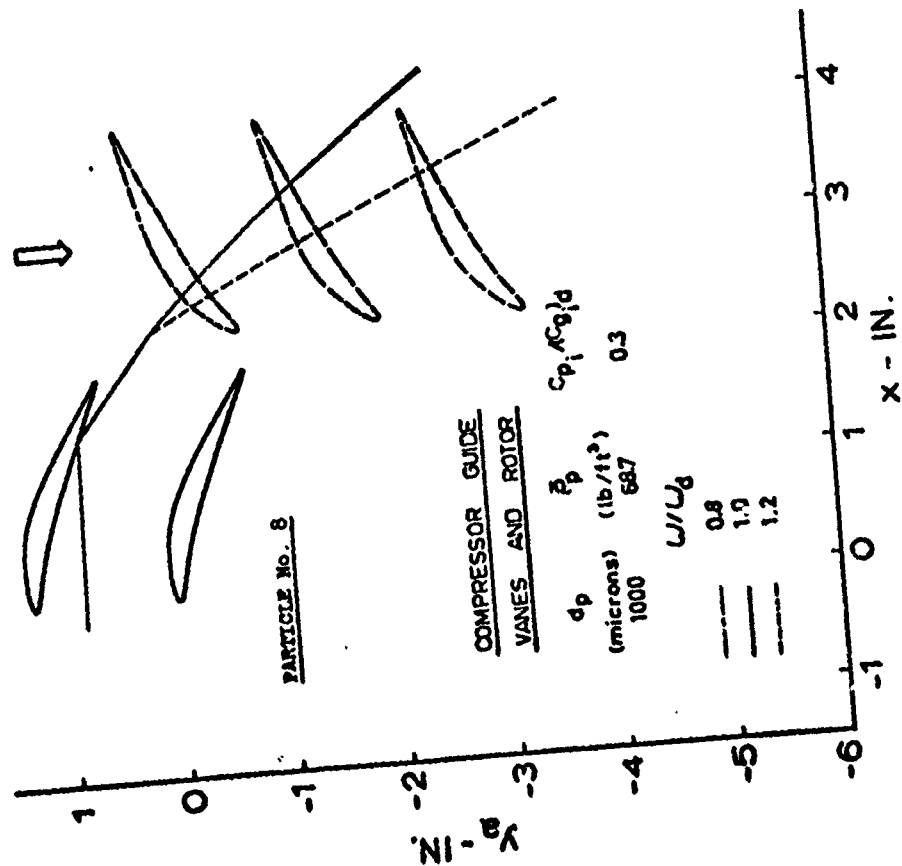


FIGURE 86 AXIAL AND TANGENTIAL COMPONENTS OF PARTICLE TRAJECTORIES (EFFECT OF U/U_d)

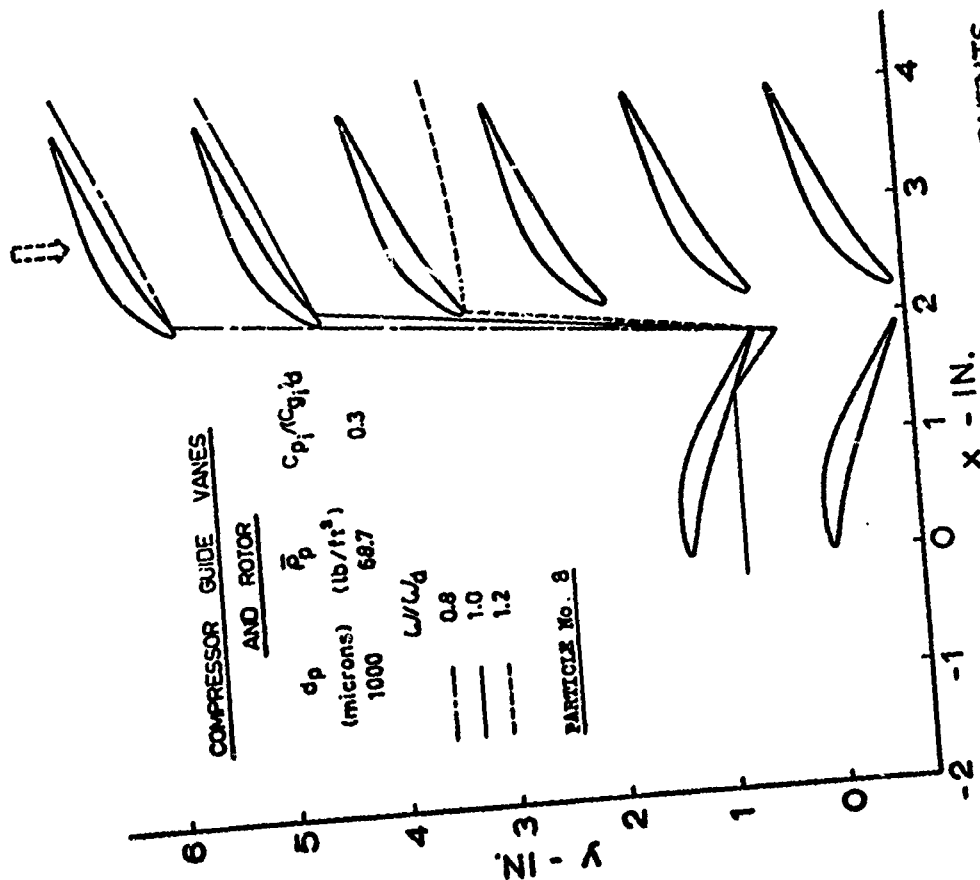


FIGURE 87 AXIAL AND TANGENTIAL COMPONENTS OF PARTICLE TRAJECTORIES RELATIVE TO THE ROTOR BLADES (EFFECT OF U/U_d)

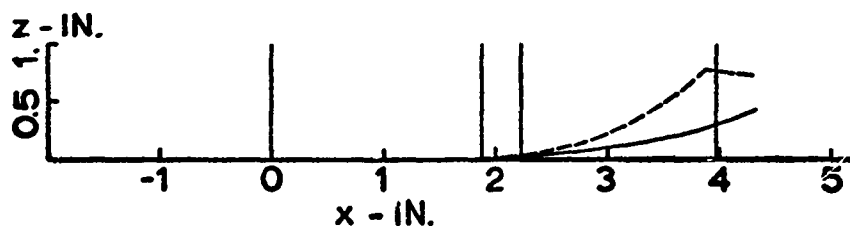


FIGURE 88 AXIAL AND RADIAL COMPONENTS OF PARTICLE TRAJECTORIES

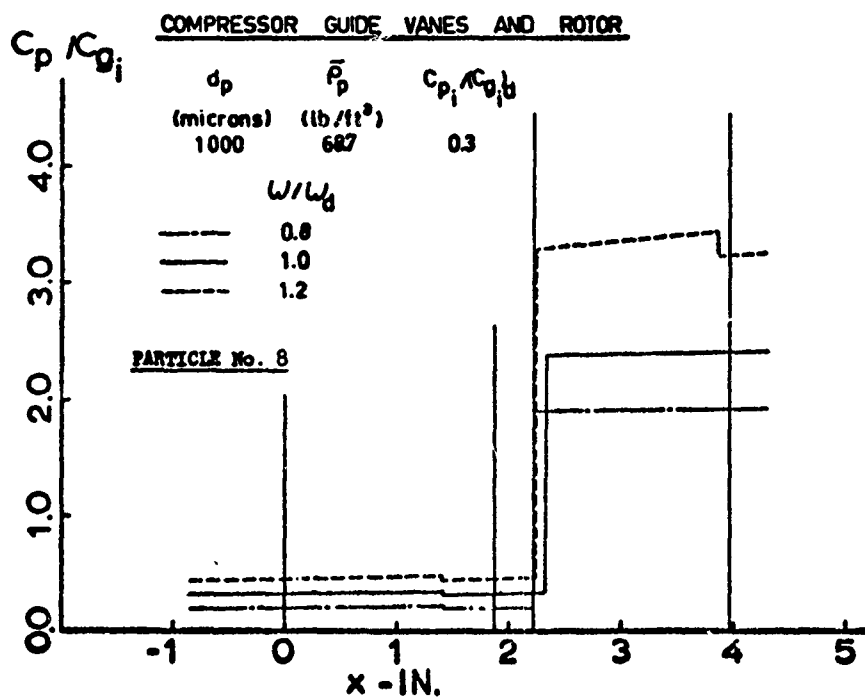


FIGURE 89 PARTICLE NONDIMENSIONAL ABSOLUTE VELOCITIES (EFFECT OF w/w_d)

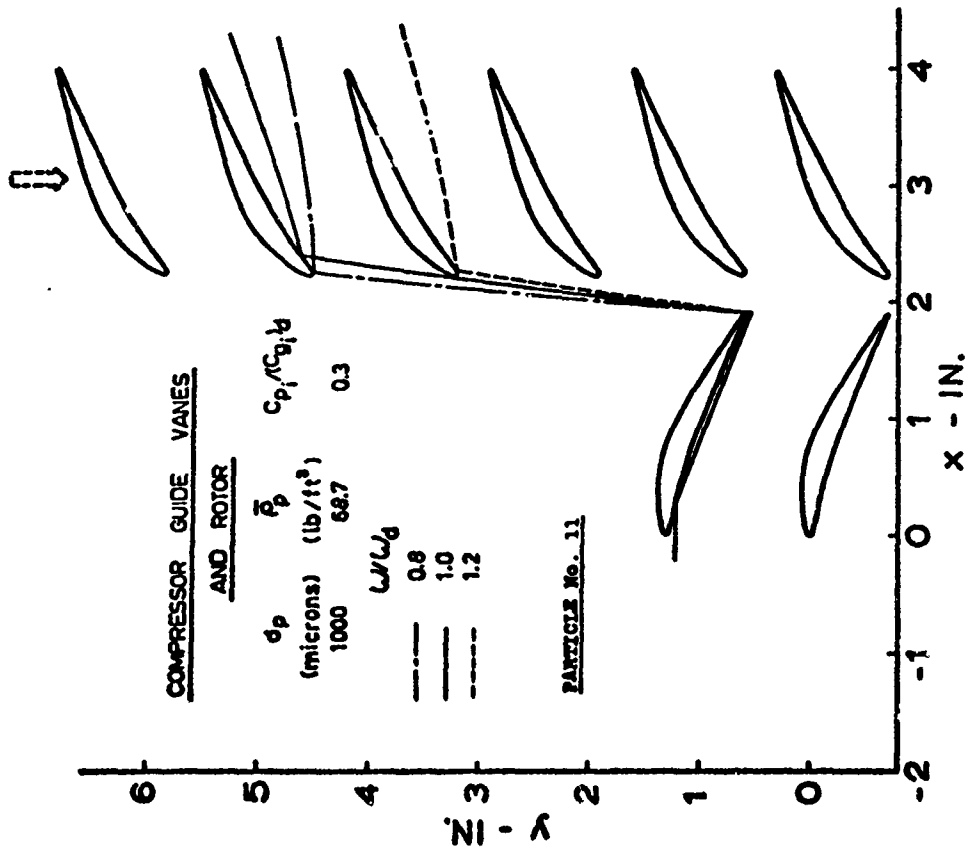


FIGURE 91 AXIAL AND TANGENTIAL COMPONENTS OF PARTICLE TRAJECTORIES RELATIVE TO THE ROTOR BLADES (EFFECT OF W/W_d)

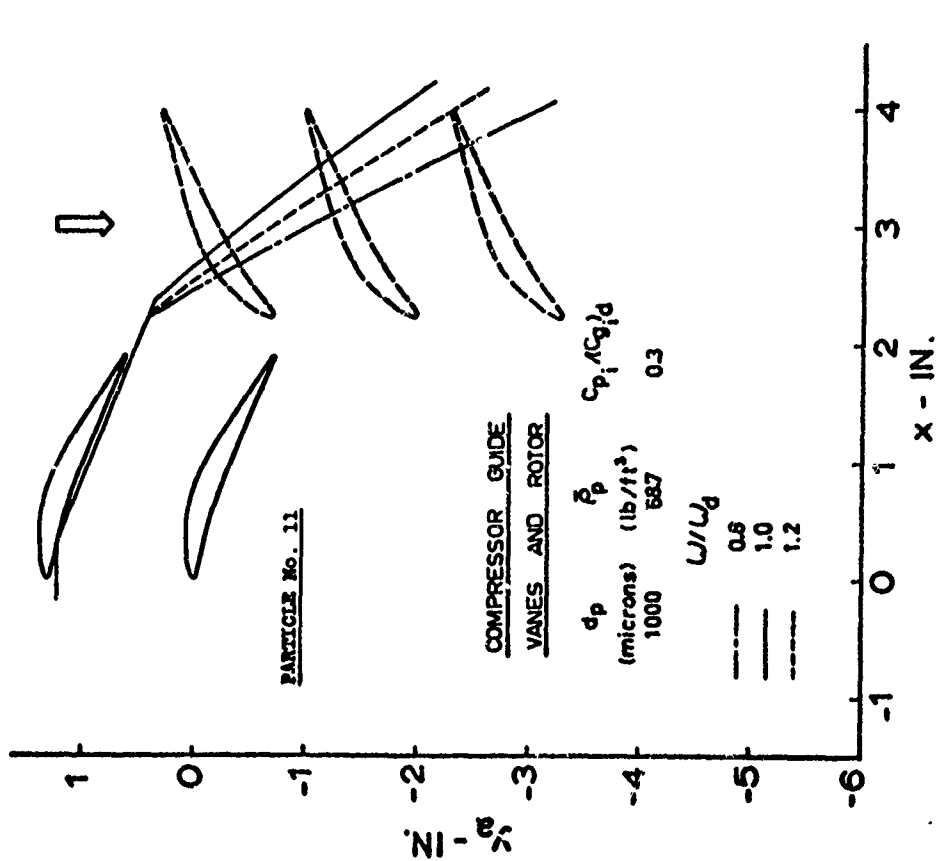


FIGURE 90 AXIAL AND TANGENTIAL COMPONENTS OF PARTICLE TRAJECTORIES (EFFECT OF W/W_d)

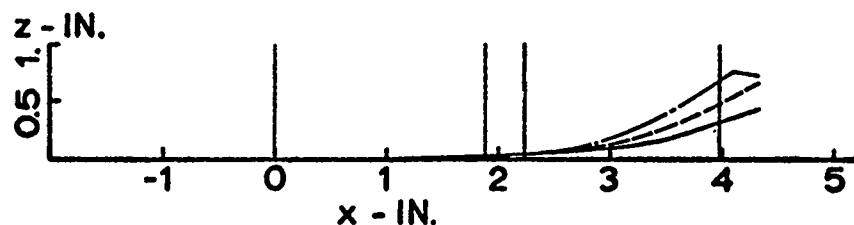


FIGURE 92 AXIAL AND RADIAL COMPONENTS OF PARTICLE TRAJECTORIES

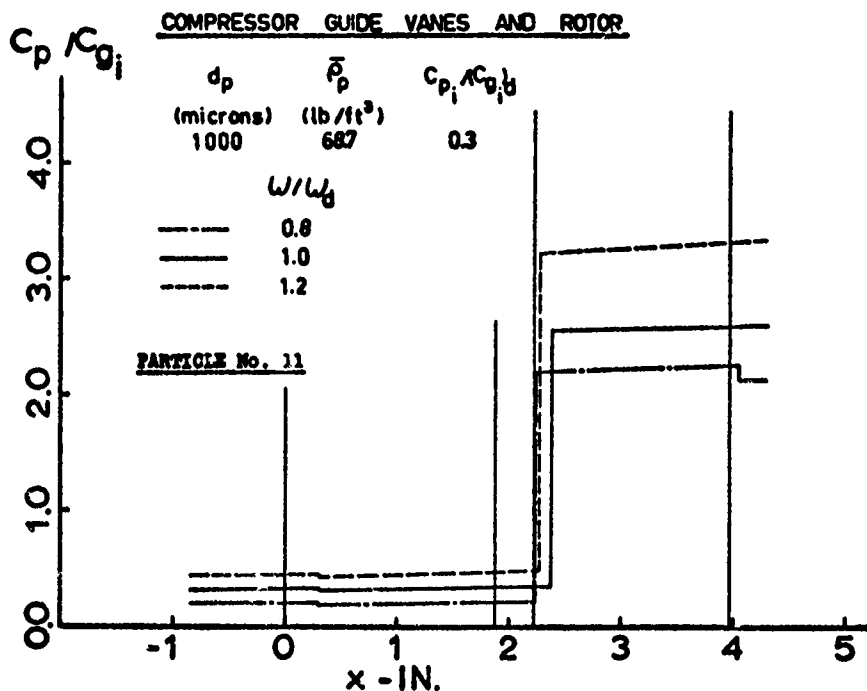


FIGURE 93 PARTICLE NONDIMENSIONAL ABSOLUTE VELOCITIES (EFFECT OF W/W_g)

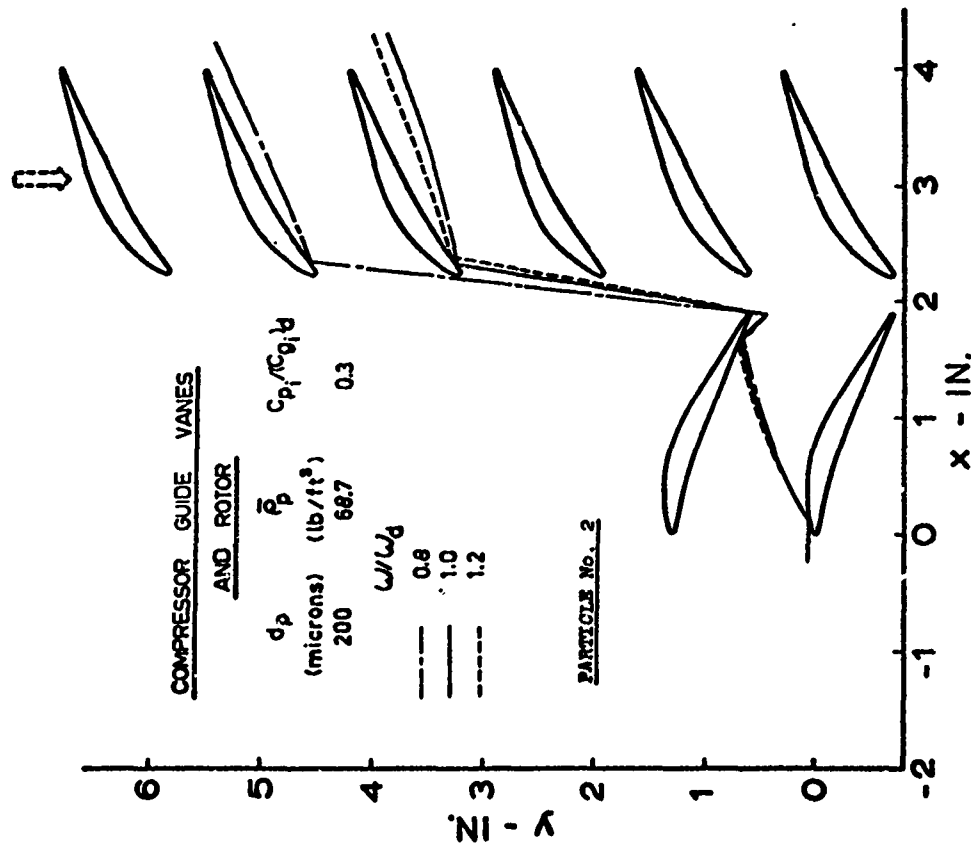


FIGURE 94 AXIAL AND TANGENTIAL COMPONENTS OF PARTICLE TRAJECTORIES RELATIVE TO THE ROTOR BLADES (EFFECT OF ω/ω_d)

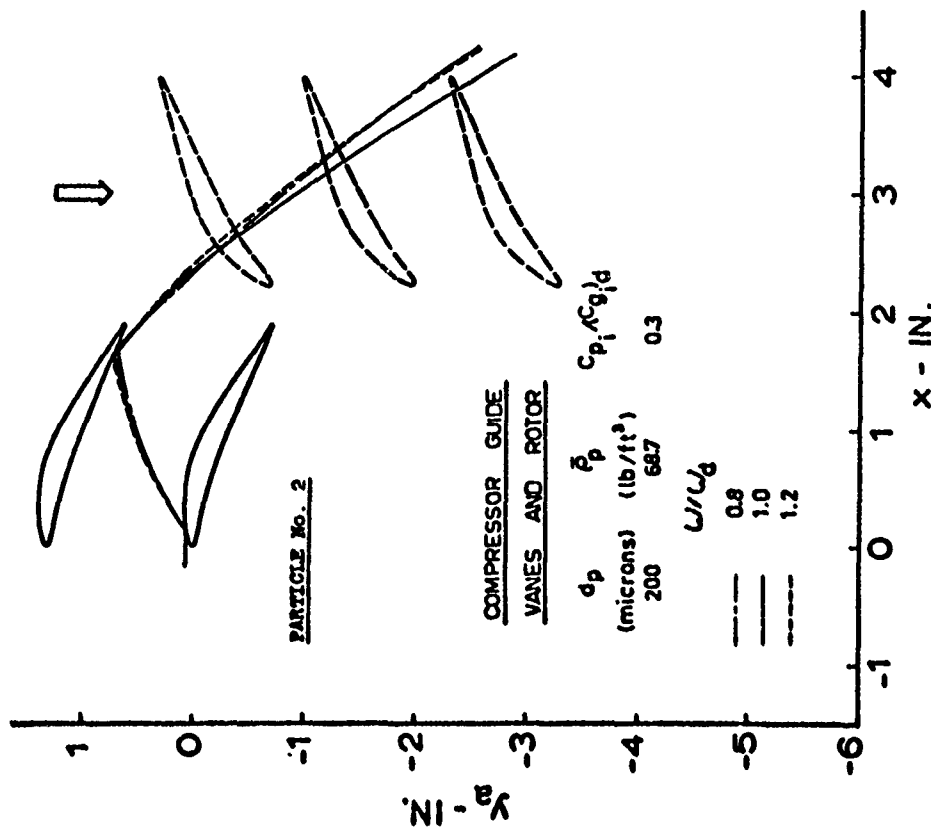


FIGURE 95 AXIAL AND TANGENTIAL COMPONENTS OF PARTICLE TRAJECTORIES RELATIVE TO THE ROTOR BLADES (EFFECT OF ω/ω_d)

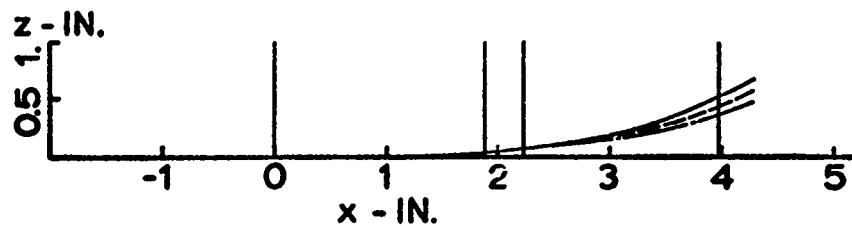


FIGURE 96 AXIAL AND RADIAL COMPONENTS OF PARTICLE TRAJECTORIES

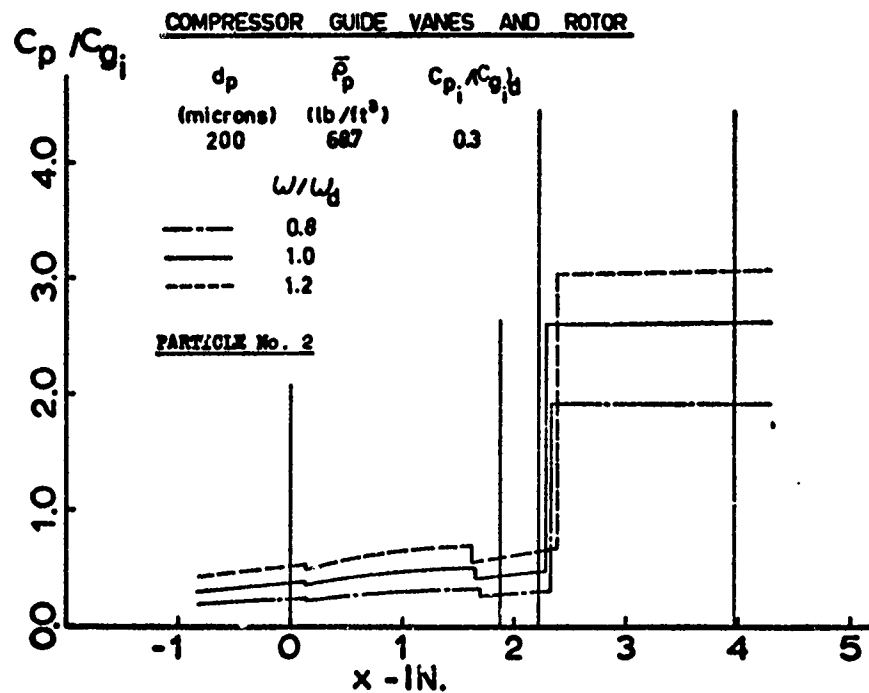


FIGURE 97 PARTICLE NONDIMENSIONAL ABSOLUTE VELOCITIES (EFFECT OF W/W_d)

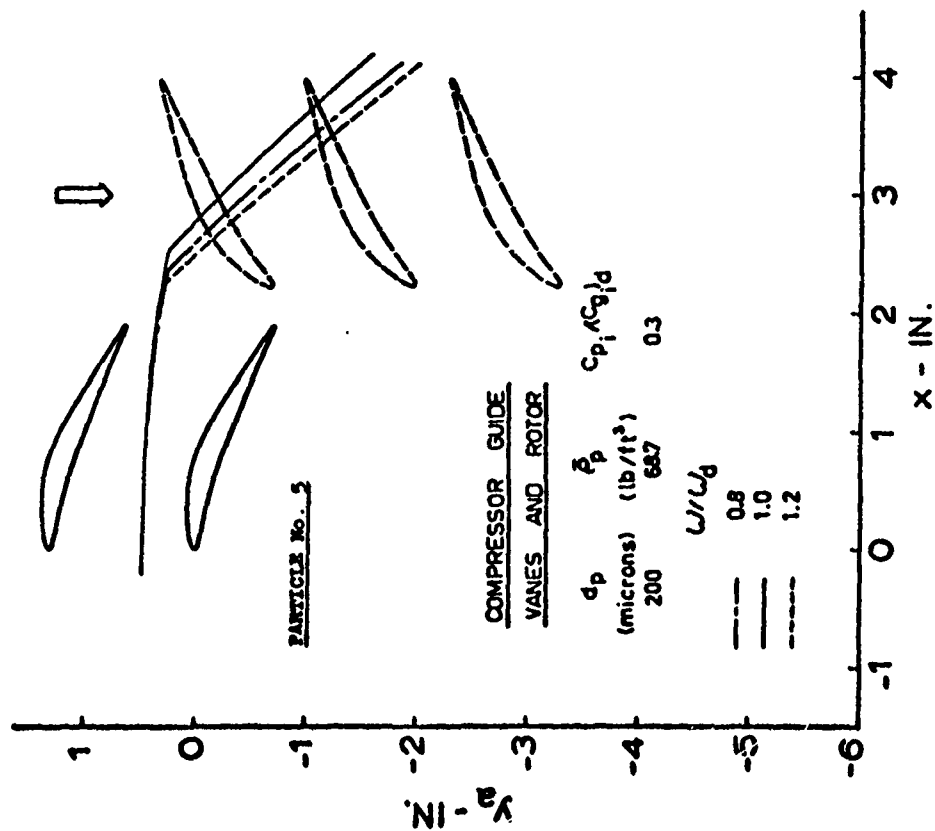


FIGURE 98 AXIAL AND TANGENTIAL COMPONENTS OF PARTICLE TRAJECTORIES (EFFECT OF w/w_d)

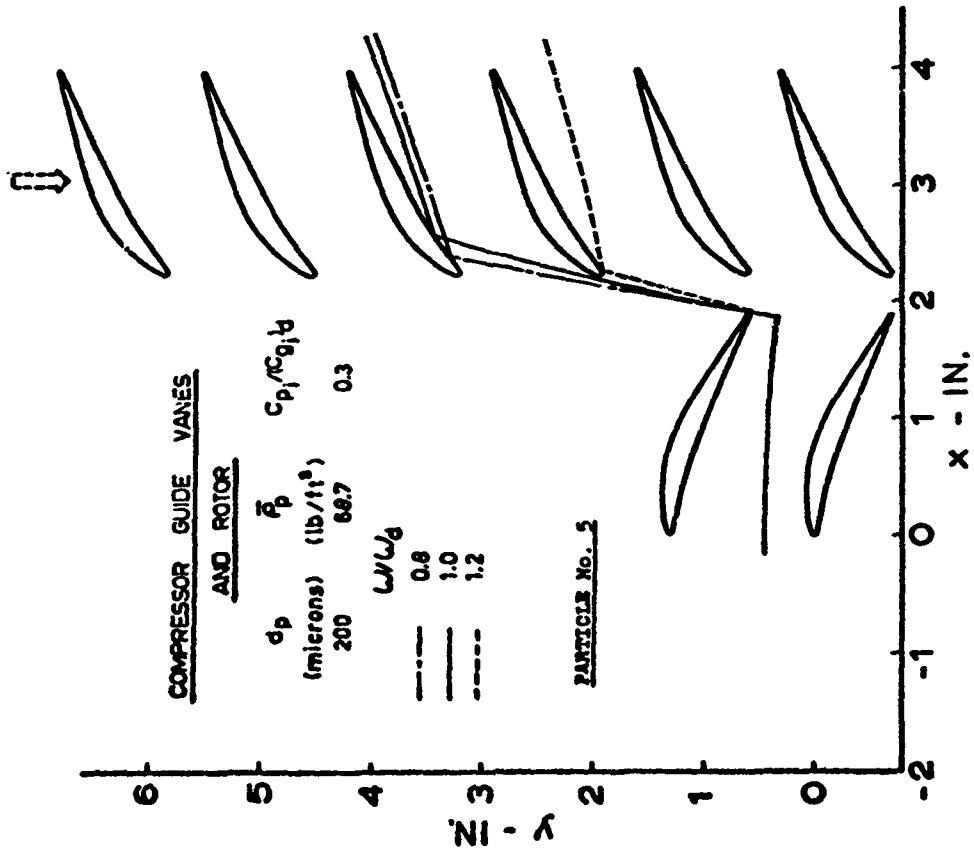


FIGURE 99 AXIAL AND TANGENTIAL COMPONENTS OF PARTICLE TRAJECTORIES RELATIVE TO THE ROTOR BLADES (EFFECT OF w/w_d)

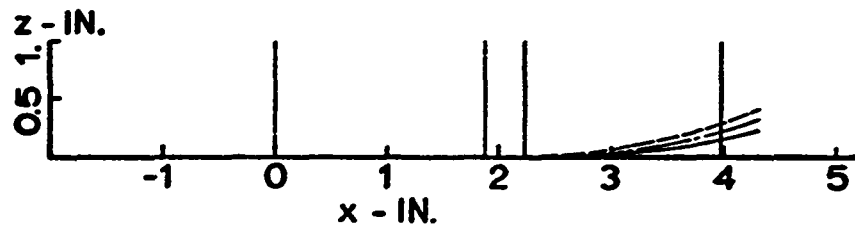


FIGURE 100 AXIAL AND RADIAL COMPONENTS OF PARTICLE TRAJECTORIES

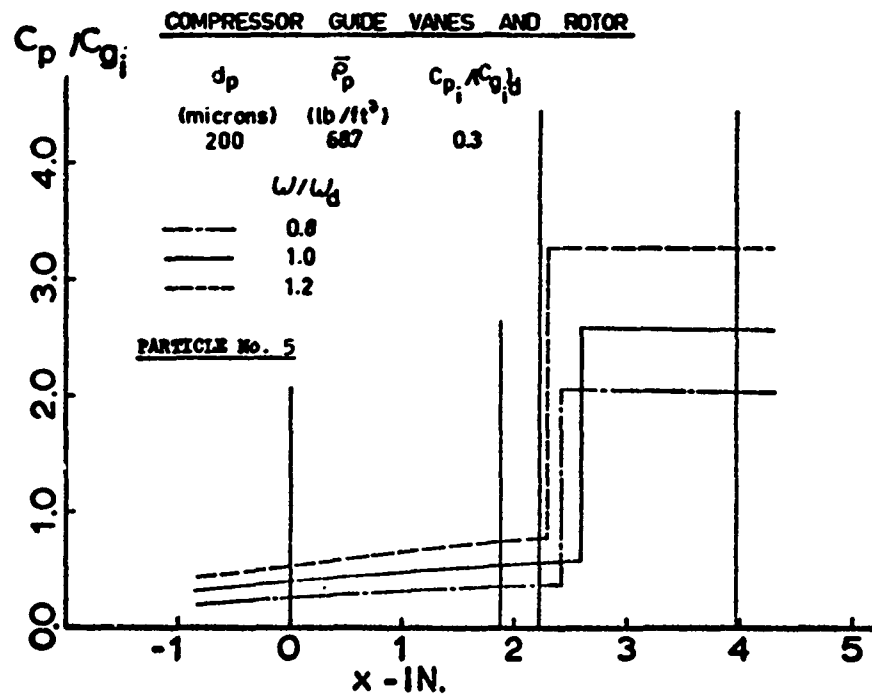


FIGURE 101 PARTICLE NONDIMENSIONAL ABSOLUTE VELOCITIES (EFFECT OF w/w_g)

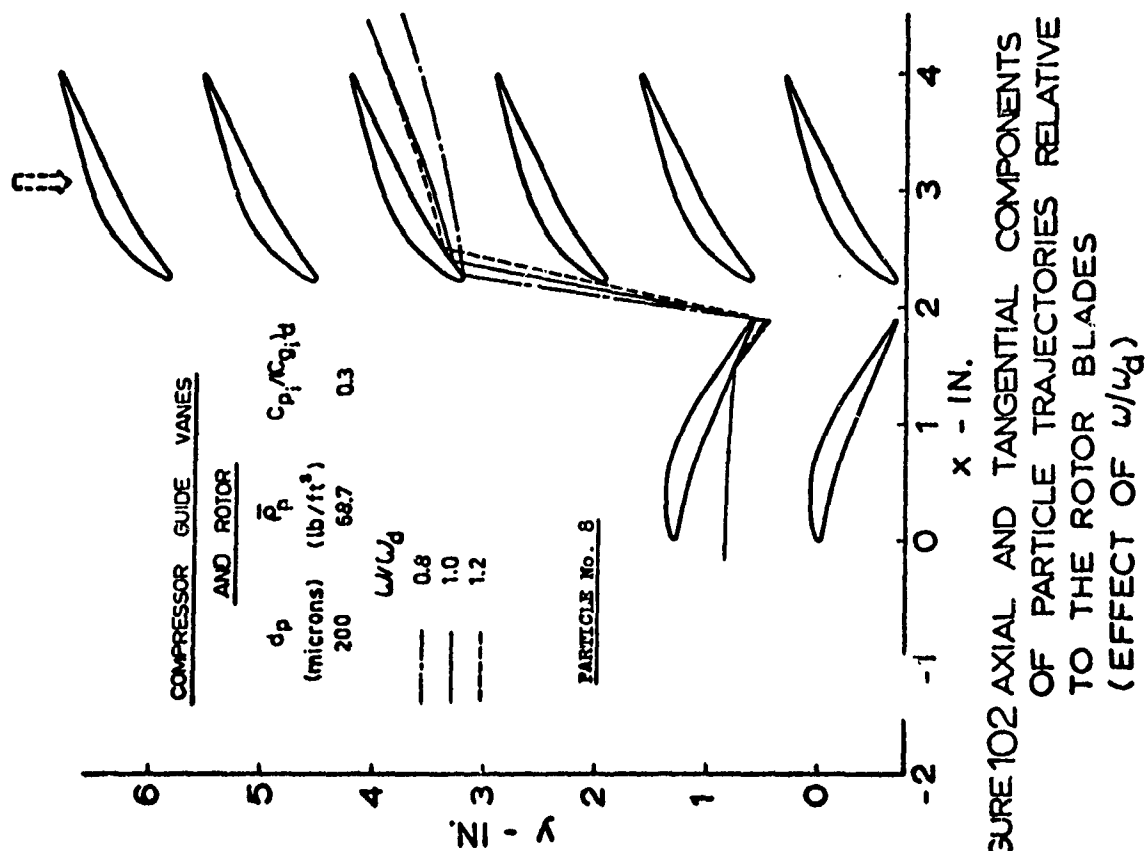


FIGURE 102 AXIAL AND TANGENTIAL COMPONENTS OF PARTICLE TRAJECTORIES RELATIVE TO THE ROTOR BLADES (EFFECT OF w/w_d)

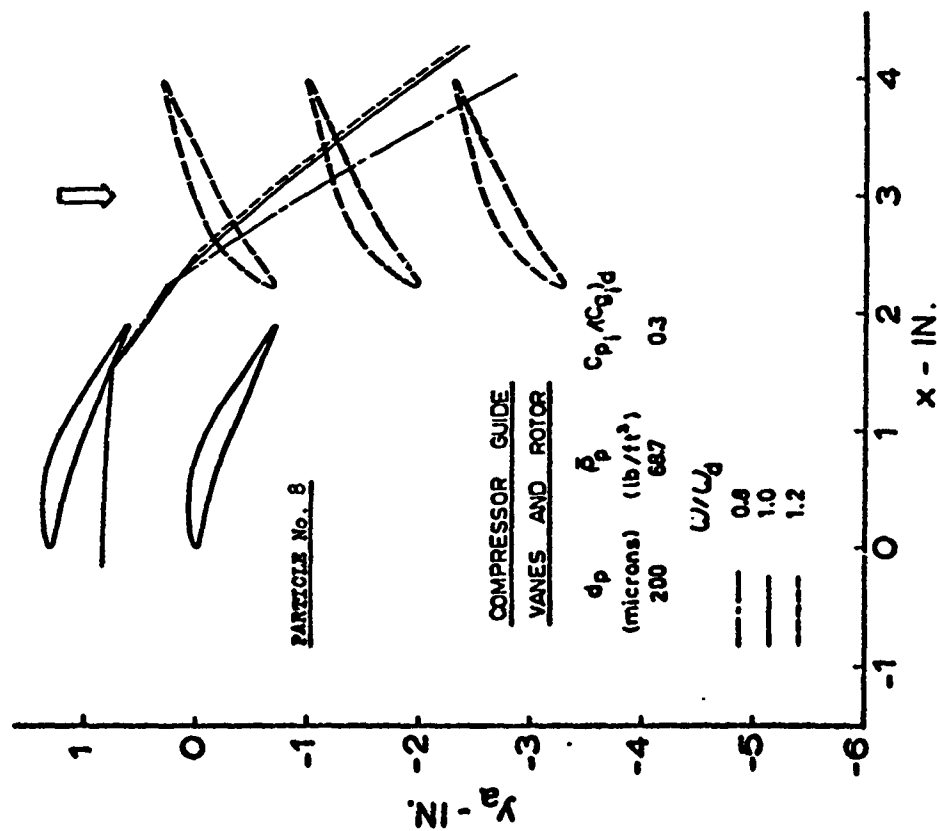


FIGURE 103 AXIAL AND TANGENTIAL COMPONENTS OF PARTICLE TRAJECTORIES (EFFECT OF w/w_d)

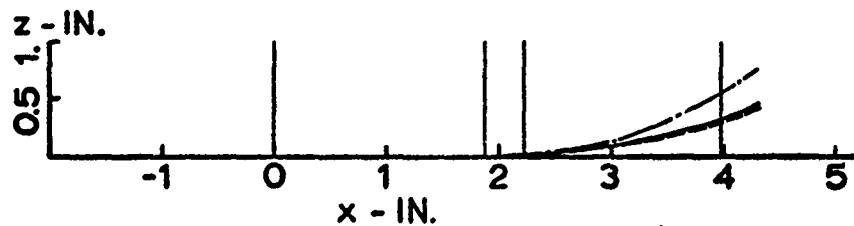


FIGURE 104 AXIAL AND RADIAL COMPONENTS OF PARTICLE TRAJECTORIES

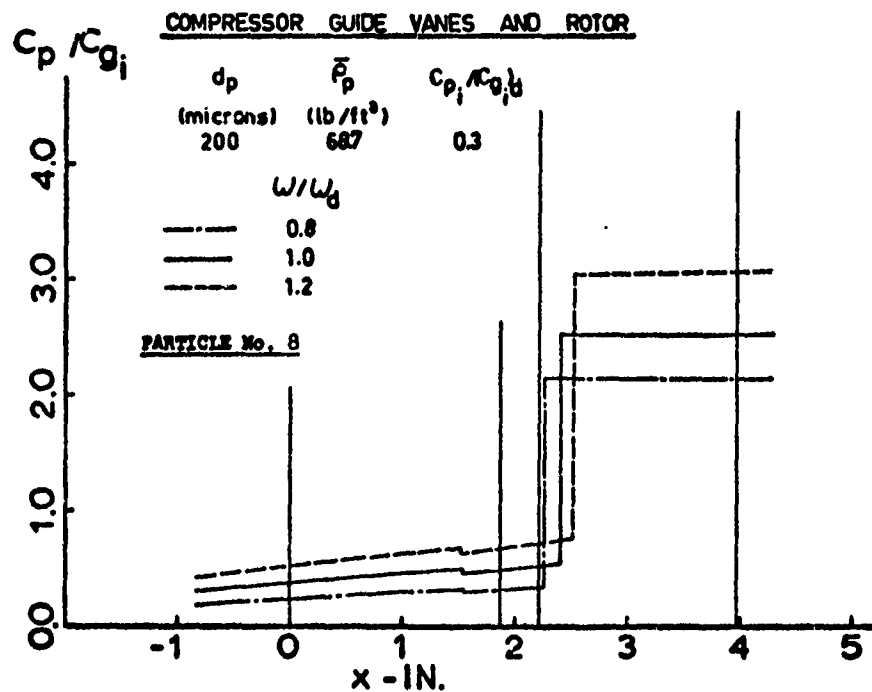


FIGURE 105 PARTICLE NONDIMENSIONAL ABSOLUTE VELOCITIES (EFFECT OF w/w_d)

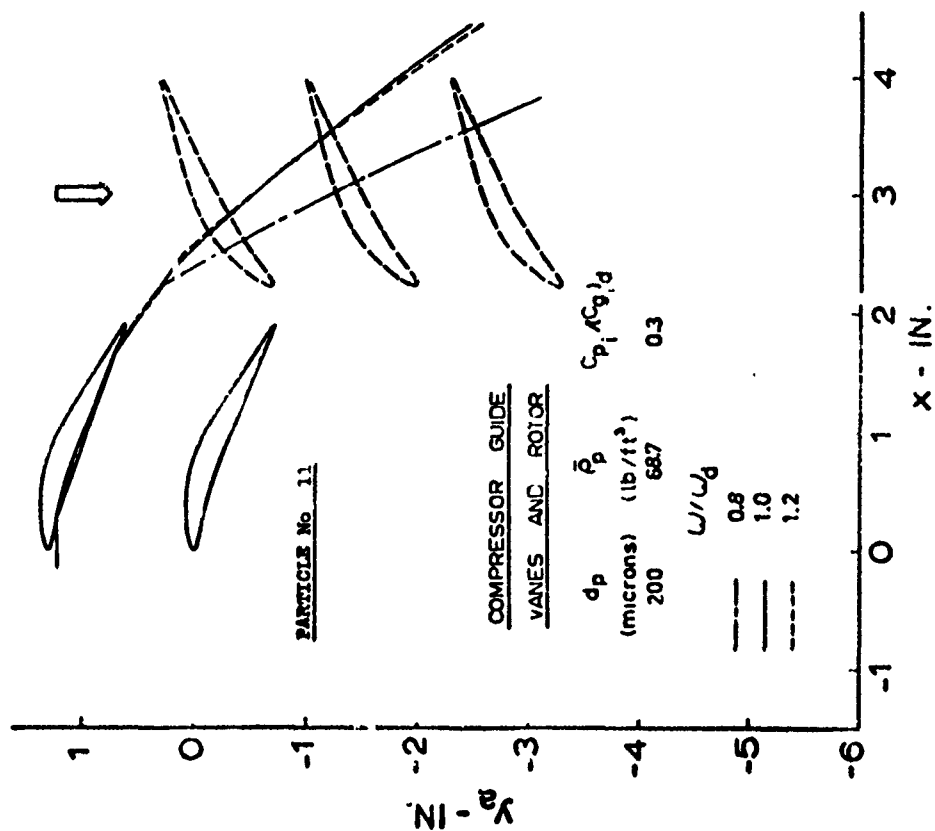


FIGURE 106 AXIAL AND TANGENTIAL COMPONENTS OF PARTICLE TRAJECTORIES (EFFECT OF W/W_d)

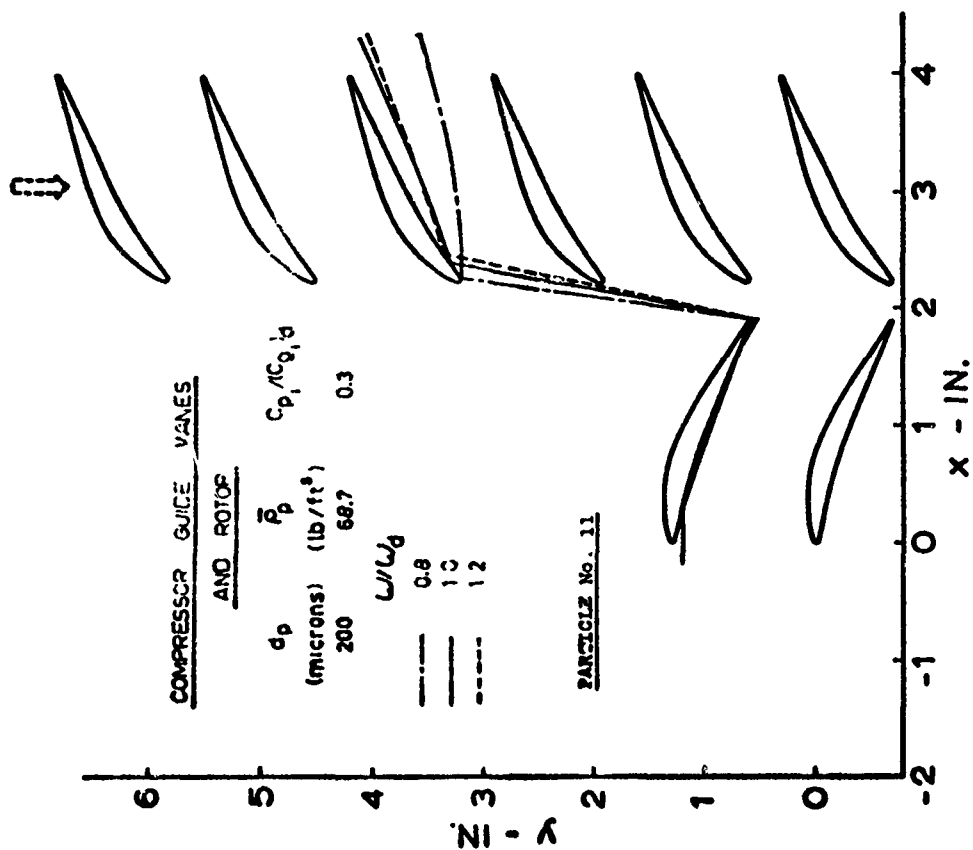


FIGURE 107 AXIAL AND TANGENTIAL COMPONENTS OF PARTICLE TRAJECTORIES RELATIVE TO THE ROTOR BLADES (EFFECT OF W/W_d)

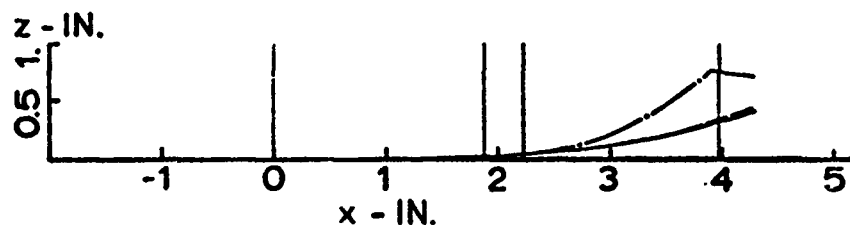


FIGURE 108 AXIAL AND RADIAL COMPONENTS OF PARTICLE TRAJECTORIES

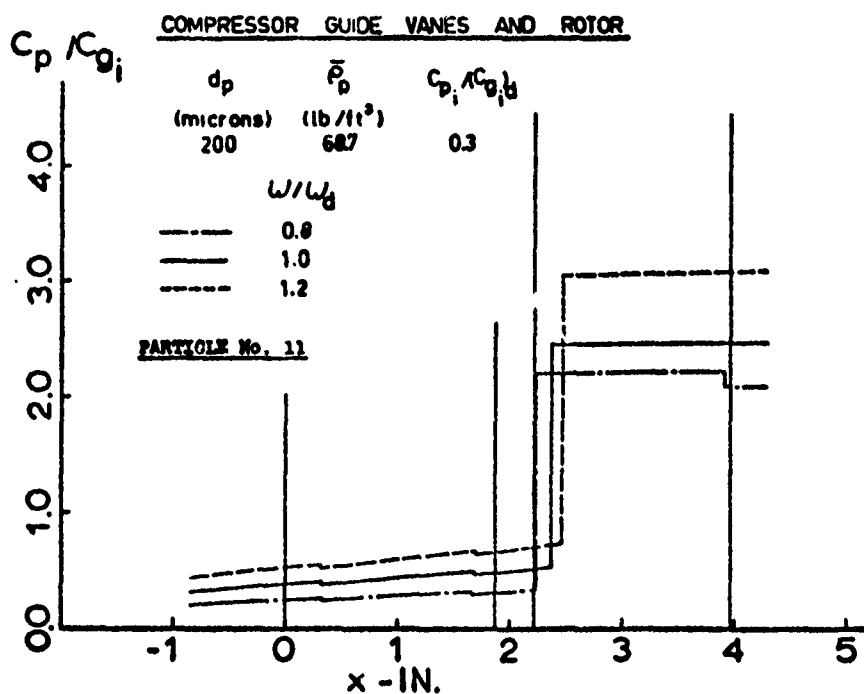


FIGURE 109 PARTICLE NONDIMENSIONAL ABSOLUTE VELOCITIES (EFFECT OF w/w_d)

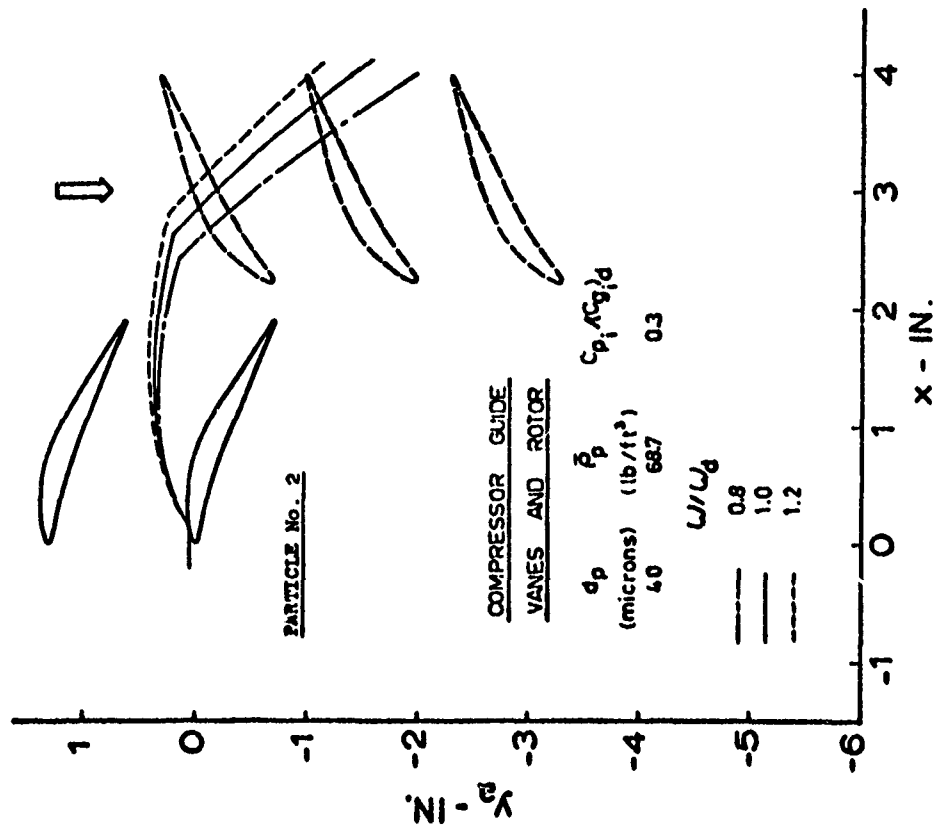


FIGURE 110 AXIAL AND TANGENTIAL COMPONENTS OF PARTICLE TRAJECTORIES (EFFECT OF ω/ω_d)

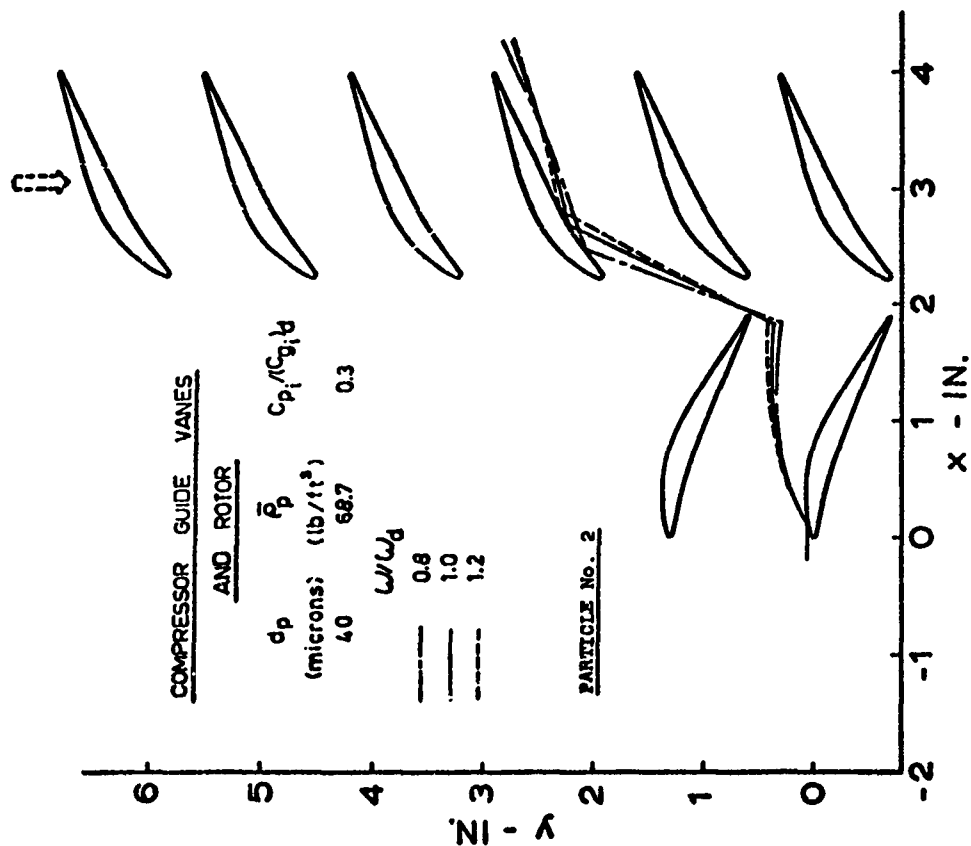


FIGURE 111 AXIAL AND TANGENTIAL COMPONENTS OF PARTICLE TRAJECTORIES RELATIVE TO THE ROTOR BLADES (EFFECT OF ω/ω_d)

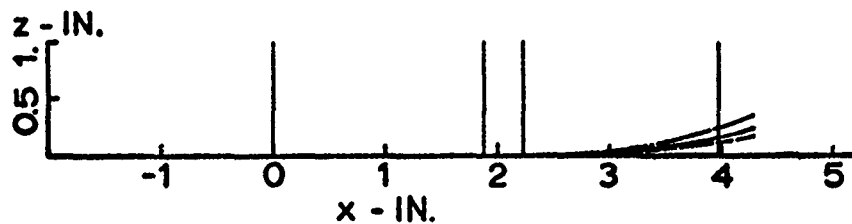


FIGURE 112 AXIAL AND RADIAL COMPONENTS OF PARTICLE TRAJECTORIES

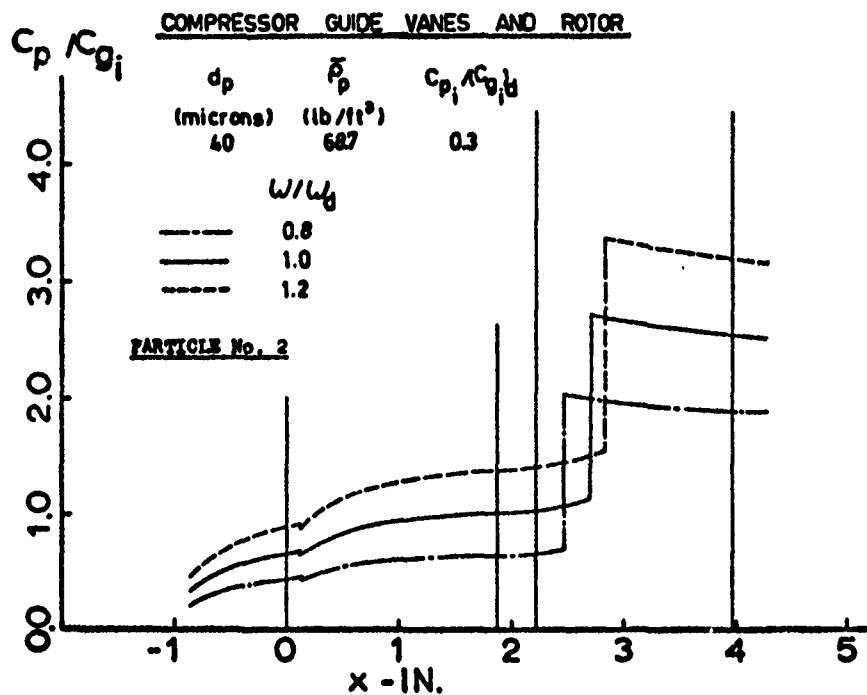


FIGURE 113 PARTICLE NONDIMENSIONAL ABSOLUTE VELOCITIES (EFFECT OF w/w_b)

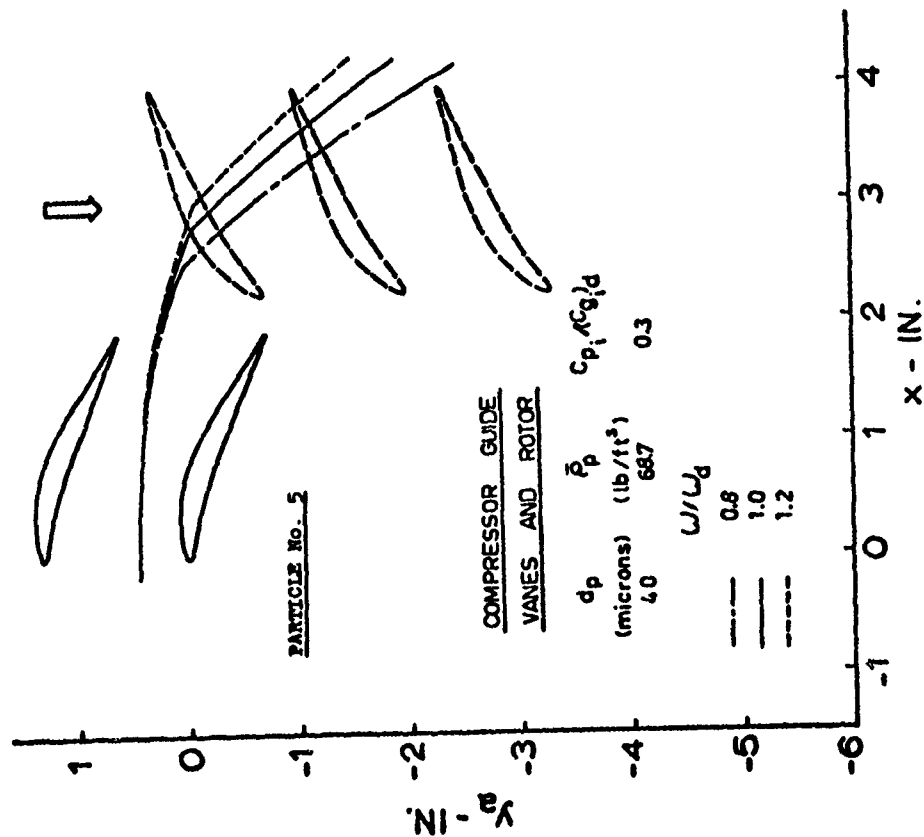


FIGURE 114 AXIAL AND TANGENTIAL COMPONENTS OF PARTICLE TRAJECTORIES (EFFECT OF ω/ω_d)

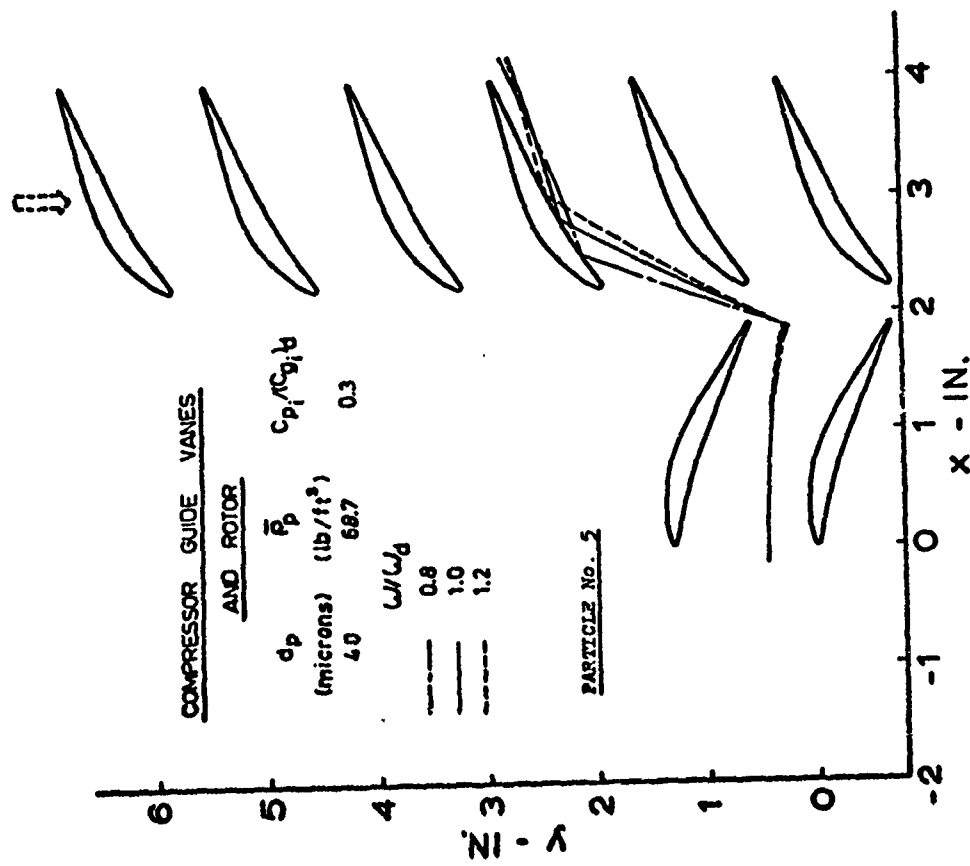


FIGURE 115 AXIAL AND TANGENTIAL COMPONENTS OF PARTICLE TRAJECTORIES RELATIVE TO THE ROTOR BLADES (EFFECT OF ω/ω_d)

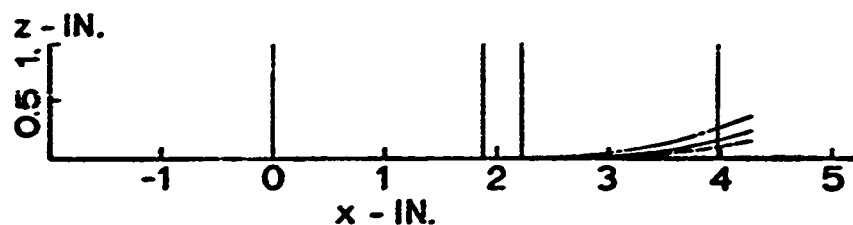


FIGURE 116 AXIAL AND RADIAL COMPONENTS OF PARTICLE TRAJECTORIES

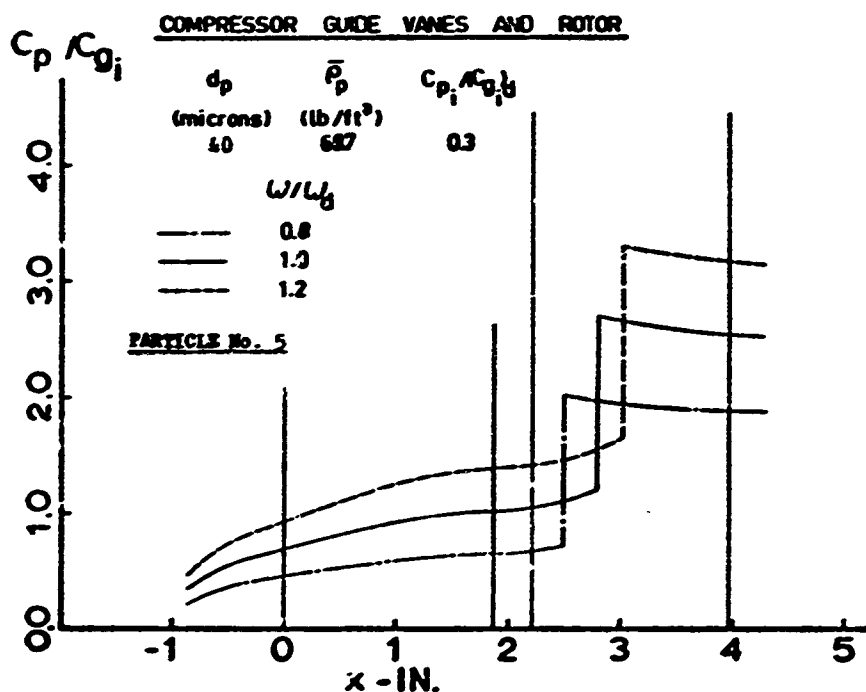


FIGURE 117 PARTICLE NONDIMENSIONAL ABSOLUTE VELOCITIES (EFFECT OF w/w_g)

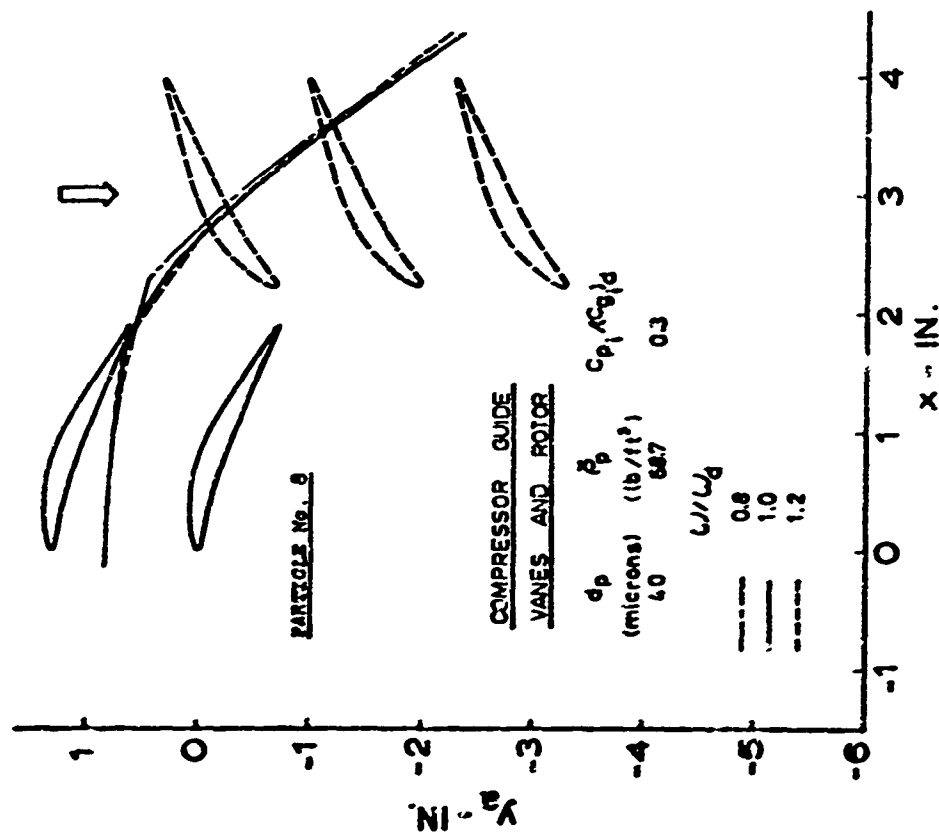


FIGURE 118 AXIAL AND TANGENTIAL COMPONENTS OF PARTICLE TRAJECTORIES (EFFECT OF w/w_d)

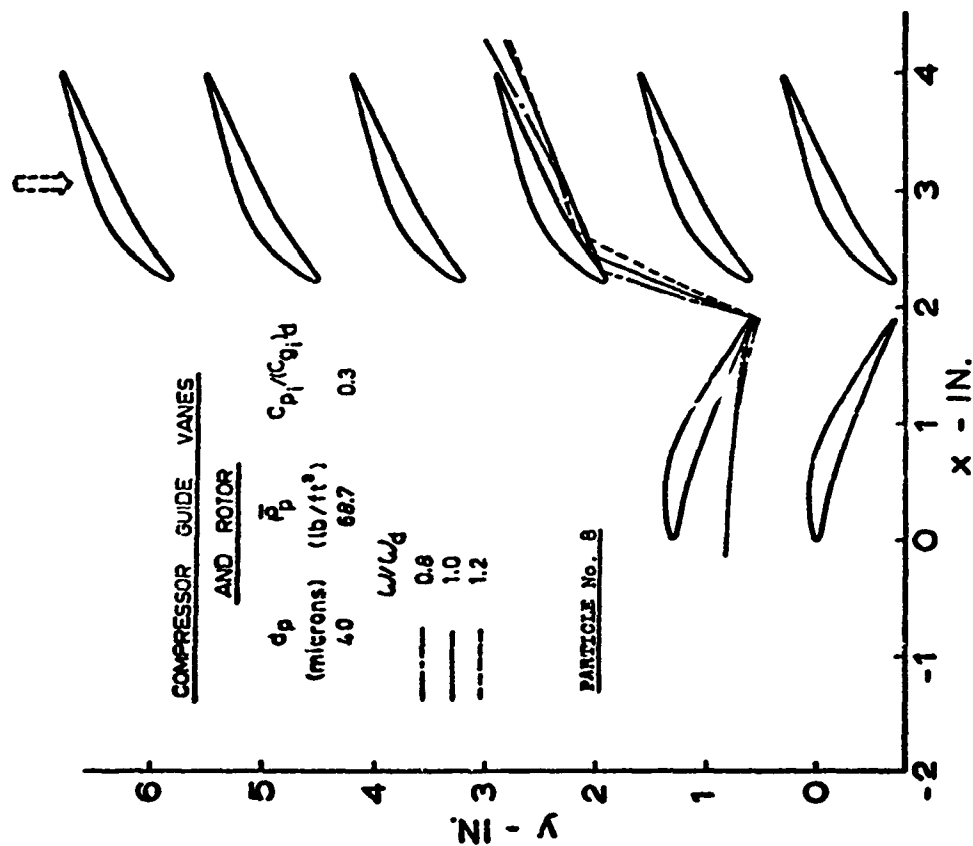


FIGURE 119 AXIAL AND TANGENTIAL COMPONENTS OF PARTICLE TRAJECTORIES RELATIVE TO THE ROTOR BLADES (EFFECT OF w/w_d)

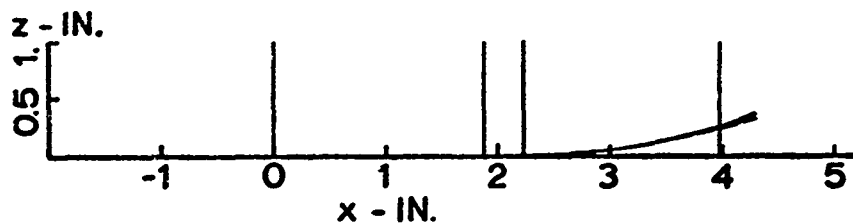


FIGURE 120 AXIAL AND RADIAL COMPONENTS OF PARTICLE TRAJECTORIES

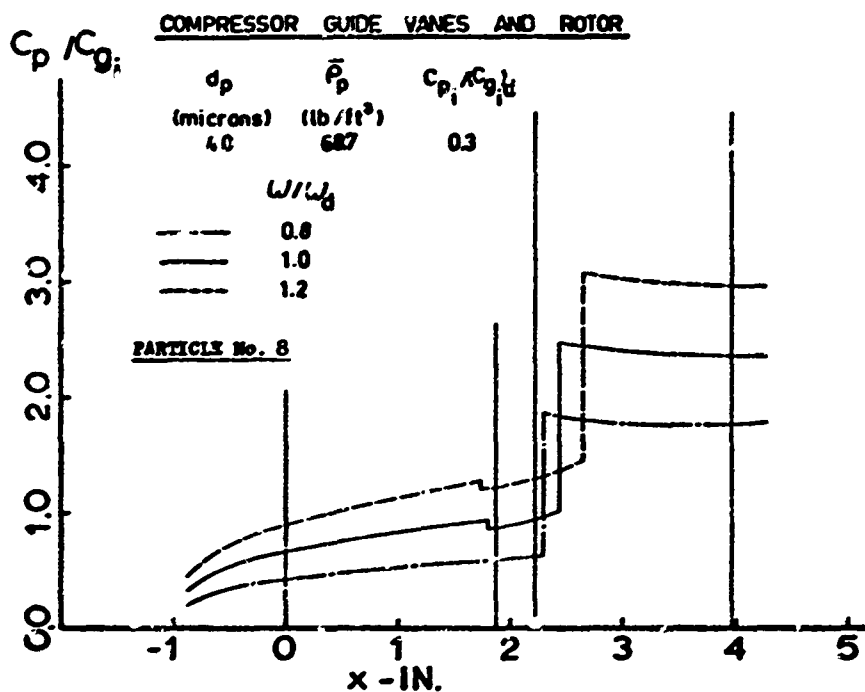


FIGURE 121 PARTICLE NONDIMENSIONAL ABSOLUTE VELOCITIES (EFFECT OF W/W_d)

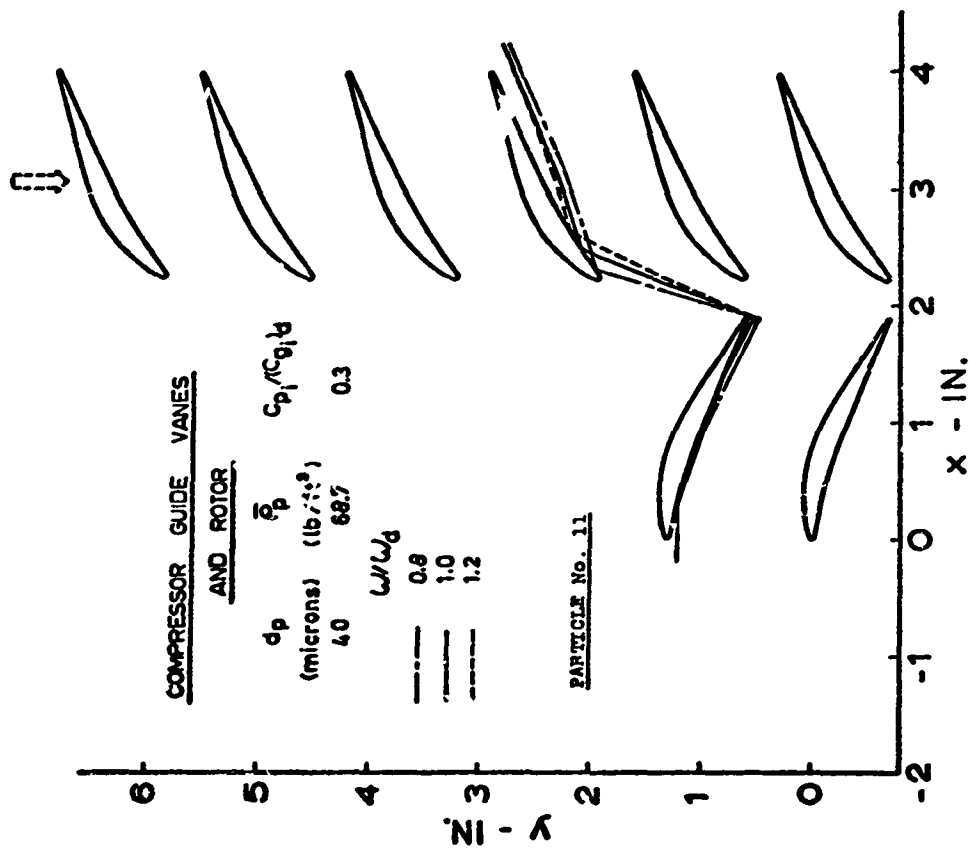


FIGURE 122 AXIAL AND TANGENTIAL COMPONENTS OF PARTICLE TRAJECTORIES (EFFECT OF ω/ω_d)

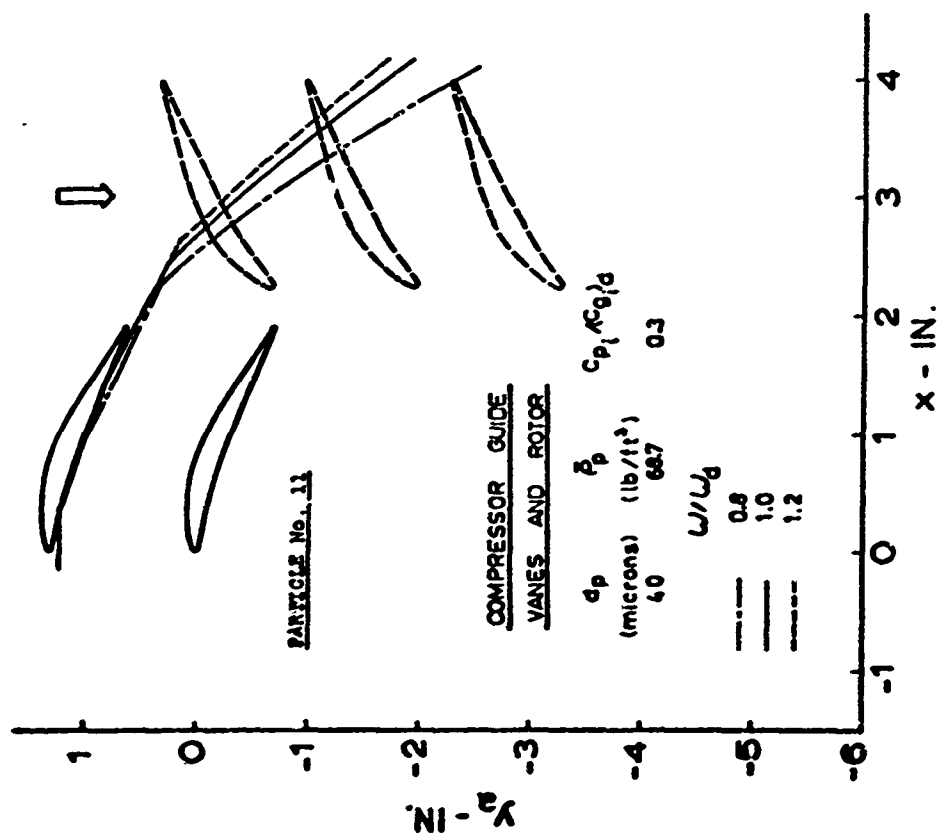


FIGURE 123 AXIAL AND TANGENTIAL COMPONENTS OF PARTICLE TRAJECTORIES (EFFECT OF ω/ω_d)

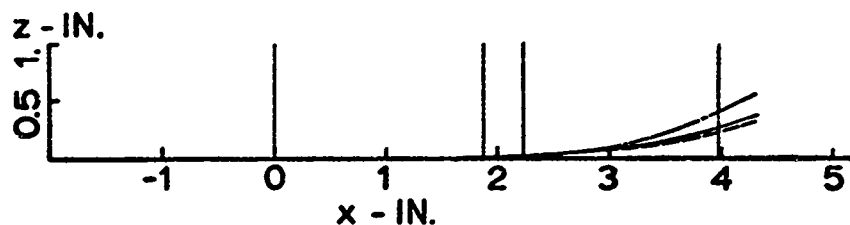


FIGURE 124 AXIAL AND RADIAL COMPONENTS OF PARTICLE TRAJECTORIES

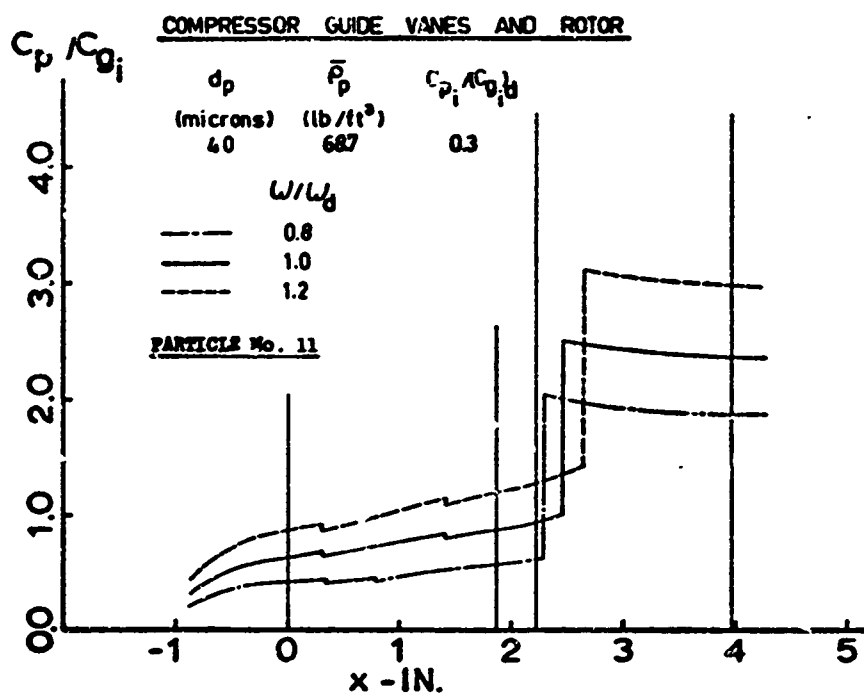


FIGURE 125 PARTICLE NONDIMENSIONAL ABSOLUTE VELOCITIES (EFFECT OF w/w_0)

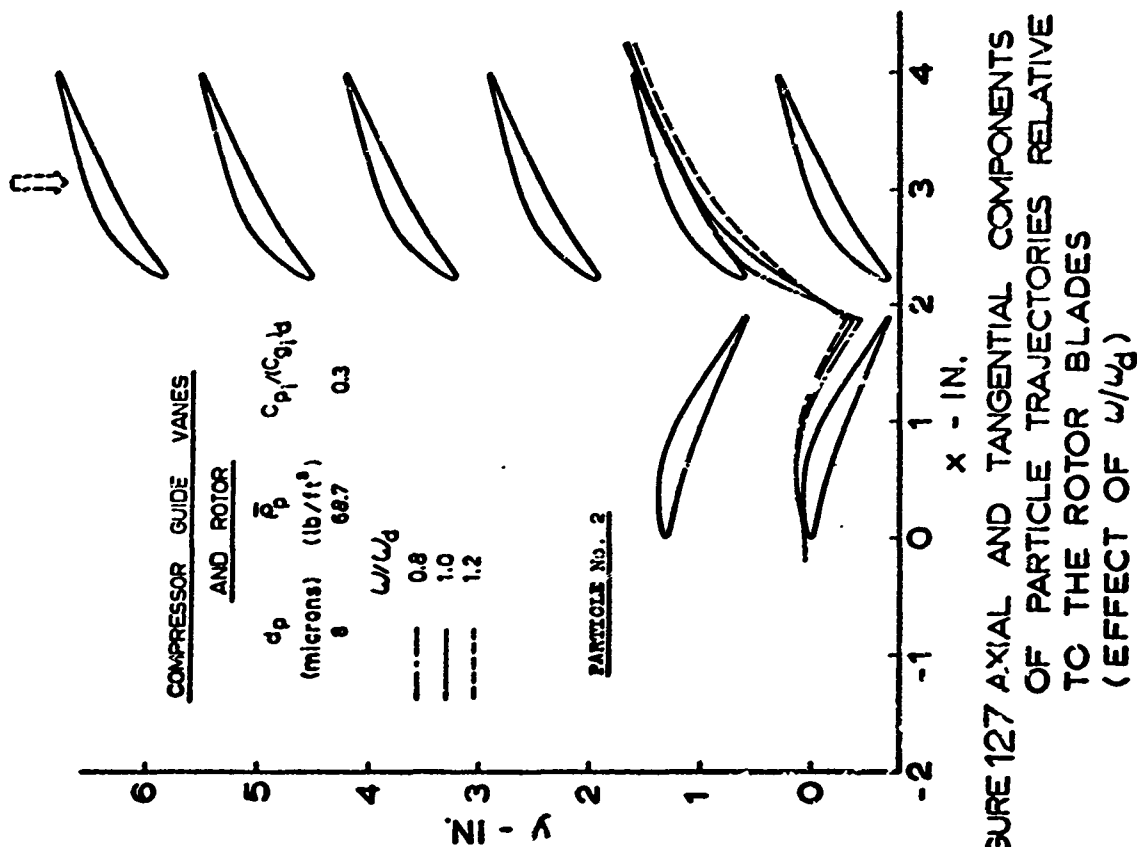


FIGURE 126 AXIAL AND TANGENTIAL COMPONENTS OF PARTICLE TRAJECTORIES RELATIVE TO THE ROTOR BLADES (EFFECT OF w/w_d)

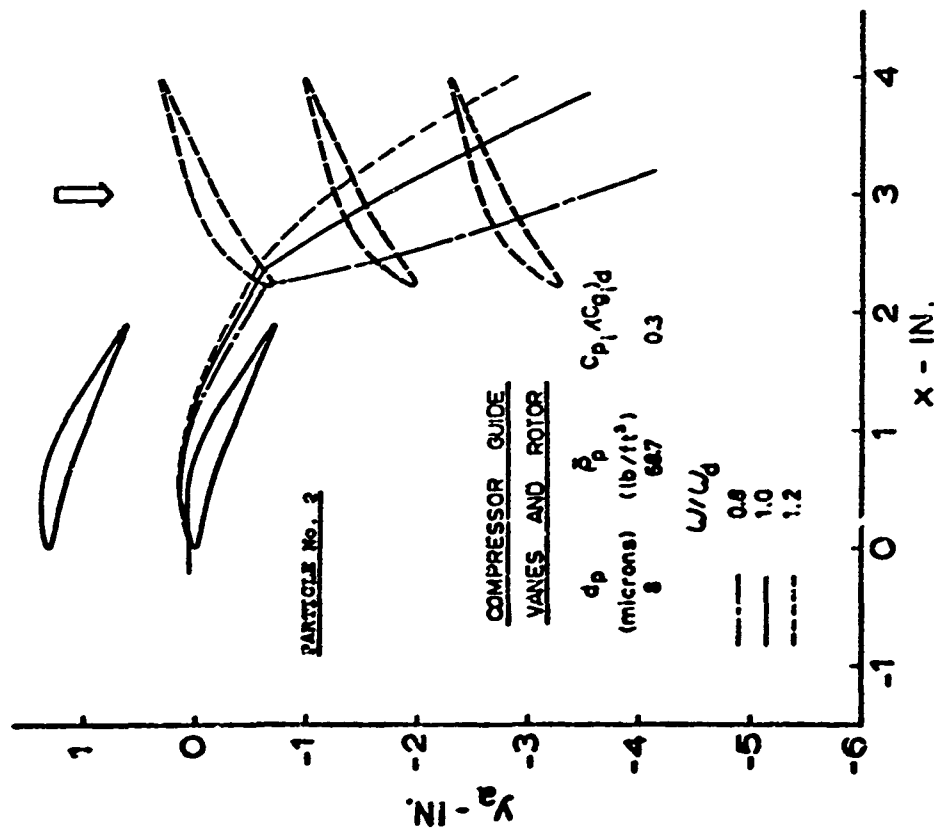


FIGURE 127 AXIAL AND TANGENTIAL COMPONENTS OF PARTICLE TRAJECTORIES RELATIVE TO THE ROTOR BLADES (EFFECT OF w/w_d)

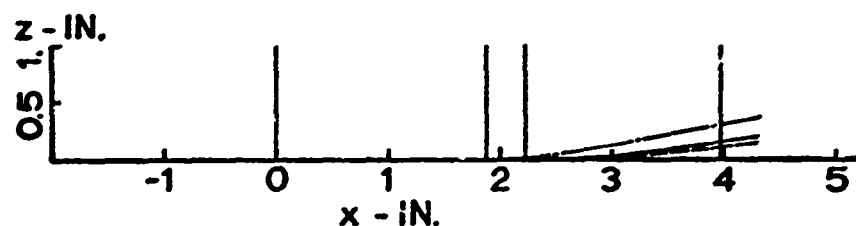


FIGURE 128 AXIAL AND RADIAL COMPONENTS OF PARTICLE TRAJECTORIES

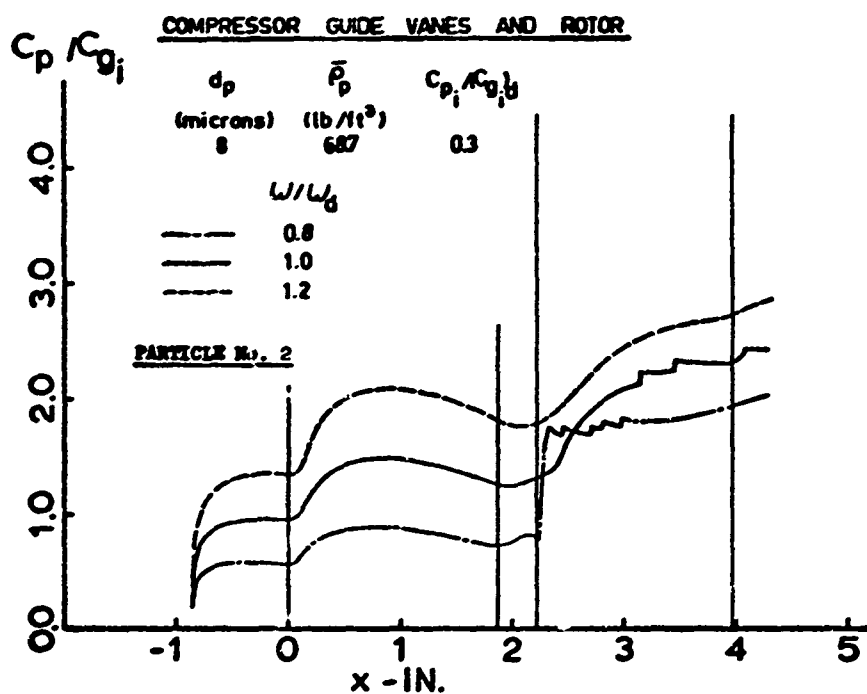


FIGURE 129 PARTICLE NONDIMENSIONAL ABSOLUTE VELOCITIES (EFFECT OF W/W_0)

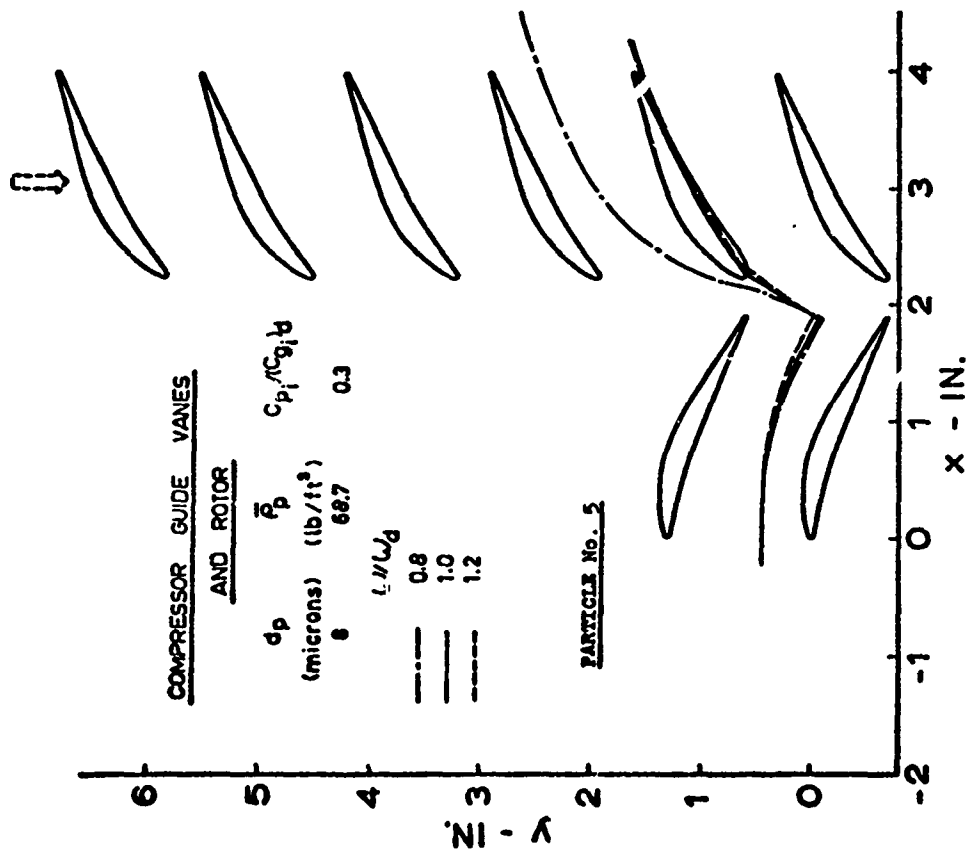


FIGURE 130 AXIAL AND TANGENTIAL COMPONENTS OF PARTICLE TRAJECTORIES (EFFECT OF w/w_d)

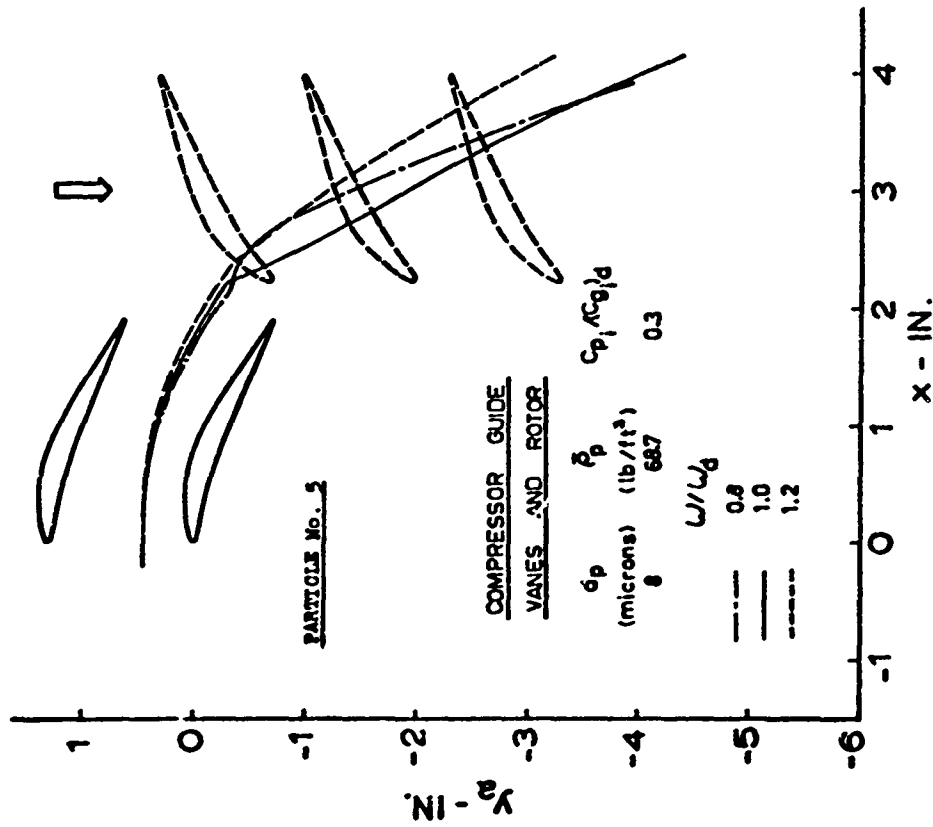


FIGURE 131 AXIAL AND TANGENTIAL COMPONENTS OF PARTICLE TRAJECTORIES (EFFECT OF w/w_d)

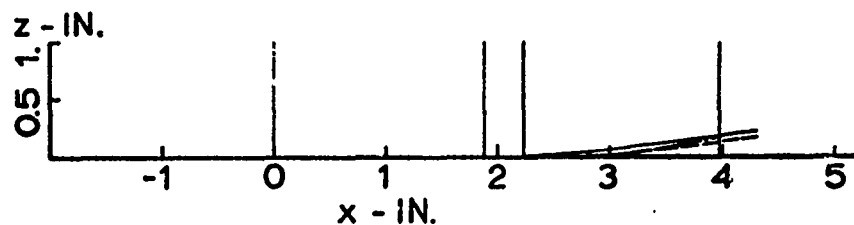


FIGURE 132 AXIAL AND RADIAL COMPONENTS OF PARTICLE TRAJECTORIES

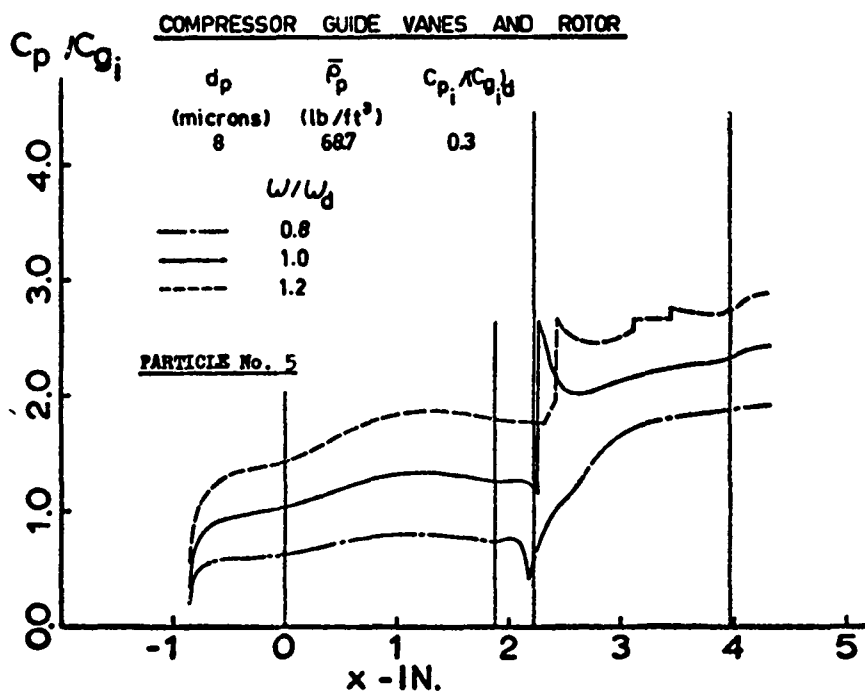


FIGURE 133 PARTICLE NONDIMENSIONAL ABSOLUTE VELOCITIES (EFFECT OF W/W_d)

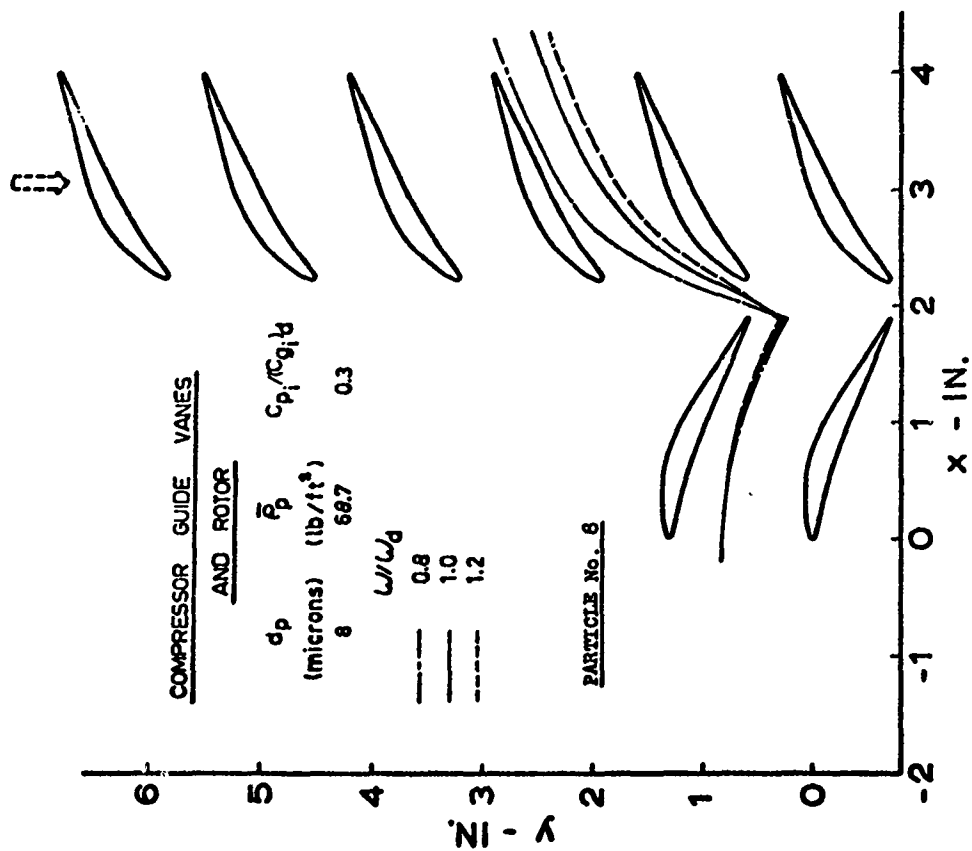


FIGURE 134 AXIAL AND TANGENTIAL COMPONENTS OF PARTICLE TRAJECTORIES RELATIVE TO THE ROTOR BLADES (EFFECT OF w/w_d)

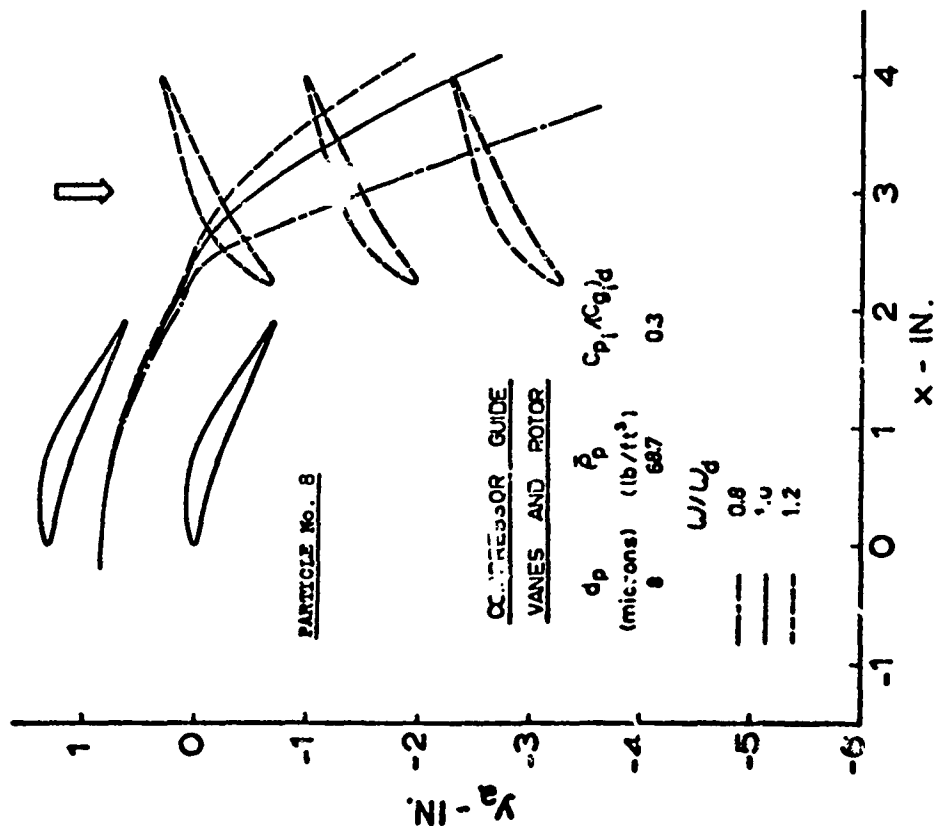


FIGURE 135 AXIAL AND TANGENTIAL COMPONENTS OF PARTICLE TRAJECTORIES RELATIVE TO THE ROTOR BLADES (EFFECT OF w/w_d)

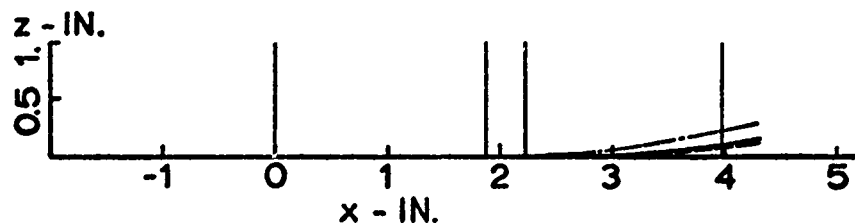


FIGURE 136 AXIAL AND RADIAL COMPONENTS OF PARTICLE TRAJECTORIES

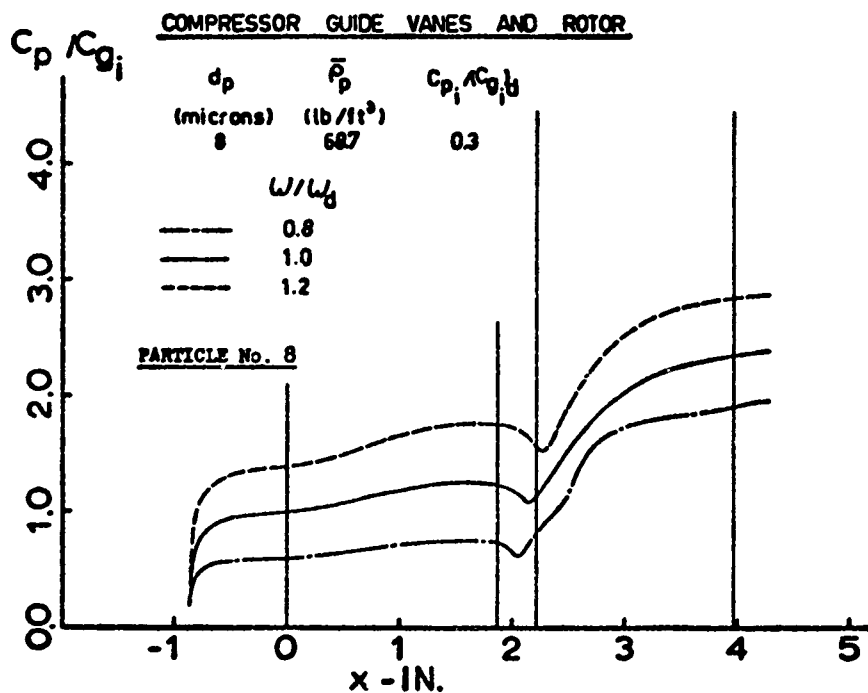


FIGURE 137 PARTICLE NONDIMENSIONAL ABSOLUTE VELOCITIES (EFFECT OF w/w_d)

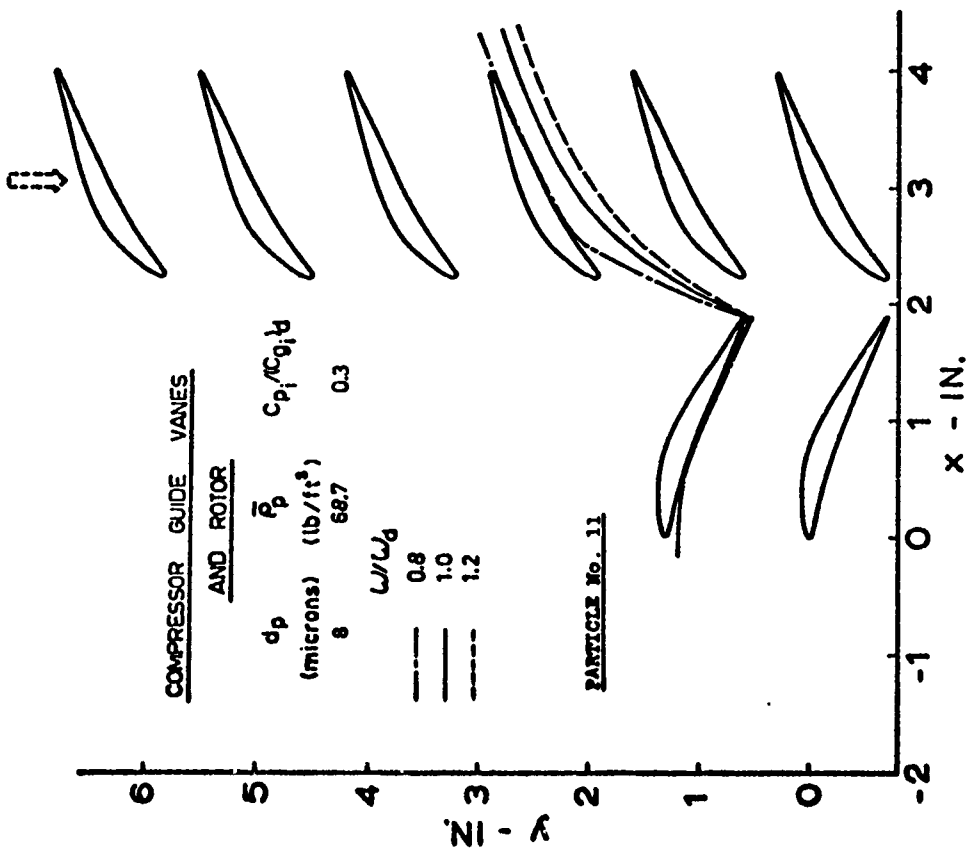


FIGURE 138 AXIAL AND TANGENTIAL COMPONENTS OF PARTICLE TRAJECTORIES RELATIVE TO THE ROTOR BLADES (EFFECT OF U/U_d)

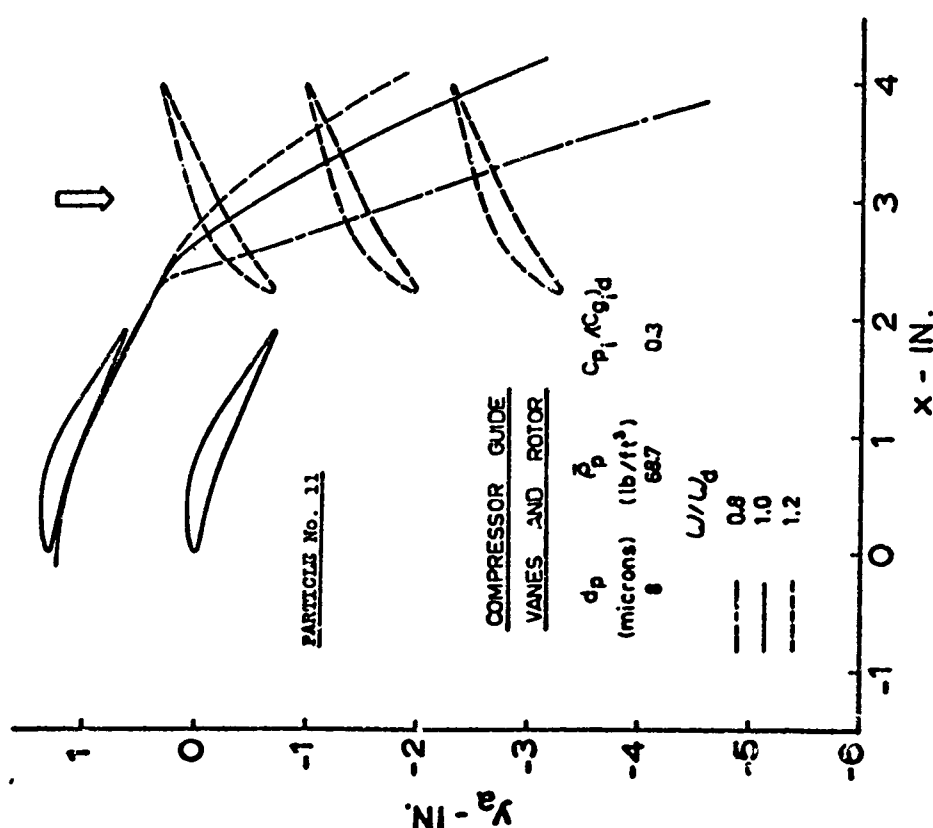


FIGURE 139 AXIAL AND TANGENTIAL COMPONENTS OF PARTICLE TRAJECTORIES RELATIVE TO THE ROTOR BLADES (EFFECT OF U/U_d)

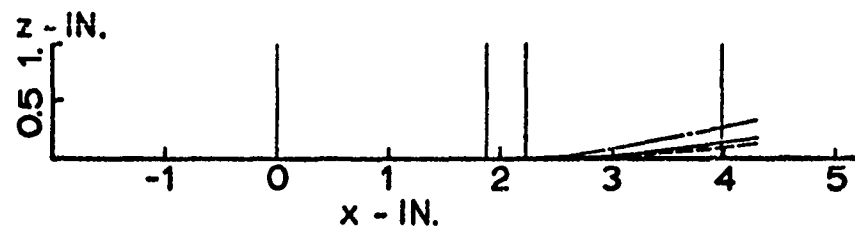


FIGURE 140 AXIAL AND RADIAL COMPONENTS OF PARTICLE TRAJECTORIES

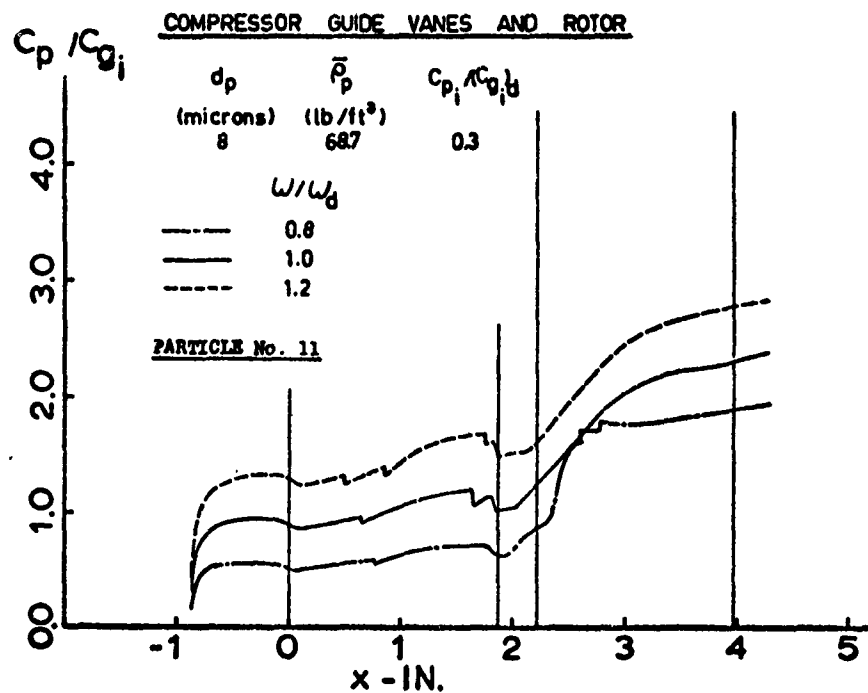


FIGURE 141 PARTICLE NONDIMENSIONAL ABSOLUTE VELOCITIES (EFFECT OF ω/ω_d)